University of Strathclyde
Department of Pure and Applied Chemistry

TUNABLE SOFT MATTER THROUGH PEPTIDE SELF-ASSEMBLY

by

GARY GEORGE SCOTT

A thesis submitted to the Department of Pure and Applied Chemistry, University of Strathclyde, in part fulfillment of the regulations for the degree of Doctor of Philosophy in Chemistry.

June 2017

Signed:

Date:

“It always seems impossible until it is done”

-Nelson Mandela

Acknowledgements

During the course of this PhD, there are a number of people that deserve special recognition for both the work they have put into it but also the support they have giving me throughout the past 4 years.

First and foremost, I must give my thanks to both my supervisors Prof Rein V. Ulijn, Dr Tell Tuttle and my sponsors EPSRC and Macphie of Glenbervie. Without them, this project would of not been possible but I would also like to thank them for their patience, understanding and helpful discussion throughout. I am sure our paths will cross again in the future. Tell – I will keep the pool table open in case you want to try and gain some pride back.

Secondly, I must thanks the postdoctoral research associates that have been there:

Dr Pim W. J. M. Frederix, you taught me everything I know about computational chemistry. The project started with your amazing idea and without it, my life would have been much more difficult.

Dr Ayala Lampel, although we only worked together for approximately a year, it was a privilege to collaborate with you. You helped me with important discussions and got me on the front cover of Advanced Materials. In addition, it was your work and perseverance that got us a publication in *Science*.

Dr Meghan Hughes, what an adventure we have been on. You have truly been an asset to the Ulijn group and a great friend. We will always have the many trips to New York and me forcing you to the pub every second day. It has been a pleasure. Also, thanks for stopping me over tipping the waitress, that would have been a major mistake.

To both research groups, Ulijn group of old and new and Tuttlelab. It was an honour to work with such a talented group of people. I am sure every single one of you will prosper in your chosen field.

To my friends back home. It was probably a struggle for yourselves as much as it was for me but your witty banter and friendly atmosphere has made the pass few years enjoyable. I probably owe most of you guys a pint.

Finally, I must give special recognition to my family. To my brothers, Kenny and Steven, thanks for all the “support” over the years, you can now get off my back as I need to start contributing to society. Mum and Dad, thanks for everything you have done over the past 9 years I have been at university. From helping out with money, accommodation, reading over reports/CVs/letters etc. your endless enthusiasm for my work has driven me forward. It will be something that I will always remember.

The Author

Publications

1 Pickering Stabilized Peptide Gel Particle as Tunable Microenvironments for Biocatalysis

G. G. Scott, S. Roy, Y. M. Abul-Haija, S. Fleming, S. Bai, R.V. Ulijn

Langmuir, **2013**, *29*, 14321-14327

2* Exploring the sequence Space for (Tri-) peptide Self-assembly to Design and Discover New Hydrogels

P. W. J. M. Frederix, **G. G. Scott**, Y. M. Abul-Haija, D. Kalafatovic, C. G. Pappas, N. Javid, N. T. Hunt, R. V. Ulijn, T. Tuttle

Nat. Chem., **2015**, *7*, 30-37

3* Tripeptide Emulsifiers

G. G. Scott, P. J. McKnight, T. Tuttle, R. V. Ulijn

Adv. Mat., **2016**, *28*, 1381-1386

4 Polymeric Peptide Pigments with Sequence-Encoded Properties

A. Lampel, S. McPhee, H-A. Park, **G. G. Scott**, S. Humagain, D. R. Hekstra, B. Yoo, P. W. J. M. Frederix, T-D. Li, R. Abzalimov, S. G. Greenbaum, T. Tuttle, C. Hu, C. J. Bettinger, R. V. Ulijn

Science, **2017**, *365*, 1064-1068

5* Trapping Tripeptide Nanostructures in Kinetically Controlled Bio-Catalytic Self-Assembly

G. G. Scott, A. Lampel, P. J. McKnight, T. Tuttle, R. V. Ulijn

Chem Commun, manuscript in progress

6 Cooperative, Ion-Sensitive Co-Assembly of Tripeptide Hydrogels

Y. M. Abul-Haija, **G. G. Scott**, J. K. Sahoo, T. Tuttle, R. V. Ulijn

Chem Commun, Manuscript under review

7* Counter-Ion Effect on Tripeptide Nanostructures and Hydrogels
G. G. Scott, N. Wijerathne, S. McPhee, T. Tuttle, R. V. Ulijn
JACS, Manuscript in progress

8 Spontaneous Amide Bond Formation by Auto-Acylation of Tripeptides
K. L. Duncan, T. K. Piskorz, **G. G. Scott,** J. van Esch, T. Tuttle, R. de la Rica, R. V.Ulijn
Angew. Chemie, Manuscript in Progress

* *Publication related to work in this thesis*

Patent Applications

1 Self-Assembling Tripeptides
R. V. Ulijn, T. Tuttle, P. W. J. M. Frederix, **G. G. Scott**, Y. M. Abul-Haija
WO2016055810

2 Stable Emulsions
R. V. Ulijn, T. Tuttle, I. P. Moreira, **G. G. Scott**, S. Bai, C. Pappas, P. J. McKnight, M. E. Ruck
WO2015177569

Conferences/Workshops

2014 RSC Biomaterials
University of Manchester, Manchester, UK
*Poster presentation

Modeling Molecules and Materials – M3
University of Strathclyde, Glasgow, UK
*Poster Presentation

ScotCHEM Computational Chemistry Symposium
Herriot-Watt University, Edinburgh, UK
*Poster Presentation

2015 Nanoscience NY

Advanced Science Research Center, New York, U.S.A

Materials Research Society (MRS) Spring Exhibit

San Francisco, California, U.S.A

ScotCHEM Computational Chemistry Symposium

University of Strathclyde, Glasgow, UK

*Poster Presentation – Prize winner

POLARIS Conference – Challenges in Nanomedicine and Regenerative Medicine

University of Minho, Guimarães, Portugal

*Oral Presentation

MARTINI Coarse-grain Workshop

University of Groningen, Groningen, Netherlands

Active and Adaptive Materials

Advanced Science Research Center, New York, U.S.A

* Poster Presentation

2016 ScotCHEM Computational Chemistry Symposium

University of Edinburgh, Edinburgh, UK

*Poster Presentation – Prize Winner

Bio|Nano|Med

Advanced Science Research Center, New York, U.S.A

*Poster Presentation

Abbreviations

AA	All-atom
AFM	Atomic Force Microscopy
AP	Aggregation Propensity
CD	Circular Dichroism
CG	Coarse grained
CHARMM	Chemistry at HARvard Macromolecular Mechanics
DIPEA	N,N-Diisopropylethylamine
DNA	Deoxyribonucleic Acid
Fmoc	9-fluorenylmethoxycarbonyl
FTIR	Fourier Transform Infra red
HBTU	O-Benxotiazole-N,N,N',N'-tectramethyl-uronium-heaxfluoro-phosphate
LCMS	Liquid chromatography Mass Spectroscopy
HPLC	High Performance Liquid chromatography
LJ	Lennard-Jones
LMWG	Low molecular weight gelator
MD	Molecular dynamics
MM	Molecular mechanics
MS	Mass spectrometry
NAMD	Nano scale molecular dynamics
NMR	Nuclear Magnetic Resonance
PBC	Periodic Boundary Conditions
QM	Quantum Mechanics
SASA	Solvent Accessible Surface Area
SDS	Sodium Dodecyl Sulphate
TEM	Transmission Electron Microscopy
VMD	Visual Molecular Dynamics

Abstract

Nanomaterials produced by molecular self-assembly has become one of the emerging technologies for the development of materials for the food, cosmetic and biotechnology industries. These materials exploit the unique properties of their molecular building blocks, which include natural molecules, such as peptides. Using the entire library of amino acids, consisting of 20 residues that are conserved across all life forms, a range of different materials can be created, such as hydrogels, emulsions, *etc.* However, such materials are normally found serendipitously or by complex molecular design and therefore the development of new systems has been challenging.

In this thesis, a combination of computational and experimental techniques is used to predict, design, synthesize and apply a range of different tripeptides. Using design rules, a subset of tripeptides was chosen to examine their self-assembling ability. It was determined that peptides with cationic amino acids at the N-terminal position (KYF, KYW and KFF) promote the formation of nanofibers and hydrogelation whereas anionic amino acids form bilayer-like assemblies (DFF and FFD). Alteration of the peptides sequence disrupts the formation resulting in loss of ordered nanostructures. Exploiting this self-assembling process can result into different materials such as emulsions. Fibrous tripeptide assemblies have the ability to assemble at the water/oil interface stabilizing emulsions *via* interfacial nanofibrous networks, whereas anionic tripeptide assemblies form surfactant-like emulsifiers. These materials can be tuned to give different emulsion stabilities. The formation of tripeptides can be controlled using enzymatic methods where physiological conditions can be altered to selectively target different tripeptides. Conditions such as pH and temperature control peptide hydrolysis allowing for the retention of highly order peptide nanostructures. The promotion of highly order nanostructures is imperative and the presence of additive such as salts can influence the self-assembling structure formed. Different salts can interact with charged amino acids, which promote crosslinking between peptides creating new tripeptide nanomaterials.

Table of Contents

1.

Introduction

1.1 Motivation for Thesis

The motivation for this research was to develop tools to identify new self-assembling peptides. With the emergence of aromatic peptide amphiphiles capable of self-assembling in nanostructures, it was envisioned that unmodified peptides could arrange in a similar fashion. Understanding the fundamentals of peptide assembly is key to identifying how short peptides can interact. These self-assembled nanostructures can then be exploited to develop soft materials. Developing soft materials such as hydrogels and emulsions is an integral part of this thesis and can lay the foundations for the utilization of such materials throughout a variety of multidisciplinary industries.

1.2 Thesis Overview

This thesis is split into individual chapters with each chapter giving an extensive description of research performed.

Firstly, Chapter 1 reviews the literature of recent research undertaken in the new area of short peptide self-assembly predominantly from the 21st century. Supramolecular interactions are explained and how these interactions are important for the self-assembly process. This then goes on to examine the key aromatic peptide amphiphiles systems and how the discovery of these peptide derivatives led to advances in peptide chemistry but also how these derivatives led to implications for industrial applications. An examination of different unmodified self-assembling peptides is carried out focusing on how these peptides may form a variety of different supramolecular structures upon changing the molecular structure. Finally, an overview of two different computational methods available for the analysis of peptide self-assembly and how the utilization of these methods can be helpful in understanding the fundamental concepts involved.

Chapter 2 introduces the peptide design element of this thesis. Design rules derived from an initial screening measuring the aggregation propensity of all 8,000 tripeptides, were used to select 'interesting' peptides. Seven peptides were chosen

with varying amino acid types and positioning on the peptide chain. A using both a collaboration of computational and experimental analysis, a difference in self-assembling nanostructures is observed. The comparison between both types of design rule with the control peptides, allow for a greater understanding of the assembling process.

Chapter 3 leads onto the applications of self-assembling peptides as tunable emulsifiers. As shown in Chapter 2, different peptides such as KYF, KYW; FFD, etc. have the ability to form different nanostructures. Thus, in Chapter 3, the ability of these peptides to self-assemble and form nanofibrous networks at the interface between water and oil is discussed. The formation of networks at the interface provide a mechanism to stabilize oil droplets, which gives rise to enhanced stability. In addition, other peptides such as FFD and DFF have shown that they assemble in a bilayer fashion, which is indicative of surfactant behavior. The comparison between the two different morphologies of peptides to identify if they have the ability to stabilize emulsions is the focus of this chapter.

Chapter 4 presents methods of controlling the synthesis of tripeptides using enzymatically-catalyzed methods. The use of enzymes such as α-chymotrypsin, have been shown to facilitate the formation of new peptide molecules. Unfortunately, reaction thermodynamics control the degradation of the targeted tripeptides to the more favored dipeptide. Controlling the physiological conditions, the equilibrium of the reverse reaction can change resulting in target synthesis of tripeptides.

Chapter 5 explores how the presence of salts, affect the self-assembling mechanism, thus, altering the forming of nanostructures. Using the tripeptide FFD, an examination of how ions such as calcium and sodium are able to interact with the free charges on the peptide, reducing charge-charge repulsion. A comparative study of the differences between both ions with four different counter ions is discussed.

1.3 Introduction to Peptide Self-Assembly

1.3.1 Self-assembly

Self-assembly is the process by which small monomeric units spontaneously organize into large ordered structures. A great deal of interest in the field of self-assembly has begun to emerge with the ideology that this behavior can be controlled and utilized for a range of different applications. The importance of self-assembly in nature was first explored in 1969 by Kushner,[1] where this behavior was examined in viruses, phages, microtubules *etc*. Not only was it seen in these types of systems, self-assembly was also examined within the human body. The human being would not be able to function without the special molecular recognition that occurs within the body. Biomolecular self-assembly has its foundation in the early 1950s where Linus Pauling[2-3] showed the formation of peptide helices. In addition, the structure of DNA, where the use of the Watson–Crick[4-5] pairing allows for the DNA strands to specifically interact, leading to the formation of doubled stranded DNA. In addition, the area of self-assembly can be expanded to cells, where cell membranes form due to the recognition between lipids, proteins, and peptides. In each case, collections of non-covalent interactions play vital roles in promoting the self-assembling behavior. A deeper understanding of the self-assembling behavior of peptides was examined and keys papers such as Hartgerink *et al*[6] and Reches *et al*[7] published towards the beginning of the millennium show that short peptides and peptide amphiphiles have the ability to self-assemble. These seminal papers preceded a rapid growth of the field and a large increase in the number of publications in the field of peptide self-assembly (Figure 1.1).

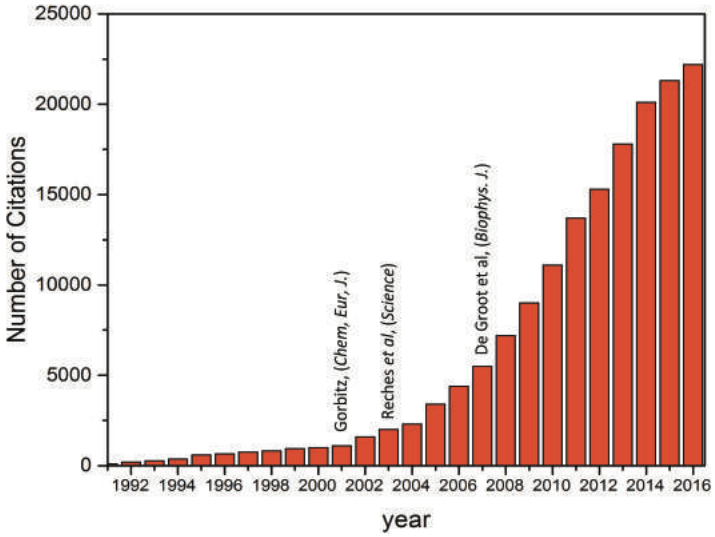

Figure 1.1: Number of citations reported per annum when searching for the term Peptide Self-Assembly with key papers indicated (data retrieved via Web of Science – on 4th April 2017, data from 2017 is not included).

Peptides are captivating molecules as their chemical sequence diversity allows for a range of completely different nanostructures creating different functionality. Their ability to form different supramolecular structures with small changes in chemical structure has begun to emerge as viable approaches for the design, discovery and development of novel nanomaterials. The key to this diverse assembly propensity is the chemical versatility of the amino acid monomers, which govern changes in the self-assembly process. There are 20 gene-encoded amino acids shared across all living species (Figure 1.2), with a variety of functionalities. The amino acid has two parts: the backbone and the side chain. For each amino acid the backbones are identical, with the exception of for L-proline, where the backbone is strained, as the terminal amine is tertiary instead of secondary. The side-chain for each amino acid is different. These side chains can be categorized into interaction types where the dominant effect on the side chain promotes the ability. These categories are: hydrophobic, hydrophilic, aromatic, positively-charge, negatively charged and "special".

1.3.2 Amino Acids

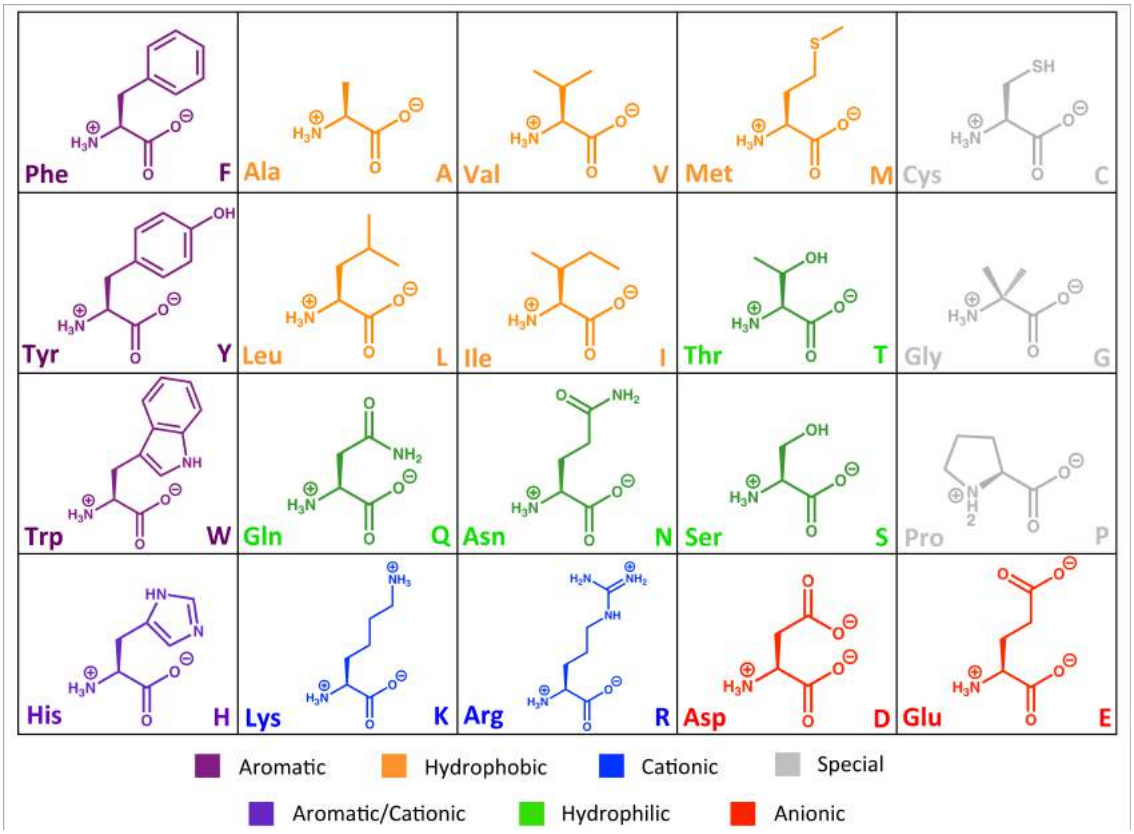

Figure 1.2: The 20 gene-encoded amino acids separated into different categories based on the most dominant interaction from the side chain.

Hydrophobic groups primarily consist of aliphatic side chains (A, V, L, I, M). In this case, no specific interaction results from the side chain, however, with the increase in hydrophobicity, this can result in an increase in hydrophobic effect. A common misconception about the hydrophobic effect is that it is thought that the presence of hydrophobic groups drives the clustering and aggregation of hydrophobic molecules. To some extent this is correct, as without the presence of such groups there would be no aggregation. In reality, however, the hydrophobic effect is driven by the stability of the water structure. Water is a unique molecule that possesses many properties, which do not follow the trends for similar molecules such as boiling point, freezing point, phase transition, surface tension, etc. The hydrogen-bonded structure of water is extremely stable and therefore the presence of hydrophobic groups that disturb this network introduces an enthalpic

energy penalty. Therefore, water aggregation of these hydrophobic groups to minimize the observed enthalpic penalty.

Aromatic residues (F, Y, W) have similar interactions to that of hydrophobic amino acids where the hydrophobic effect plays a pivotal role in the aggregation of such molecules. In addition, the presence of the delocalized π-system creates areas of increased electron density, which can result in induced dipoles. For example, π-systems can interact with each other in several different conformations resulting in alignment of these planar rings allowing for optimum induced dipole – induced dipole interactions.

Hydrophilic amino acids consist of groups that contain polar side groups such as amines or alcohols (S, T, Q, N). In this case, the side chains have the ability to interact with water molecules *via* hydrogen bonds. Although there is some disruption to the stable structure of water, the effects are reduced.

Charged amino acids (K, R, D and E) have groups on the side chains where the loss or gain of a proton can occur. These side groups can be separated into cationic, lysine and arginine, and also anionic, aspartic acid and glutamic acid. Cationic peptides consist of terminal amine groups, which have the ability to pick up an extra proton, creating a net positive charge. Anionic groups have carboxylic acid termini side chains and therefore the loss of a proton is achieved with ease. Due to susceptibility for charged groups to change their ionization state, the choice of pH promotes the presence of electrostatic interactions. pK_a values of K, R, D and E are 10.5, 12.4, 3.9 and 4.1 respectively.[8] Therefore at pH 7, cationic amino acids have protonated side chains whereas the anionic amino acids have their side chains deprotonated. This introduces the electrostatic interaction between side chains creating salt-bridges, however, the converse is also apparent where repulsion between similar groups can occur. In addition, choice of solvent can affect the charged group to interact with another charged species. Solvent affects the polarisabilty of the amino acids, therefore the dielectric controls the effective range electrostatic interactions are able to have. In addition, similar observations can be made, where the amino acids end up in and environment where the

ionization can be suppressed or enhanced due to the chemical nature of surrounding moieties.

Histidine has properties that fit into both the aromatic and the basic categories. Histidine has a side chain of an imidazole ring, which promotes aromatic-aromatic interactions allowing for the formation of stacked structures. In addition, upon changing pH, the protonation state of the nitrogen within the imidazole ring changes. Below pH 6.0 the second nitrogen becomes protonated and therefore the ring becomes positively charged, a process, which affects the potential stacking of these residues. Furthermore, the histidine residue is most commonly involved as part of a catalytic triad for enzymatic reaction due to the stabilization of charges which will be discuss in more detail in Chapter 4.

Special amino acids (C, P and G) have different side chains, which cannot be categorized with others due to the structure, types of atom and flexibility:

The first example of a special amino acid is cysteine. Cysteine has a terminal thiol group, which has the ability to be involved in enzymatic reactions acting as the nucleophile. In addition, the thiol side chain is susceptible to oxidations. As a result, the formation of disulphide bridges occurs. This is a covalent bonded unit joining up two-cysteine groups forming a disulphide bridge. These additional interactions are normally found in large proteins and play an important structural role for these proteins. [8]

Proline is the only amino acid that has a secondary amine as the amino groups is incorporated into the side chain of the amino acid. The distinctive cyclic structure of proline give the amino acid enhanced rigidity therefore it is classed as a structure disrupter especially in β-sheet and α-helical structures.[8] In proteins, secondary structures are dependent on the torsion angles along the backbone allowing for the conformational change to create the helix or sheet. Within proline the φ angle is locked at approximately -65°, and therefore disrupts the formation of secondary structures.

Finally, glycine is the most simplistic of all the 20 amino acids. The side chain on glycine consists of a solitary hydrogen atom making it the only amino acid that is not chiral. Thus glycine does not possess the ability to have intermolecular interactions with other amino acids apart from the backbone. In addition, the presence of a smaller side chain results in an increase in flexibility of the backbone creating a less rigid structure.

1.3.3 Supramolecular Assembly

Spontaneous supramolecular assembly is based on the formation of interactions that result in a decrease in the Gibbs' free energy (ΔG). In this case the main energetic contributions associated are: enthalpy (H) and entropy (S). The creation of stable interactions gives a favorable decrease to the enthalpic term ($\Delta H < 0$) where entropically, the formation of ordered nanostructures is unfavorable ($\Delta S < 0$).

$$\Delta G = \Delta H - T\Delta S \qquad \text{Equation 1.1}$$

A number of different interactions are vital for peptides to assemble into supramolecular nanostructures. Requirements for the formation of different nanostructures differ in the chemical make up of each system. The energetic benefits are greatly enhanced, which is why self-assembling systems are enthalpically driven to overcome the entropic penalties. Examples to these interactions included hydrogen bonding, electrostatic, van der Waals, and π-stacking. Each of these interactions have different energy outputs and are all important for the ability of a molecule to self-assemble. However, there is also a significant entropic contribution from freeing water molecules from solvation shells. Water molecules are released from the solvation structure around hydrophobic moieties, resulting in entropic gain.

Hydrogen Bonds

Hydrogen bonding occurs when a hydrogen bond donor, for example –OH/-NH, can interact with a hydrogen bond acceptor, C=O.[9] Hydrogen bonding mostly arises from the electrostatics, due to the partial charges on the atoms.[10] In addition,

approximately 10% of hydrogen bonding can be classified as covalent nature.[11-12] This has a directional implication as the lone pair of electrons present on the hydrogen bond acceptor can interact with the σ* orbital from the C-H. At 180° there is a good overlap between these orbital and therefore there is a covalent nature associated with the hydrogen bond. Digressing away from 180° the overlap becomes weaker, and therefore less of a covalent nature is observed, which results in a weaker hydrogen bond[13]. As a result, enthalpic energy gain from this interaction means that the strength of a hydrogen bond is distance and angle dependent. For systems where there is a greater covalent nature, the energy gain can be up to 120 kJ mol^{-1}.[14] This energy decreases to approximately 12 kJ mol^{-1} for hydrogen bonding dominated by electrostatics; varying the hydrogen-bonding angle and distance can have a dramatic effect on the stabilization *via* hydrogen bonding. Types of secondary structures resulting from hydrogen bonding include β-sheet, α-helix, and polyproline III helix. For β-sheet formation, the hydrogen bond distance is slightly decreased to an approximately 1.8 Å, allowing for a much stronger covalent overlap. The angle of the hydrogen bond differs depending on the orientation of the hydrogen bond on whether the overall peptide structure is arranged parallel (*i.e.* N→C in neighboring strands), which will have an offset angle, or antiparallel (*i.e.* alternating N→C and C→N in neighboring strands), in which the angle will be close to 180° (Figure 1.3). These conformations are based on the hydrogen bond interactions between adjacent peptide/protein backbones where the amide linkages provide both the donor and acceptor moieties for the formation of these structures.

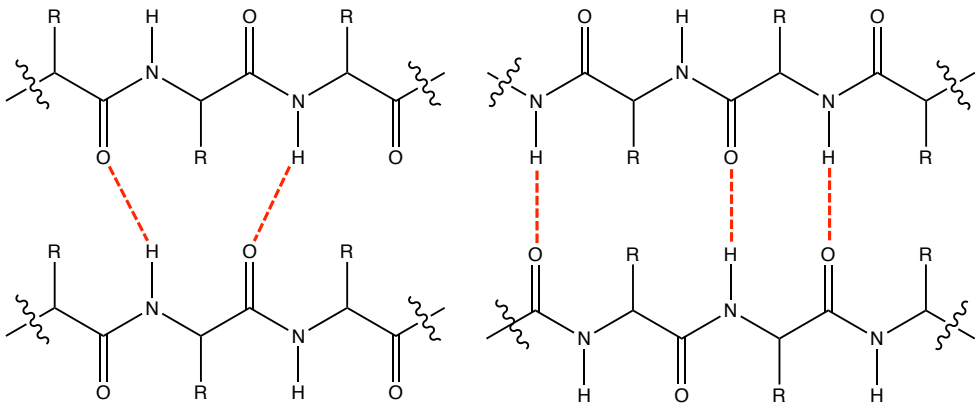

Figure 1.3: Hydrogen bonding observed from the backbone of peptide in the parallel and antiparallel arrangements

Secondly, α-helix is a secondary structure that is present with protein folding which can be extrapolated for peptide self-assembly (Figure 1.4). For this type of structure to occur the dihedral angles of φ and ψ are 60° and 45° respectively.[15] Each amino acid is hydrogen bonded with the amino acid that is four positions along in the chain with the hydrogen bonds parallel to the helical axis. [16]

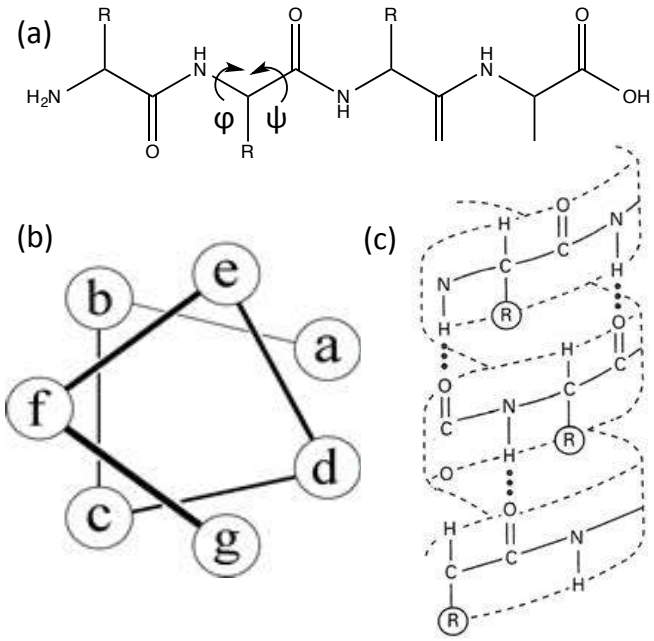

Figure 1.4: Formation of α helix indicating the observed hydrogen bonds and twisting

π-π stacking

As previously stated, there are four residues (F, W, Y, and H) that are capable of forming π-π interactions. The π-conjugated ring system that is apparent within the each of the three amino acids residues create delocalized regions of high electron density and low electron density. These regions of charge can interact allowing aromatic rings to be situated closer together. There are 4 different types of orientation that aromatic rings can adopt, parallel stacked, parallel displaced, T-shaped and edge-on-edge. (Figure 1.5)[17]

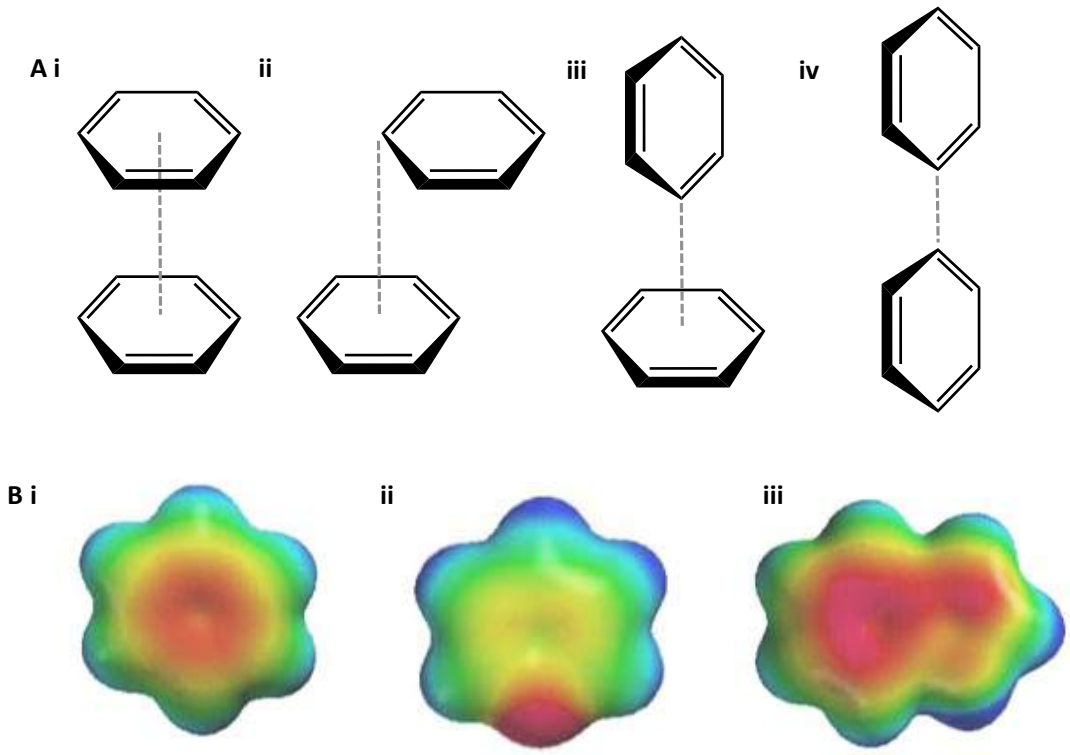

Figure 1.5: Different orientations of π-stacking i) parallel stacked ii) displaced parallel stacked iii) T-shaped iv) edge-on-edge. B) Electron density surfaces of i) phenylalanine, ii) tyrosine, and iii) tryptophan side chains

The stability of each arrangement is based on the interaction of the electron cloud between the aromatic rings.[18] Parallel-stacked conformations are repulsive between the two rings residues. The high-density electron clouds between the aromatic rings overlap, forcing them to separate from each other. A similar observation is made with the edge-on-edge conformation where the localized areas of low electron density repel the rings.[19] On the other hand, the displaced parallel stacked conformation is shown to be the more stable out of the available orientations, as the positively charge edges of each ring can interact with the negatively charged core. Finally T-shaped stacking of aromatic rings can occur with the interaction between the electrostatic potential of the outer edge of the rings and the high-density electron cloud within the center of the corresponding ring.[19] The separation of the adjacent π-systems are approximately 3.5 Å and the addition of π-π stacking can contribute approximately 0-50 kJ mol^{-1} [14] to the enthalpic term depending on the type of π-system that is interacting.

Van der Waal Interactions

Van der Waals forces are weak interactions that occur due to the close proximity of the electron clouds of neighboring atoms. The polarization due to the two dipoles formed by the small variation on the electrons creates and transient electric dipole. The dipoles are weakly attracted to each other; however, the electron clouds start to repel as the nuclei become close.[20] Interactions can be divided into attractive interactions, called London dispersion forces, and the repulsive term.[20] The attractive term arises from the fluctuating multipoles of adjacent molecules, which are more dominant at longer distances. The repulsive forces are more established at shorter distances. These forces can give an approximate energy of 2-5 kJ mol^{-1}.[14]

Charge-Charge Interactions

Electrostatic interactions are among the strongest non-bonding interactions that occur within supramolecular self-assembly. These interactions can contribute approximately 200 kJ mol^{-1} to the enthalpic energy term.[14] The interactions themselves are based on the Coulombic interactions where the charge on each atom (q_i, q_j) and the distance between them (r_{ij}) is taken into account to determine the strength of the interaction. Charges can be screened due to solvent effects (ε).

$$F = \frac{q_i q_j}{4\pi\varepsilon r_{ij}} \qquad \text{Equation 1.2}$$

The Coulombic Law states that as the distance between the charges decrease the force will increase. For amino acids, the Coulombic law is important as peptides can alter their charged states according to the pH of the surrounding media. pK_a values for the charge groups indicate the ionized state of the peptides. At lower pH values, 1-3, carboxylates groups will become protonated and therefore will lose their negative charge. The opposite is apparent at higher pH, 9-14, where the free amines will become deprotonated and will therefore lose their positive charge.[21] This indicates that at neutral pH, where both the free amine and carboxylate will be at their ionized state, charge-charge interactions are feasible. The formation of salt bridges within peptides can be a major driving force for the promotion of self-

assembled structures due to the energy gain observed with the ion pair.[22] As previously stated, the ionization of the side chains is influenced by the solvent. In addition, upon self-assembled structure then ionized groups can alter their environment, which can affect the ionized state of the molecules, which can give rise to different types of interactions. This occurs due to the shifts in apparent pK_a values as a result of the changes in the environment.[23]

Hydrophobic Effect

The hydrophobic effect is one of the most misunderstood supramolecular self-organization processes. Often mistaken as a force, the hydrophobic effect is dependent on the structure of polar solvents; particularly water, rather than the interaction between the hydrophobic groups themselves. This process is observed in the immiscibility of oil and water where the completely separate phases are formed.[14, 16, 24-25] The hydrogen-bonding network that water possesses allows for a strong attraction between each of the water molecules resulting in the observed accumulation of hydrophobic groups as they are pushed together (Figure 1.6). This process may suggest that hydrophobic groups drive the organization, and to some extent, these hydrophobic groups do interact *via* Van der Waals and (in the case of aromatic residues) π-stacking, however, it is the strong interaction between the water molecules that is the major driving force that leads to the hydrophobic collapse.

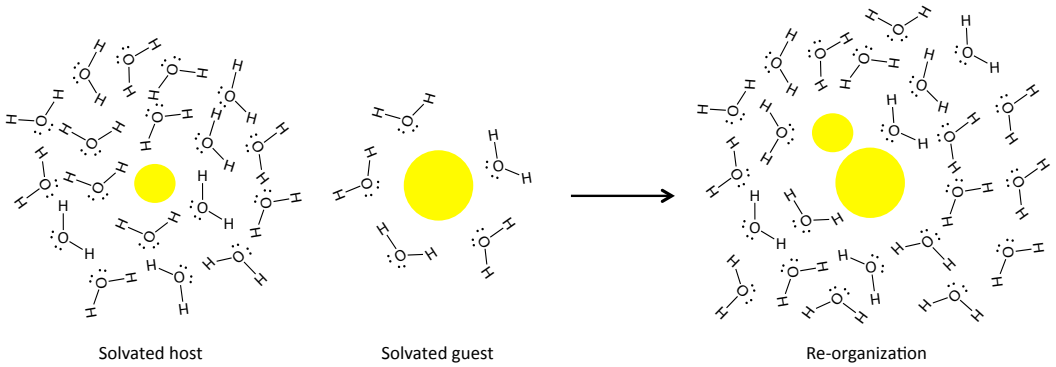

Figure 1.6: Agglomeration of two hydrophobic groups and the stabilization observed by the hydrophobic effect.

Within the field of self-assembly, the hydrophobic effect is one of the main driving forces for the formation of self-assembled nanostructures, and it is this process that gives rise to the formation of fibers and fibrous networks observed in

hydrogels. As with all areas in self-assembly the energetic output must be favorable, as such, the two main contributions to the energy are enthalpy and entropy. The enthalpic contribution to the system comes from the stabilization of the water molecules. The reorganization of the water in order to maximize the number of hydrogen bonding interactions is the greatest contribution, although any interactions the hydrophobic groups can partake in with other hydrophobic groups is an added bonus. However, with the formation of a "cavity" where the hydrophobic groups reside, there are sacrificial water molecules that are unable to interact fully with other water molecules and are therefore high in energy. Entropic contributions due to the hydrophobic effect result in both favorable and unfavorable interactions. As the self-assembly process result in the ordering on molecules, the entropic term (ΔS) becomes more negative. As a consequence, the Gibbs free energy (ΔG) within the system increases (See Equation 1.1). However, the reorganization of the peptide molecules frees water molecules into the bulk solvent phase, which results in an entropic gain – more stable.[26-28]

1.4 Short Self-Assembling Peptides

1.4.1 Aromatic Peptide Amphiphiles

The conjugation of aromatic substituents at the N-terminal amine position on the peptide chain has been shown to enhance the self-assembling behavior of peptides. The development of modified peptide amphiphiles have become of great importance within the past 30 years giving rise to a number of applications. These large aromatic groups that are typically used provide order and directionality for the formation of fibrillar nanostructures. Aromatic peptide amphiphiles were first explored in the mid 90s when Vegners *et al*,[29] examined the self-assembly behavior of fluorenylmethoxycarbonyl (Fmoc) substituted dipeptides. Aromatic peptides such as Fmoc-LD, Fmoc-AD, and Fmoc-ID were found to self-assemble into fibrullar nanostructures resulting in the formation of hydrogels. A decade later the self-assembling work carried out by Xu and co workers[30-31] rediscovered this concept and demonstrated new types of Fmoc-dipeptide hydrogelators where the hydrogels responded to biological ligand receptors. Simultaneously, work carried out by Gazit and others demonstrated the role of aromatic groups on the side chains for the formation of large aggregates *via* the reductionist approach for understanding the aggregation of polypeptides in the formation β-amyloid plaques. It was discovered that the central motif within the β-amyloid peptide was the diphenylalanine dipeptide. It was this key short peptide that led the way for the understanding of short peptides, which will be discussed in greater detail in Section 1.5.

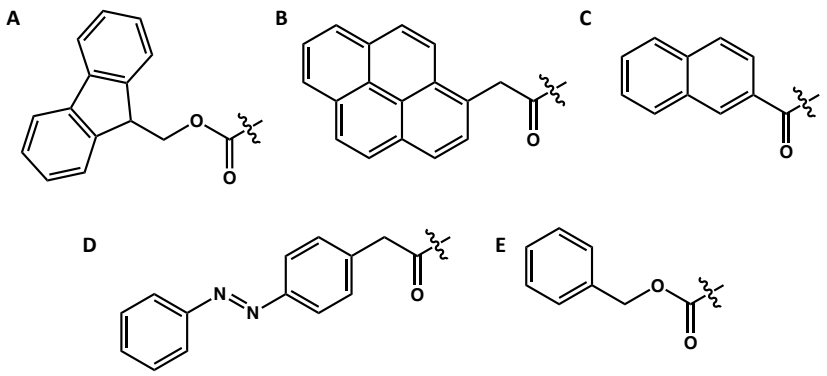

Figure 1.7: Different types of aromatic moieties reported to promote self-assembly[32]. A) Fmoc B) Pyrene C) Naphthalene D) Azobenzene and E) Phenyl.

Since 2006, the field of aromatic peptide self-assembly has rapidly increased and as a result a number of new self-assembling peptides have been discovered. This was driven in large part by the recognition that moieties such as Fmoc could be used to promote the self-assemble of peptide sequences.[32] In addition, aromatic groups such as napthalene, pyrene, phenyl and azobenzene, (Figure 1.7) have all been used in a similar fashion. [33-48]

An excellent review from Fleming and Ulijn[32] gives an overview on the diverse moieties that can be utilized as aromatic capping ligands. In addition this review summarises the observation that small modifications in chemical structure can give rise to a number of different types of supramolecular structures, which illustrates the versatility of these systems. Additional modifications can be introduced in the linker section that attaches the aromatic moiety to the N-terminus. It has been widely seen that slight modifications to this linker can dramatically affect the packing of the peptide molecules.[49-52] These linkers such as methoxy, carbonyl and carbamate linkers can all affect the self-assembly process. Fortuitously, for self-assembled systems containing Fmoc, the carbamate was shown to assist in the self-assembly process. Slight modification of the aromatic group, linker, amino acid or C-terminal groups can result in different packing arrangements of the peptides. Aromatic peptide amphiphiles tend to assemble in a β-sheet conformation, either in the parallel or anti-parallel arrangement. As a result, this can give rise to a number of supramolecular nanostructure from fibrils, tape, tubes, worms etc. each with their own unique properties. (Figure 1.8)

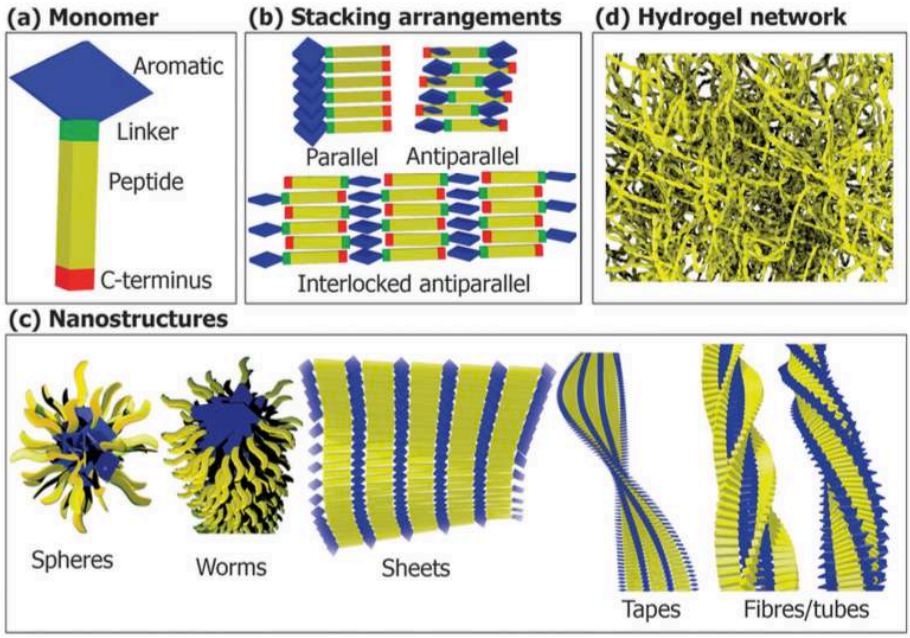

Figure 1.8: Overview of aromatic peptide self-assembly. A) Monomeric aromatic peptide amphiphile b) different arrangements of the self-assembled peptide C) observed supramolecular structures from peptide self-assembly D) Nanofibrous network. Reproduced from Ref. 32 with permission from The Royal Society of Chemistry.

Although there are many advantages and potential applications of aromatic peptide amphiphiles, issues can arise when certain industries such as the drug, food, or cosmetic industries utilize this type of technology. Large aromatic groups, such as Fmoc, may introduce a risk of toxicity due to their ability to intercalate with DNA.[53-54] This intercalation can interfere with the overall structure of the DNA resulting in mutations. Therefore, the introduction of unprotected peptide gelators (i.e., systems that contain only peptidic components) would provide similar properties of the aromatic gelators with a significantly decreased risk of toxicity.

1.4.2 Discovery of Diphenylalanine

The development of insoluble fibrils due to the aggregation of polypeptide chains (*ca.* 30 – 40 amino acids in length) results in the formation of Amyloid.[55] These amyloid fibrils arise due to the inappropriate folding of sequences within the polypeptide chain.[56-57] Amyloid fibrils are naturally occurring nano-fibrils (Figure 1.9) that are the main cause of a number of human diseases, that include Alzheimer's, Parkinson's and diabetes.[58-59] There are approximately 20 diseases that are known to be associated with amyloid.[55]

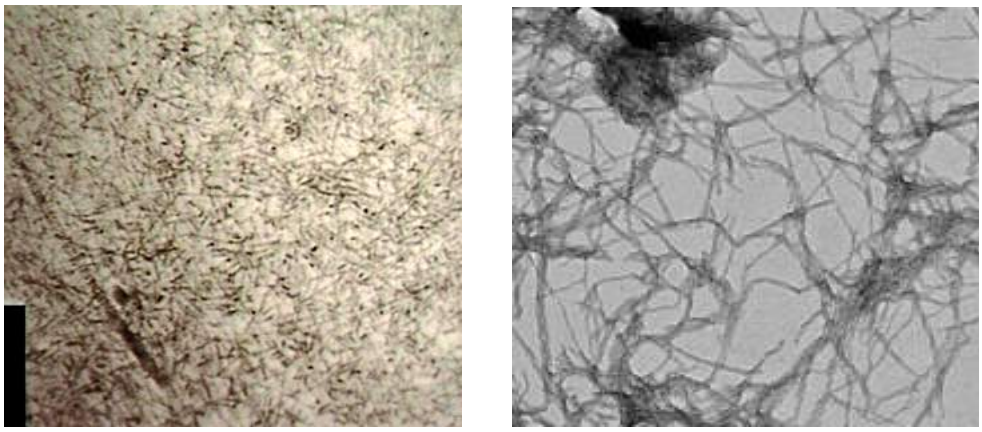

Figure 1.9: Amyloid formation into fibrils (Image taken from Ref. 39)

At the core of this polypeptide, resides the short sequence KLVFF. Tjernberg *et al*[60] showed the importance of KLVFF in its ability to control the formation of the fibrils. It was determined that KLVFF was central to the aggregation of the polypeptide, furthermore, the importance of the residues were confirmed upon mutation of the KLVFF peptide. This resulted in the inhibition of the fibril formation by substituting each amino acid separately with alanine and measuring the binding to the β-amyloid peptide. Here, Tjernberg shows the importance of the VFF fragment[61] within the peptide in the binding to β-amyloid as the binding was reduced when VFF was substituted with the alanine controls. The development of this research was accelerated by Ehud Gazit who, using the reductionist approach, uncovered the key motif diphenylalanine, which was central to the peptide ability to form aggregates[7]. Work published in *Science* in 2003 by Gazit and Reches showed developments in the self-assembly of the core dipeptide, diphenyalanine (FF). FF was solubilized using pure 1,1,1,3,3,3-hexafluoro-2-propanol (HFIP) and displayed instantaneous self-assembly, upon dilution with water, into ordered nanotubes. Discovery of these nanotubes was utilized to show the ability to cast metal nanowires. The inner cavity of the nanotubes promotes the reduction of silver ions to metallic silver within the nanotubes, which after enzymatic degradation resulted in the production of discrete silver nanowires. Since 2003, developments of new self-assembled peptides have started to become apparent, resulting in a large increase in publications within the field (see Figure 1.1)

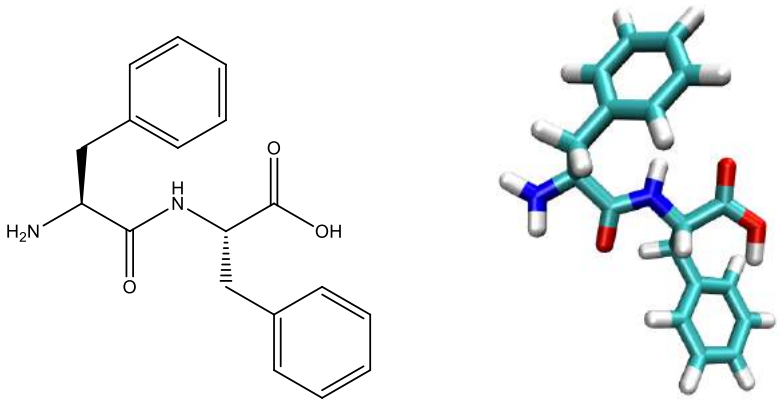

Figure 1.10: 2D and 3D representation of diphenylalanine.

Independently from Gazit, in 2001, Carl Gorbitz used crystal structures of LL, LF, FL and FF to characterize these dipeptides to understand the self-assembling nature of FF[62-63]. It was shown through the characterization of different solvates from alcohols that FF was able to self-assemble into nanotubes. (Figure 1.11) Furthermore, on comparison with structures formed from FF and LL, Gorbitz was able to demonstrate that the interactions between side chains were also crucial in determining the resulting nanostructure and therefore the formation of the nanostructures was not fully dependent on the hydrophobicity of the peptides.

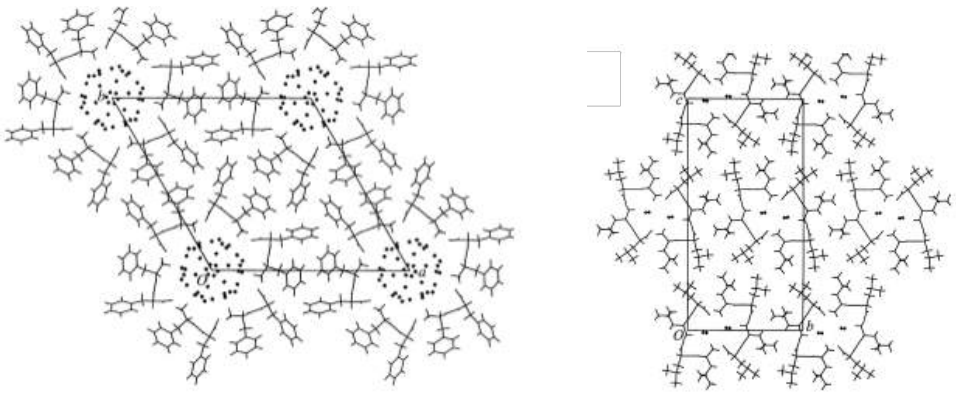

Figure 1.11: Crystal structures of diphenylalanine and dileucine showing the channel forming tubes upon assembling. Unit cell of the crystal structure is highlighted. Figure taken directly from publication Figure adapted from Ref. 62 by permission of John Wiley & Sons, Inc. Copyright 2000 by John Wiley & Sons, Inc.

The presence of phenylalanine resulted in a greater packing of the molecules, which resulted in cylindrical channels through the crystal. Comparison with the crystals obtained from leucine, indicated that these channels were less organized

resulting in a greater number of channels, with less water based within. This gave the first inclination that the presence of phenylalanine in short peptides introduces another stabilizing interaction. It was observed that a large clustering of water molecules is apparent within the channels formed upon self-assembly. This indicates the importance of the hydrophobic effect, but in addition, the greater size and organized structure observed for FF shows that π-stacking also has an influence on the self-assembling nature of these nanostructures.

To gain a greater insight into what supramolecular interactions have a significant factor in the peptides ability to form supramolecular nanostructures, modifications to the FF backbone was examined. Reported by Gazit and Reches,[64] examination of the electrostatic capabilities of FF upon self-assembly by blocking the charged termini indicates how the electrostatic contribution of peptide can affect the conformational and also the spatial aspects of the self-assembled structure. In this case, in addition to the zwitterionic form previous explored, FF analogues Ac-FF-NH_2, and H-FF-NH_2, were examined. In both cases, the formation of nanotubes was detected, which indicates that the formation of the nanotubes is not predominantly driven by the potential electrostatic interactions. Differences between the examined systems were changes in the directionality of the nanotubes. Non-charged analogue of the FF nanostructure was non-orientated, where, on comparison with the positively charge analogue, unidirectional well-aligned tubular structures were formed. Therefore, for the case of FF, electrostatic interactions are not important for the formation of nanotubes, but these interactions do participate in the directionality of the nanotubes and control the alignment of the nanostructures.

Finally, the success of FF resulted in a number of attempts to modify the residue of the peptide structure to examine new functionality and structure. Further work by Reches and Gazit examined the behavior of diphenylglycine[65-66], where the β-carbon atoms have been removed. The removal of these atoms result in reduced flexibility of the phenyl rings (Figure 1.12). As a result, the side chains become more rigid and are unable to rotate thus prohibiting the phenyl rings to π-stacking.

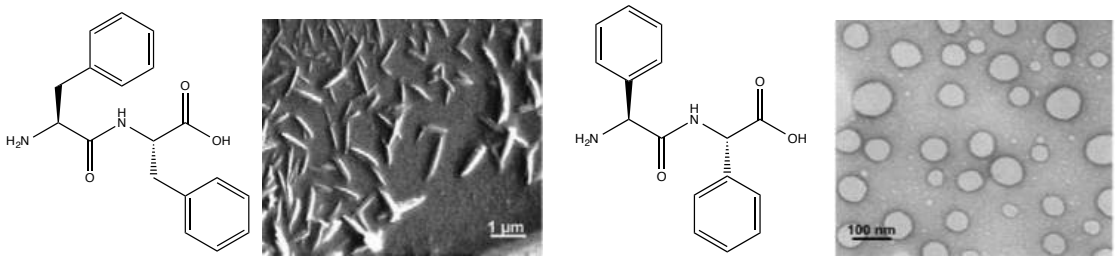

Figure 1.12: Structure of Diphenylalanine and Diphenylglycine with their associated TEM images indicating the nanoscale structures that are formed. Adapted with permission from Reches, M. Gazit, E. (2004), *Nano. Lett.* Copyright (2004) American Chemical Society

Diphenylglycine was visualized *via* TEM imaging where the formation of nanospheres instead of nanotubes was detected.

1.4.3 Short Self-Assembling Peptides

The discovery of the self-assembling ability of FF initiated the beginning of the development of short peptide based nanomaterials.[67] The diversity of amino acids, allows for manipulation of the peptide sequence allowing for the development of new nanostructures. De Groot *et al*.,[68] altered the dipeptide sequence of FF, where, substitution of the a single phenylalanine residue with isoleucine (Ile-Phe, IF) and valine (Val-Phe, VF) gave different structural affects even though the difference is a single methyl group. VF does not show formation of assembled structures, whereas IF demonstrates self-assembling behavior – the formation of fibrils entangled to form self-supporting hydrogels (Figure 1.13). These fibrillar structures show similar dimensions to those of the self-assembling FF, although it was the first reported case for a dipeptide having hydrogelation capabilities. Examining the supramolecular assembly on a molecular level, the use of FTIR data showed the presence of a shift in the typical carboxylate group to a lower wavenumber, ca. 1570 cm^{-1}, suggesting a head-to-tail electrostatic interaction between the terminal groups. On examining the amide I region, differences were observed between the wet and dry samples. No peaks were observed in the wet sample. This is potentially due to the weak interactions that are forming within the wet samples and the destructive nature of this method disrupts the interactions. Within the dried sample the peptides are 'locked' in their assembled state. Dried samples

show peaks at 1618 and 1678 cm^{-1} indicating the presence well-ordered hydrogen-bonded structures.

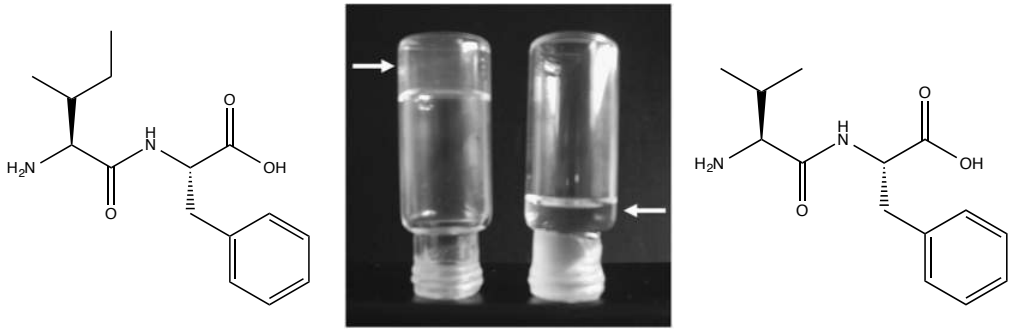

Figure 1.13: Representation of hydrogel forming IF compared with non-hydrogel forming VF. Adapted from De Groot *et al*, *Biophys. J.*, 2007, *92*, 1732-1742. Copyright (2007) with permission from Elsevier.

Using the Whimley-White scale[69-70] as reference, the hydrophobicity of isoleucine is greater than that of valine. This suggests that the hydrophobic effect has an important role in the formation of nanostructures. The presence of more hydrophobic groups intensifies the aggregation of the peptides. However, the ordering of the peptides, which created the nanostructures, is due to the supramolecular interactions.

The effects of peptide chain length can have an effect of the self-assembling properties of each peptide. The addition of another amino acid to form tripeptides introduces more supramolecular interactions, with another hydrogen bonding segment on the backbone to the side chain interactions. These effects were explicitly seen with the addition of cysteine to the N-terminal position of diphenyalanine.[71-72] The effect of introducing this additional amino acid changes the resulting structure from nanotubes to nanospheres, indicating the disruptive effect that alteration of the peptide sequence can have.

Work by Tamamis *et al.*[73] has developed this area by comparing between the self-assembly of FF and the addition of a third phenylalanine group to give FFF (Figure 1.14). The addition of the third amino acid will introduce another possible aromatic interaction. It was identified that the addition of another phenylalanine caused the self-assembly of plate-like structures.

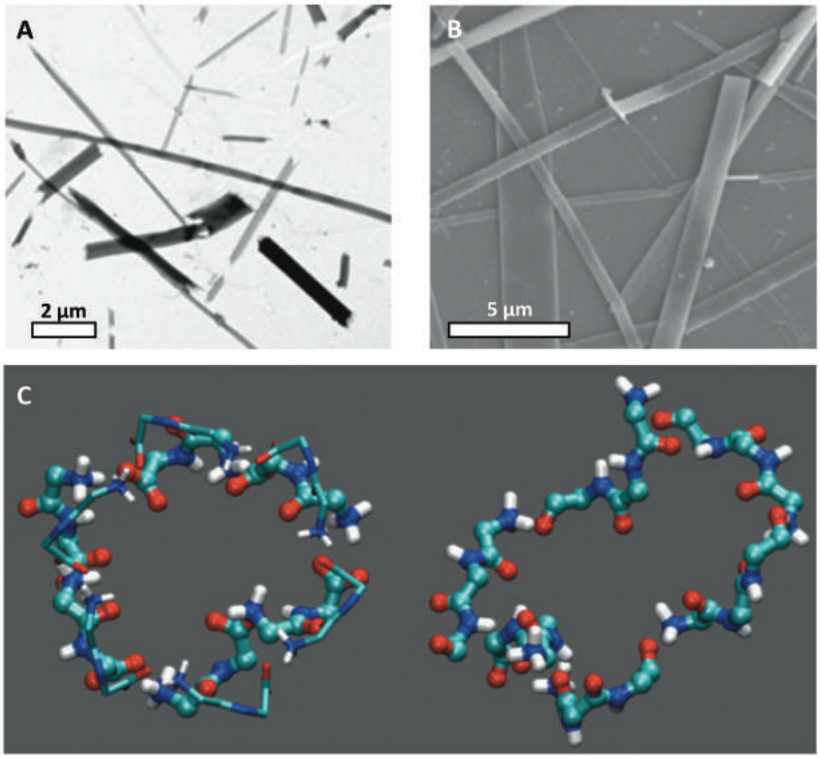

Figure 1.14: A) TEM of FFF nanostructures B) SEM of FFF nanostructures C) Representation of FF (*left*) and FFF (*right*) assemblies after molecular dynamics simulations showing the changes in structure that arise from the presence of another amino acid on the backbone.. Adapted from Tamamis *et al*, *Biophys. J.*, 2009, 96, 5020-5029, Copyright (2009) with permission from Elsevier

Conformational differences between nanotubes (FF) to plates (FFF) are related to the difference in strength involved with the electrostatic interactions between the peptides, the increase in hydrogen bonding sites and also the stacking interactions between adjacent structures.[73] The shorter chain length of FF, allows more turns in the nanostructures to optimize the stabilizing interactions, resulting in the tubular structure. In order to optimize these interactions in FFF, there is an elongation of the nanostructure. The additional hydrogen bonding in FFF stabilizes the self-assembled structure further, thus, FFF is more stable than FF. The orientation of the phenyl rings situated on the outer face of the structure allows for stacking between neighboring structures, resulting in the cluster nanostructures, observed by Reches *et al*.[7] these observations are in line with the crystal structures shown by Gorbitz,[62] where the stacking of the peptides and location of the phenyl rings are determined. In addition, spectroscopic measurements have shown the formation of β-sheets. FTIR shows similar observations to what is seen with FF, in that a sharp peak around 1630cm^{-1} is consistent with sheet-like formation and the

Thioflavin T staining assay, which binds to β-sheet structures giving an enhancement of the fluorescence.

Increasing this chain length to tetra- and pentaphenylalanine, give rise to similar observations as seen with FFF. Issues arise with extending this chain length as the solubility of the sample become less, therefore the addition of various solvents are carried out to solubilize the sample. Minimal amounts of glacial acetic acid were shown to improve the solubility of the FFFF and FFFFF so that analysis of these samples could be made possible.[74] Microscopy images of these samples show bundling of fibrils, which demonstrate that the π-stacking of the phenyl rings cause the fibers to assemble into the ordered clusters. FTIR measurements of these structures show a single peak at 1630 cm^{-1}, which is indicates the formation of β-sheets. More interestingly, it has been reported that the change of temperature can alter the morphology of the structures. It was observed that at lower temperatures shorter and thinner structures are formed. Furthermore, FFFFFF (F_6) was enzymatically and chemically synthesized as part of work carried out by Pappas *et al,*[75] where in this work they created a dynamic combinatorial library while monitoring the constant condensation and hydrolysis of unprotected dipeptides in the presence of thermolysin (Figure 1.15). This gave rise to the fibrous structure of F_6, in addition, structures of L_6 (fibers), W_4 (micelles/fibers) and F_2L_2 (block-like fibers) were observed. These morphological changes are accompanied by spectroscopic differences. For F_6, dramatic shifts in FTIR peaks observed at 1674 to 1625 cm^{-1} indicate strong intermolecular hydrogen bonding between the backbone amides, while the reduction in intensity of the carboxylate peak at 1580cm^{-1} suggest suppression of the carboxylate group. This indicates the C-terminus becomes trapped in the self-assembled hydrophobic structure.[75] The formation of L_6 shows the transformation from L_2 to L_6 where FTIR indicates the formation of ordered hydrogen bonding interactions. In addition, this is seen macroscopically, with the system transforming from an opaque free flowing solution to a self-supporting hydrogel. The formation of spherical aggregates observed with W_4, are supported with FTIR indicating the disruption of hydrogen bonding interactions. Although, an intense peak is observed at 1580 cm^{-1}, indicating the ionized state of the C-terminus, there is a clear suppression of the

peaks within the amide I region showing the disruption of ordered hydrogen-bonding interactions.

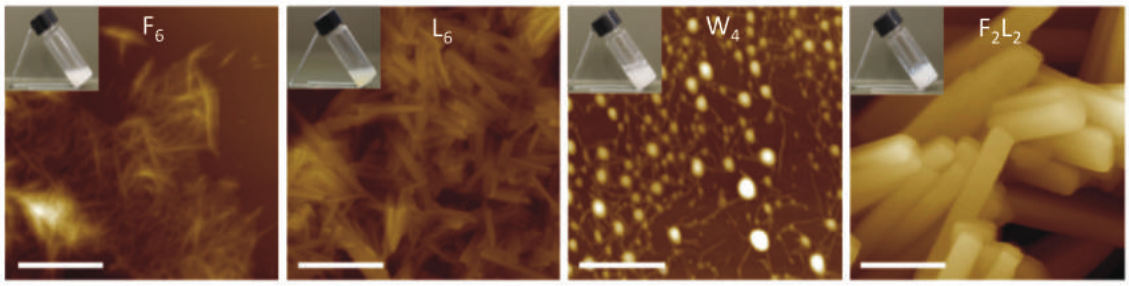

Figure 1.15: AFM images of the dynamic combinatorial library peptides F_6, L_6, W_4 and F_2L_2 and there macroscopic image. Adapted with permission from Macmillan Publishers Ltd: (Nature Nanotechnology) Ref. 75, copyright (2016)

Subtle changes in the amino acids on the peptide chain, such as chirality, affect the ability to self-assemble. Work by Marchesan et al.[76-80] has shown that, although chirality effects have an important role, positioning of the D-amino acid can have an influence on the self-assembled structure of the peptide. In this work, the focus again was on the key section within the β-amyloid fibril: KLVFF. Using the main characteristics of this sequence, it has been shown that VFF and FFV can have different physical effects such as sol-to gel-transition depending on the chirality of some of the amino acids. It has been shown that the L-tripeptide sequence VFF does not lead to formation of distinct self-assembled structures. The most dramatic change observed was when the chirality of the amino acid at the N-terminus was altered. FTIR showed that the N-H amide I region had shifted to lower frequencies, indicated by the presence of the peaks at 1637 cm^{-1} and the broad peak at 1680-1690 cm^{-1}, suggesting that the presence of ordered β-sheets for ^{D}VFF whereas no shift is observed for VFF. When the same process was carried out on ^{D}FFV, where the chirality of the N-terminus amino acid (in this case F) was again changed, similar changes, compared with ^{D}VFF, were seen. Another specific interaction that is observed through these modifications is the formation of electrostatic interactions. Similar to the observations for hydrogen bonding, a shift in the carboxylate stretching frequency (~1595 cm^{-1}) to lower wavenumbers (1570 cm^{-1}) is observed, indicating the presence of the head to tail salt bridge interaction. FTIR has not been the only way of observing the changes in structure. Visual

inspection has shown that the sample with the D-amino acids found at the N-terminus hydrogelate, which was the first time this type of self-assembly has been reported for non-protected tripeptides. The continuation of this work has shown the formation of structures with LFF (Figure 1.16). Similar to VFF and FFV the changing of the chirality of the amino acid at the N-terminus to the more unnatural D-amino acid induces the formation of structures and gelation.

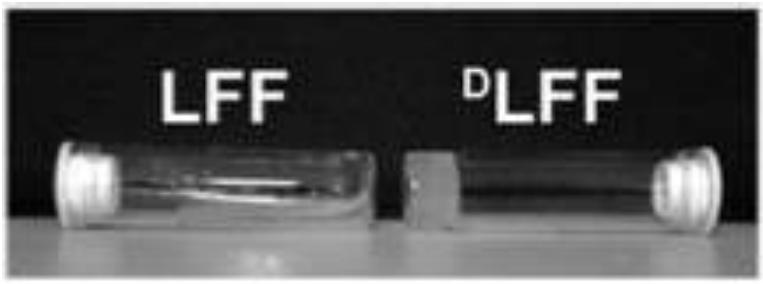

Figure 1.16: Macroscopic image of LFF and DLFF highlighting the importance of chirality on the amino acid with the formation of a hydrogel found in the D- form of the amino acid. Adapted from Ref. 76, with permission from the Royal Society of Chemistry.

Molecular modeling has provided some explanation as to the molecular origin of the differences between LFF and DLFF. The effect of a 'phenylalanine zipper' (Figure 1.17) results from an extra interaction that comes into effect with the DLFF.

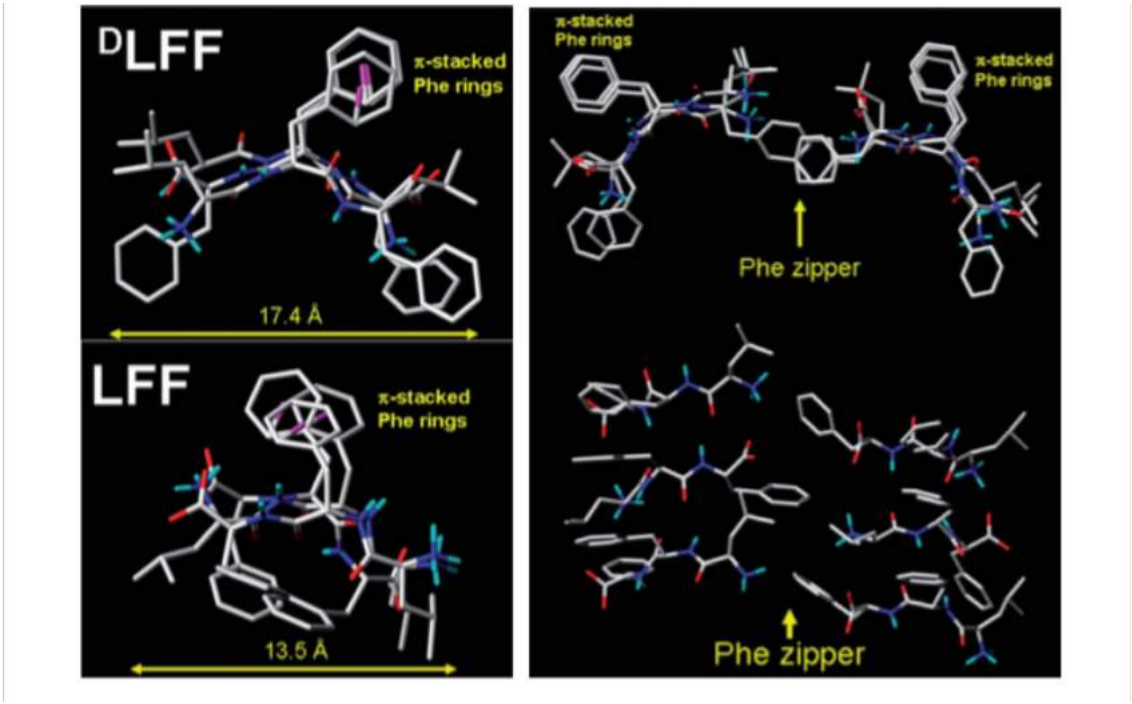

Figure 1.17: Representation of the assembly of LFF and ^{D}LFF showing how alteration of the chirality of the N-terminal amino acid- alters the packing of the peptides. Adapted from Ref. 76 with permission from the Royal Society of Chemistry.

Assembly of the peptides result in a π-stacking overlap of the phenyl rings. The π-stacking of the phenyl rings within the core of the self-assembled structure is not observed for LFF, due to steric hindrance with the L- amino acids. The hindrance observed between the L- amino acids affect the phenyl rings ability to stacking in an optimal fashion. On the other hand, in the presence of D- amino acids, this steric hindrance is reduce allowing the phenyl rings to situate themselves in close proximity with their neighbors to form stable π-stacking interactions.

Gazit[71] showed that changes in ionization, alters the orientation and consequent assembly behavior of the peptides. Changes at the termini can also give rise to different self-assembling structures. The most common change is the amidation of the C-terminus.[81-82] This causes the removal of the charge from the terminus reducing the ability for the peptides to form ionic interactions, which promotes the self-assembling behavior. The disappearance of the favorable ionic interactions means weaker interactions, such as hydrogen bonding and π-stacking, are used to form the self-assembled structures. This can be seen in a paper by Cao *et al*[83]

where modifications to the termini reduce/remove the electrostatic capabilities. In addition, they have shown that alteration of the aroimatic amino acids have an affect of the type of self-assembling structure. Protected tripeptides Ac-FFK-NH_2, Ac-FYK-NH_2, Ac-YFK-NH_2 and Ac-YYK-NH_2 all have the ability to self-assemble into different types of structures. This highlights the importance of the aromatic hydrophobic effect from the tyrosine and phenylalanine side groups. The comparison between Ac-FFK-NH_2 (long tubular structures) and Ac-YYK-NH_2 (spherical aggregates) indicated the importance of π-π interactions for the formation of nanostructures (Figure 1.18). The additional hydroxyl groups present in the tyrosine, do not allow for the required rearrangement of water molecules, key for the self-assembly. With the focus on Ac-FYK-NH_2 and Ac-YFK-NH_2, these structures form clustered fibers. The additional –OH group on the tyrosine acts as an electron-withdrawing group, which makes the aromatic groups more electron deficient and reduces the role of the π-π stacking. The constraints on the structure are also relaxed as the π-π stacking is not as predominant which allows for flexibility in the aromatic rings' orientations. There is also an increase in the possible hydrogen bonding sites with the addition of the –OH group on the tyrosine. This reasoning was used to explain are why Ac-FFK-NH_2 forms fibers, Ac-FYK-NH_2/Ac-YFK-NH_2 form weaker fibers and Ac-YYK-NH_2 form spherical aggregates. Similar observations will be discussed in Chapter 2, with changes to the aromatic residues affect the strength of the nanostructures formed. Similarly, Shlomo *et al*[84], showed the assembling behavior of tripeptides where F is located at both terminal position with glutamic acid as the central amino acid (FEF).

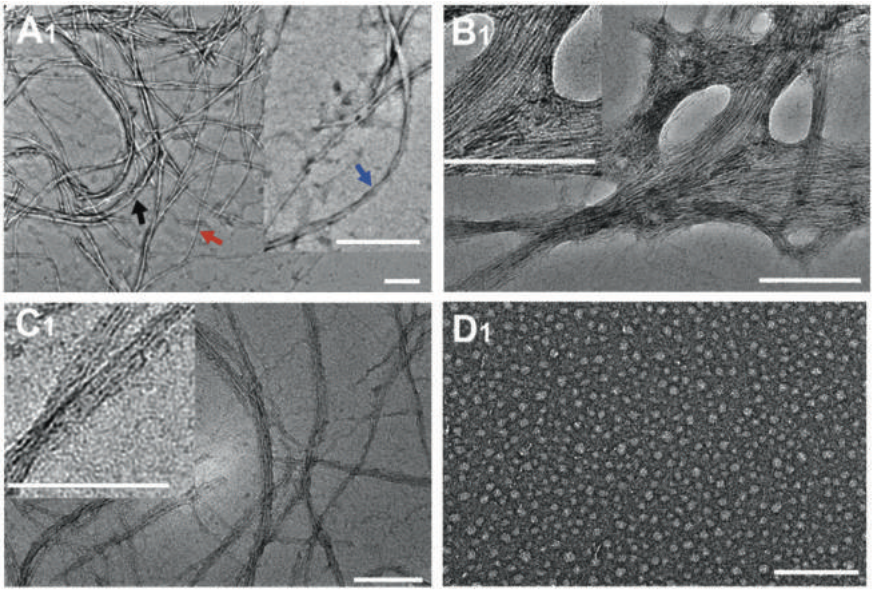

Figure 1.18: TEM images of A) Ac-FFK-NH_2 B) Ac-FYK-NH_2 C) Ac-YFK-NH_2 and D) Ac-YYK-NH_2. Adapted from Cao et al, J. Colloid. Interface. Sci, 2013, 407, 287-295. Copyright (2013) with permission from Elsevier

In addition, peptides Ac-IVD[85], Ac-IVF, Ac-IVW and Ac-IVY[86] have the ability to self-assemble into different structures. Ac-IVD and Ac-IVF assembled into nanofibers with a resultant hydrogel whereas Ac-IVW and Ac-IVY only formed amorphous aggregates. From these we can conclude that removal of the electrostatic interactions makes the peptide more prone to aggregation. The reduced electron repulsion that would be apparent in a highly charge species is no longer apparent allowing for a more ordering of the nanostructures.

Other peptides have also shown self-assembling behavior when they are co-assembled with other materials such as polymers. For example, when VYV is studied in the presence of sodium dodecyl sulfate, the resulting sample can form micelles.[87-88]

In this section, we have reviewed the area of minimalistic peptide self-assembly. A number of different short peptides have been found and the types of interactions that each of the peptides utilized are all-important for self-assembly. Although, there are many different types of peptide derivatives that have been found to self-assemble, it is increasingly clear that candidates that have not been modified can show self-assembling behaviors in water at physiological conditions. The drive for

this work is to examine peptide sequences that assemble into different nanostructures and form supramolecular hydrogels. In order to assess how these peptides can interact, computational techniques are widely utilized to determine the likelihood of peptides forming supramolecular structures. In the next section, an overview of both atomistic and coarse–grained techniques will be explored highlighting key papers that are useful for understanding the benefits of computational chemistry.

1.5 Computational Methods for Peptide Self-Assembly

The principle of molecular dynamics (MD) simulations is to treat interactions between atoms in the system classically by solving Newton's equations of motion. MD is widely used to examine the interactions between different molecules in greater detail. The level of detail can vary from all-atom representations to coarse-grain where the system is simplified. This literature review presents an overview of both all atom MD and coarse grain methods. While a comprehensive review on all molecular dynamics studies is not provided, key papers are discussed.[89-90]

1.5.1 Atomistic Modeling

Traditional atomistic molecular mechanics methods are based on a simple force field that takes into consideration the bonded and non-bonded interactions. (Equation 1.3)

$$
\begin{aligned}
U(r) = & \sum_{bonds} K_b\,(b - b_o)^2 \\
+ & \sum_{angles} K_\theta\,(\theta - \theta_o)^2 \\
+ & \sum_{torsions} \frac{1}{2} V_n\,[\,1 + \cos(\eta\omega - \gamma) \\
+ & \sum_{improper} K_\varphi\,(\varphi - \varphi_o)^2 \\
+ & \sum_{electrostatics} \frac{q_i q_j}{4\,\pi\,\varepsilon_o\,r_{ij}} \\
+ & \sum_{Van\ Der\ Waals} \varepsilon_{ij}\left[\left(\frac{R_{min,ij}}{r_{ij}}\right)^{12} - 2\left(\frac{R_{min,ij}}{r_{ij}}\right)^{6}\right]
\end{aligned}
\qquad \text{Equation 1.3}
$$

Bonded Terms

Where: K_b = bond stretching constant K_θ = angle bending constant

b = bond length θ = angle

b_o = equilibrium bond length

V_n = barrier height

η = multiplicity

ω = torsional angle

Υ = phase factor

θ_o = equilibrium angle

K_φ = improper angle constant

φ = improper angle

φ_o = equilibrium improper angle

Non-bonded Terms

q_i and q_j partial charges in atoms i and j

ε_o is the effective dielectric constant

r_{ij} is the distance between i and j

ε_{ij} is the Lennard-Jones well depth

$R_{min,\,ij}$ is the Distance of the Lennard-Jones minimum

The first 4 terms in the force field equation refer to the bonded interactions: bonds, angles and torsions/dihedrals (Figure 1.19). Improper torsions are defined as the change in the dihedral angle due to the planarity of molecules.

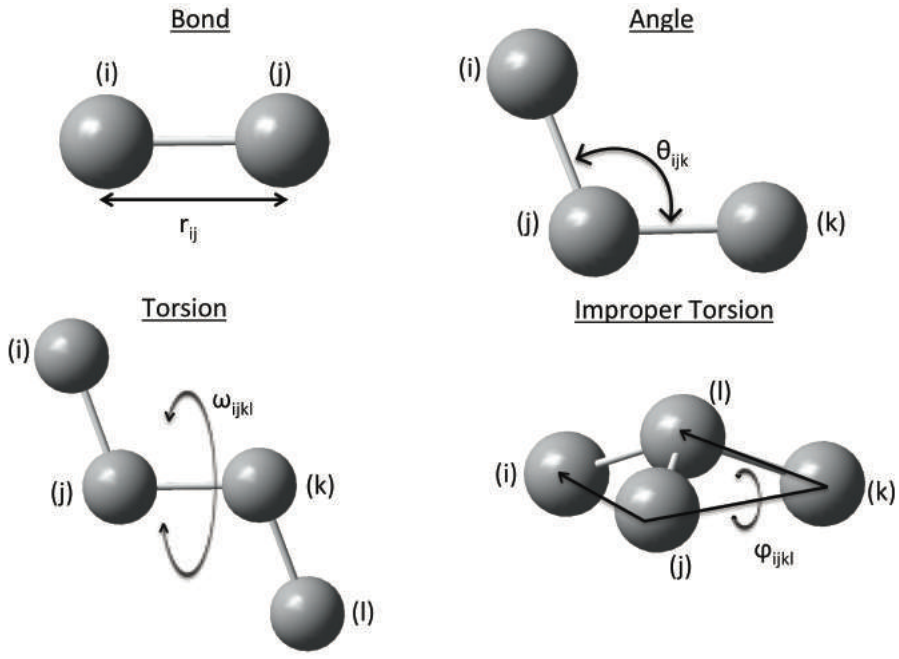

Figure 1.19: Representation of the 4 different types of bonded interactions

The first bonding interaction examines the variations in bond stretching where the energy varies with the bond length. The alteration of the bond distances was first described using the basic Morse potential (Equation 2).

$$v(b) = D_e\{1 - \exp[-a(b - b_0)]\}^2 \qquad \text{Equation 1.4}$$

This takes into consideration the depth of the potential energy minima D_e and a, which is dependent on the reduced mass and the frequency of the bond vibrations. This model of the bonding energy is not usually used in the overall force field, as it depends on three variables for each bonding interaction, which is not efficient. Furthermore, bond stretching results in only small deviations from the equilibrium bond distances. As a result the harmonic approximation is applied using Hooke's law.[89, 91]

$$v(b) = K_b\,(b - b_o)^2 \qquad \text{Equation 1.5}$$

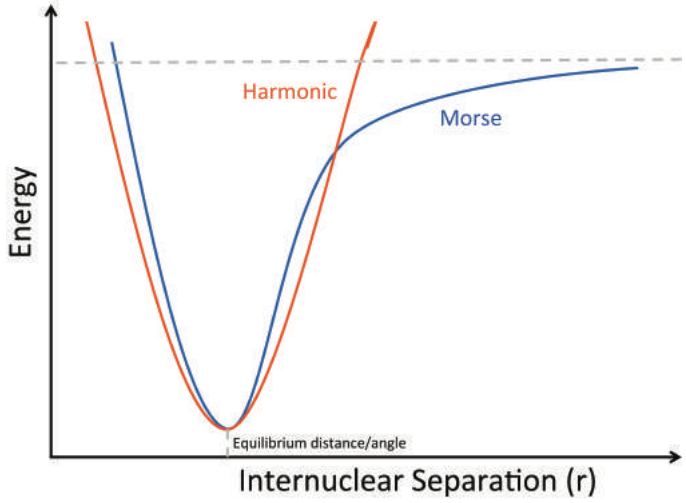

Figure 1.20: Comparison of the Harmonic and Morse Potentials

From Figure 1.20, the Harmonic potential (Hooke's Law) shows slight changes in comparison with the Morse potential. The major differences between the two potentials occur at relatively large internuclear separations; therefore Hooke's law is a reasonable approximation for the shape of the potential energy surface around

the equilibrium bond length. In addition, variations in angle bending interactions can also be defined by Hooke's law:

$$\upsilon(\theta) = K_\theta\,(\theta - \theta_o)^2 \qquad \text{Equation 1.5}$$

In a similar fashion to the bond stretching, deviation from the reference angles creates an energetic penalty for the system. In contrast to the stretching terms, the penalty for deviating the angle is often lower so less energy is required.

Torsional terms refer to the variations in the dihedral angles between 4 atoms. The rotations along the dihedral angle introduce energetic barriers, where the atoms rotate giving an energy profile for each orientation. This rotation introduces steric effects where large groups are on the same face as others creating a strained system. Examination of this energy profile is carried out using Equation 1.6.

$$\upsilon(\omega) = \sum_{dihedrals} \tfrac{1}{2}V_n\,[1 + \cos(\eta\omega - \Upsilon) \qquad \text{Equation 1.6}$$

For systems that contain more repulsive terms, more potentials need to be carried out to obtain a more accurate representation. By changing one of the variables this gives a new potential energy representation of the system.[91]

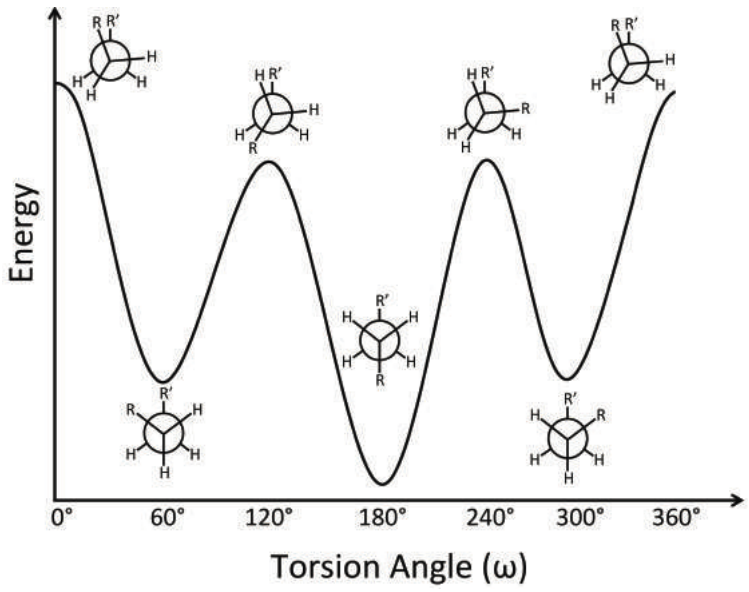

Figure 1.21: Energy changes which changing the torsional angle of butane

The combination of these different potential energy functions allows a more flexible description of the potential energy surface. (Figure 1.21) The peaks correspond to the areas of high energy, which corresponds to the eclipsing of groups. The troughs are where the large groups are away from each other resulting in an energy minimum. [89]

The latter two terms in Equation 1.3 refer to the non-bonded terms. These interactions result in the majority of the computational time used for calculating the energy of a system.

Electrostatic potentials are an example of non-bonding interactions, which is an important interaction in the force field. The difference in electronegativity of the atoms within the system is represented within the force field through point or partial charges of atoms. The interaction of these point charges can then be modeled by through Coulombs law:

$$v(q) = \sum_{i=1}^{N_A} \sum_{j=1}^{N_B} \frac{q_i q_j}{4\pi \mathcal{E}_o r_{ij}} \qquad \text{Equation 1.7}$$

Where q_i and q_j represent the charge on the specific interacting atoms (*i* and *j*) that are separated by a distance of r_{ij}.[89, 91] (Figure 1.22) If the charges have the same sign, this results in a positive term, which is a repulsive. If these have different signs then the overall term is negative resulting in an attractive interaction.

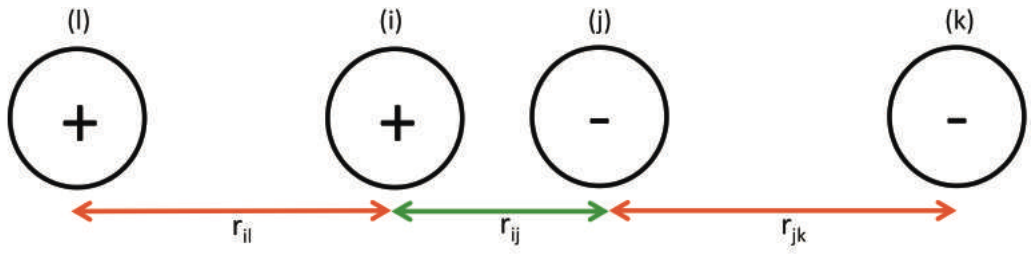

Figure 1.22: Electrostatic interactions indicating the repulsive interact between two positively charge species (r_{il}), 2 negatively charged species (r_{jk}) – red - and the attractive interaction between oppositely charged species (r_{ij}) – green

There are also non-bonding interactions that exist between uncharged, non-polar molecules. Examples of this would be such molecules that contain no dipole moment, so there cannot be a dipole-dipole interaction. Nobel gases are examples of these, as they contain no partial charges, therefore they are supposed to behave like *ideal* gases. However, the deviation from the ideal gas behavior was first observed by Johannes Diderik Van der Waal and thus these interactions have been called Van der Waals interactions.[92]

For Van der Waals interactions, there are both repulsive and attractive forces that the atoms can display. The attractive term is normally classed as long range. This contribution occurs via the dispersive forces or London forces. London forces describe the instantaneous dipole created by the fluctuations of the electron clouds. This instantaneous dipole can then induce a dipole on a neighboring atom creating an attractive inductive effect. The repulsive term is explained by the Pauli principle. The Pauli principle states that no two electrons can have the same quantum number. The interaction is due to the electrons having the same spin therefore the electrons coming into close proximity of each other will induce this repulsive interaction. For a force field, we require a means to measure the interatomic potentials accurately using a simple expression. The Lennard-Jones 12-6 potential is most commonly employed for measuring the van der Waals forces due to its accuracy and computational efficiency.

$$v(r) = \varepsilon_{ij} \left[\left(\frac{R_{min,ij}}{r_{ij}} \right)^{12} - 2 \left(\frac{R_{min,ij}}{r_{ij}} \right)^{6} \right] \qquad \text{Equation 1.8}$$

The Lennard-Jones potential takes into consideration the repulsive component of the van der Waals interaction denoted by the (12) term, and the attractive component, which is denoted by the (6) term. $R_{min,ij}$ is the separation in which the energy is zero. The ε term is the well depth of the potential, which is the magnitude of the minima with the potential. [89,91]

There are a number of different force fields that are widely available that have been well parameterized for proteins, lipids, biomolecules etc. CHARMM

(Chemistry at Harvard Molecular Mechanics),[93-95] GROMOS (Groningen Molecular Simulation),[96-98] AMBER (Assisted Model Building and Energy Refinement),[99-100] *etc*. The force field of choice is a matter of preference or availability depending on the type of system that is being examined.

Several research groups have utilized molecular dynamics techniques to examine the behavior and interactions of biomolecules. Hauser and co-workers examined tri- to hexapeptides, arranged in an amphiphilic nature with the hydrophilic head groups and hydrophobic tails.[85] results indicate that for the larger hexapeptide Ac-LIVAGD, there was a tendency for the peptides to dimerise after approximately 4 ns. This observation was observed for Ac-IVD but at a much slower rate. This was associated with the lower hydrophobicity of the tripeptide and therefore the aggregation of the peptide occurs at the slower rate (Figure 1.23). Extended simulations were carried out for the larger hexapeptide, which showed the fibre structure that formed, remained stable after 20 ns.[85]

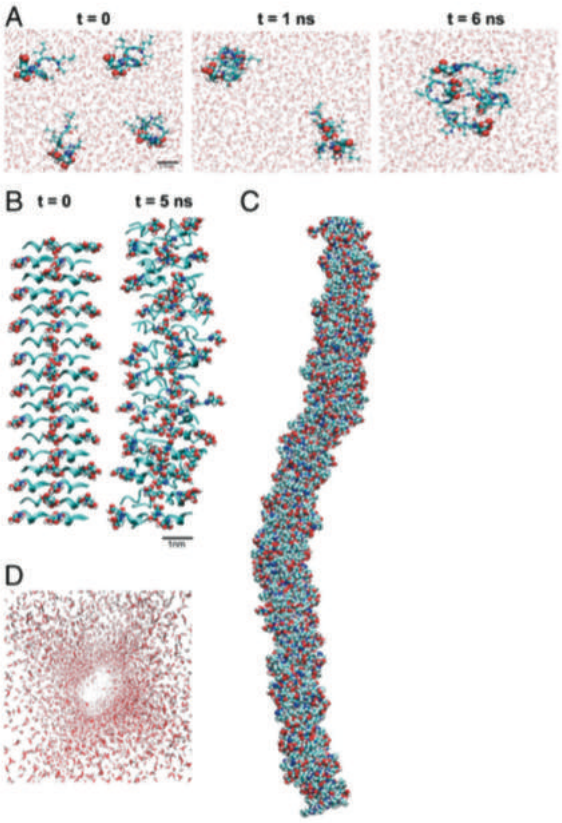

Figure 1.23 Self assembled structure of Ac-LIVAGD. A) Spontaneous assembly after 6 ns B) Snapshot of 72 molecules C) Final snapshot of fiber formation after 20 ns D) distribution of water molecules after

self-assembly indicating lack of water molecules within the fiber. Copyright (2010) Ref. 85 National Academy of Sciences

In addition, further work by the same group shows the self-assembling ability of Ac-NFGAIL, a fragment of the islet polypeptide (IAPP). In this work, they show that all systems give rise to fiber formation. This work was consequently examined computationally by Wu et al.,[101] where they observe that the peptide partially organize into parallel and anti-parallel β conformations. They suggest that the large disordered aggregates act as a nucleation point for other fibrils, which result in the formation of the plaques observed in amyloid disease.[102]

1.5.2 Coarse Graining

Over the past few decades the molecular size accessible with MD simulations has increased significantly so that the methods can be applied to biomolecular systems. With the achievements of enhanced computing power and speed requirements for the running and processing of data, this allows simulations to be carried out in the ten-to-hundred nanoseconds range. However, for most relevant simulations for biological systems, such as docking, protein-protein interactions, protein folding *etc.* the timescales tend towards the microsecond to millisecond. With the introduction of these systems, the timescale is between 4-6 orders of magnitude greater than what is currently feasible.[103-104] Coarse-grained (CG) methods have been around for many years. They introduce a simplified description of the systems which reduce a large number of degrees of freedom on the system into a smaller more manageable system.[105]

CG is a modeling approach that approximates true molecular systems, however, these approximations allow for much larger systems and over longer timescales relative to the fully atomistic models.[106-111] There have been older systems that have been used to display the usefulness of CG models. Elastic Network models have been used that to determine the fluctuations of proteins.[112] The model represents a node (center of mass) at each α-carbon within the proteins. Similar to the atomistic level, the harmonic approximation is used to model the interactions where the spatial interaction between each node is represented by a harmonic

spring. This level of coarse graining was first proposed by Tirion[113] in 1996 and it was a year later that the work was further developed for amino acids.[114-115] Another model that was specially design for protein folding was the Gō model. In the original Gō model the amino acids were represented by a single bead, with the structure determined by the between the attractive and repulsive interactions between the beads. Unfortunately, this simplified representation is not able to reproduce the thermodynamics and kinetics of the protein folding, resulting in an inaccurate description of the system as it fails to properly represent the metastable folding states.[112]

These issues resulted in a more sophisticated model, where new energy terms are added to be able to examine these states. Most issues arise from the balance between the amount of information between the atomistic and the coarse grain level, thus the number of beads that represent each system. As with the systems that are focused on the single bead system, these systems do not have enough information to get a full description of the interactions therefore for large systems this is not the most efficient procedure. The increase in the number of bead and bead types will allow a broader description of interactions and therefore the models can become more efficient in their descriptions. As with most systems, the choice of model is important, as each model will have benefits depending on the system.

MARTINI Model

The MARTINI model was initially developed for CG simulations of lipid membranes, but since 2007 the model has been extended to other biomolecules such as peptides, protein,[116-117] carbohydrates[118], lipids[119], *etc*. A recent review by the designers, Marrink and Tieleman,[120] give an overview on the design, principles and applications of the MARTINI force field. The philosophy of the force field was to develop a model, which could be accurately transferred from atomistic to coarse-grain as a whole. This means the model can be widely used for a range of biomolecular systems without the need to alter parameters and bead types between simulations.

The MARTINI CG model is based on a 4:1 mapping system where four heavy (non-H) atoms are combined into a single bead type. There are four distinct types of bead: polar (P), non-polar (N), apolar (C) and charged (Q).[106] The labeling of the certain bead types is important as this distinguishes between the types of interaction. Each type of bead is subdivided into different classes depending on the strength of interaction. For example, a range of 1-5 has been denoted depending on their polarity and also subscripts such as d, a, da, 0 are used for hydrogen bonding capabilities.

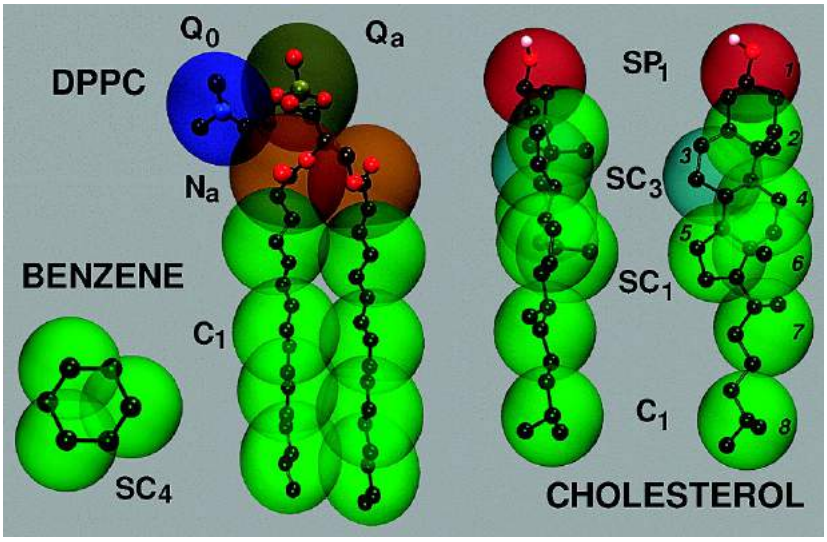

Figure 1.24: Coarse Grain Representation of different molecules according the MARTINI force field, with the bead types indicated. Adapted with permission from Marrink *et al*, *J. Phys. Chem. B.*. 2007, 11, 7812-7824. Copyright (2008) American Chemical Society.

Figure 1.24 shows the breakdown of the typical beads types and the interactions that they can possess. Comparison between the atomistic and coarse-grained force fields shows subtle differences. The non-bonded terms are still denoted by the Lennard-Jones potential with slight differences

$$\sum_{nonbonded} 4\varepsilon_{ij}\left[\left(\frac{\sigma_{ij}}{r}\right)^{12} - \left(\frac{\sigma_{ij}}{r}\right)^{6}\right] \qquad \text{Equation 1.9}$$

This represents a shifted Lennard-Jones potential where σ_{ij} represents the closest distance of approach (Equation 1.9). The *effective distance* is set at 0.47 nm except

for special cases of rings, as there are different constraints that apply for CG ring systems.[106]

For particles involved in constrained rings (phenylalanine, tyrosine, tryptophan, histidine etc.), the mapping is altered slightly as the 4:1 mapping system is inadequate. For the system to achieve a 4:1 map for ring structures the geometry of the ring system would change and therefore different interactions would be observed compared to what you would normally get if it were an all atom system. To counteract these issues in the mapping system, ring systems change to a 2-3:1 map, so for every 2-3 heavy atoms these are replaced with a bead, which allows the geometry of the ring to be established. The interaction size and strength of the must be reduced compared with normal bead molecules. The Lennard-Jones potential, σ_{ij}, is reduced to 0.43nm with the ε scaled by 75%, which allows the ring systems to pack closer together without freezing.[106]

The bonded terms remain relatively unchanged as the details in the bonding terms have been reduce due to the mapping system.

Although there are many positives associated with the use of coarse graining for simulations, the systems do have their limitations. As the beads are groups of heavier atoms, the resolution of the individual atoms is lost and therefore the information regarding the relative importance of specific interactions is limited. There is also the loss of the detailed interactions that you would normally get from the all atom simulations. Interactions such as H-bonding between certain donors and acceptors are not explicitly observed and directionality of the H-bonding is lost. The fine detail of specific interactions that are lost in the coarse graining procedure can change the conformation and potentially the overall structure of the system, therefore the lowest energy minima may not be observed.[106]

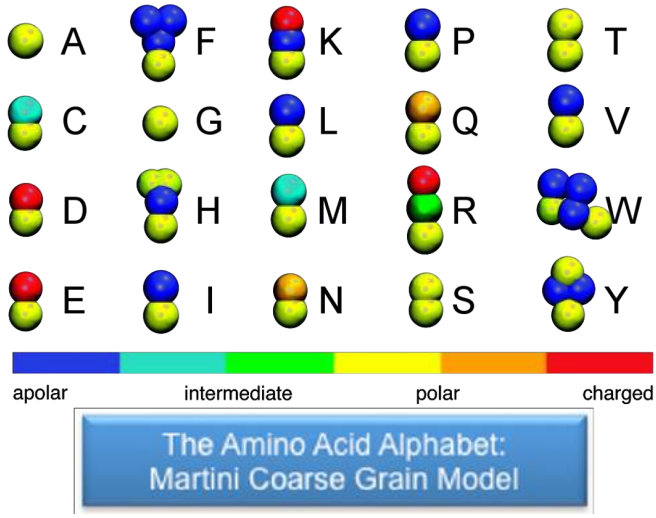

Figure 1.25: Difference in bead types for all 20 amino acids in relation to the parameters devised by the designers of the MARTINI force field. Adapted with permission from Monticelli *et al*, *J. Chem. Theory. Comput.* , 2008, *4,* 819-834. Copyright (2008) American Chemical Society.

Within this thesis, CG is used to identify the self-assembly of tripeptide molecules. Using publically accessible parameters designed for MARTINI coarse-grained proteins, tripeptides are converted into the coarse grain representation and then simulated together in a solvated system.

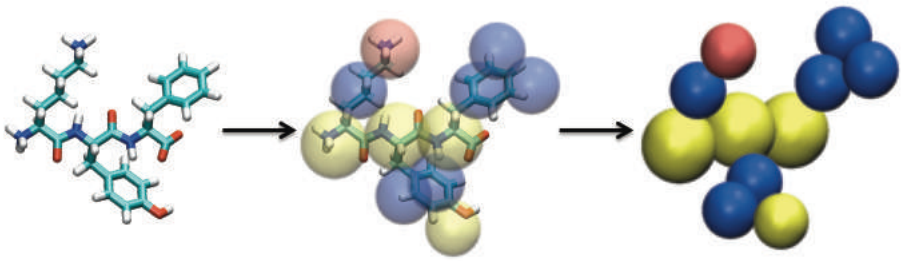

Figure 1.26: Conversion of Atomistic KYF tripeptide to coarse grain representation using MARTINI Force Field. Colour code refers to interaction bead type observed in Figure 1.25

As can be seen from Figure 1.26, the atoms are grouped together into large beads, depending on their size and conformation. The color-coding of the beads illustrates the different parts of the peptide. The side groups are given the beads corresponding on the types of interactions they can have, described previously (Figure 1.25).

The utilization of the MARTINI force has successfully been carried out to determine the aggregation behavior of dipeptides. Frederix *et al*,[121] showed the aggregation propensities of all 400 dipeptides in water and could demonstrate that their results agreed with all known published examples for dipeptide assemblies. In addition, a paper by Guo *et al*[122] describes the use of the MARTINI coarse grain model to determine the supramolecular structure of FF as a function of concentration (Figure 1.27). As it has previously been discussed, the formation of nanotubes was observed with FF, confirming the observations made by Gorbitz and Gazit, where the phenyl ring orientate on the outer side of the structure with the amide linkages arrange within the core of the assembled structure[62, 123]

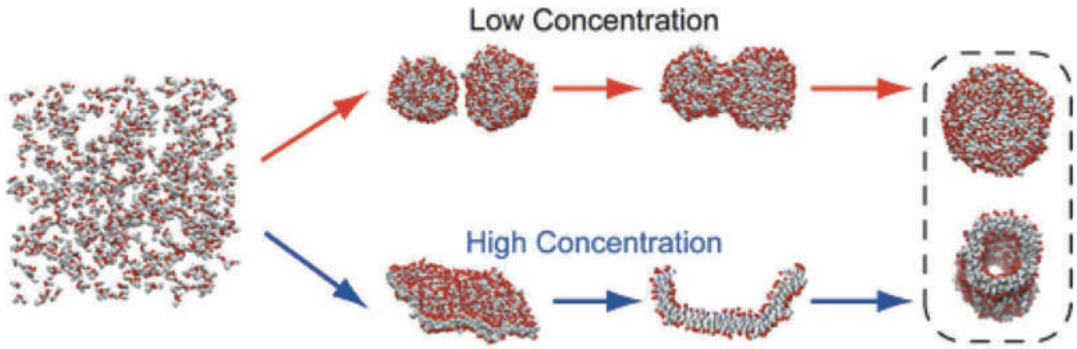

Figure 1.27 Self-assembling of FF forming nanovesicles at low concentration and nanotubes at high concentration using the MARTINI force field. Adapted with permission from Guo *et al*, *ACS Nano.*. 2012, 6, 3907-3918. Copyright (2008) American Chemical Society.

In this section, an overview of atomistic and coarse-grain computational methods was discussed. Atomistic forces are well established and can be used for a number of different biomolecular systems. The fundamentals of each force fields are primarily the same and are derived using Newton's laws of motion. However, with increasing size and complexity of biomolecular systems, the computational time can be expensive. The development of coarse-grains methods, where the number of interactions has been decrease has shown to be valid for a number of larger systems. A number of publications have been shown to use coarse-grain methods for understanding self-assembling processes. In particular, a close examination of the MARTINI coarse-grain force field identifies the benefits of using such force fields. Utilization of the MARTINI force field has shown to give results that are comparable to atomistic simulations whilst examining the systems at greater time scales.

2.

Designer Tripeptide Nanostructures: A Computational and Experimental Prediction of Short Peptide Self-Assembly

* This work was published in part as: P. W. J. M. Frederix, **G. G. Scott**, Y. M. Abul-Haija, D. Kalafatovic, C. G. Pappas, N. Javid, N. T. Hunt, R. V. Ulijn, T. Tuttle; Exploring the sequence Space for (Tri-) peptide Self-assembly to Design and Discover New Hydrogels; *Nat. Chem.*, **2015**, *7*, 30-37

Declaration of contribution to published article: Any reproduced practical work from the aforementioned published article; I was solely responsible for, unless otherwise stated.

2.1 Introduction

As discussed in Chapter 1, short peptides have enormous potential for the creation of different nanostructures. The changing of amino acid order, alteration of the amino acid sequence and changes in amino acid chirality have all shown to play a role in guiding the assembly. Unfortunately, the discovery of nanostructures is often serendipitous.

The design of new tripeptide nanostructures has taken a considerable step forward with the introduction of design rules for the ordering of the amino acids in all 8,000 tripeptides. Work from the Tuttle group[124] computationally examined the aggregation propensity of all 8,000 tripeptides by studying the different levels of aggregation for each tripeptide, and then comparing how the position of each amino acid within the peptide alters the overall structure. This examination was based upon computationally monitoring the aggregation of tripeptides at the coarse grained level, using the MARTINI force field[106] over a short simulation of 50 ns. Calculation of the solvent accessible surface area (SASA) was carried out as a quantitative measurement for determination of the aggregation propensity (AP) achieved by each sequence (Equation 2.1). The balance of hydrophobic groups and hydrophilic groups is essential for the development of hydrogelators. The peptides need to be able to aggregate together to form fibers, and these fibers require favourable interactions with water molecules in order to form fibrous networks capable of trapping water. Therefore, hydrophilicity-weighted scores (AP_H) were introduced, to provide a means for predicting tripeptides capable of aggregating together but with a required level of hydrophilicity by incorporating the *logP* in a normalized AP' (Equation 2.2). The normailisaed AP' score can be further weighted depending on how much af an dominant effect of the AP is required by alterating the alpha. These hydrophilicity-weighted values are then used to identify tripeptides with the potential to form hydrogels.

$$AP = \frac{SASA_{initial}}{SASA_{final}} \qquad \text{Equation 2.1}$$

$$AP_H = (AP')^{\alpha}.logP' \qquad \text{Equation 2.2}$$

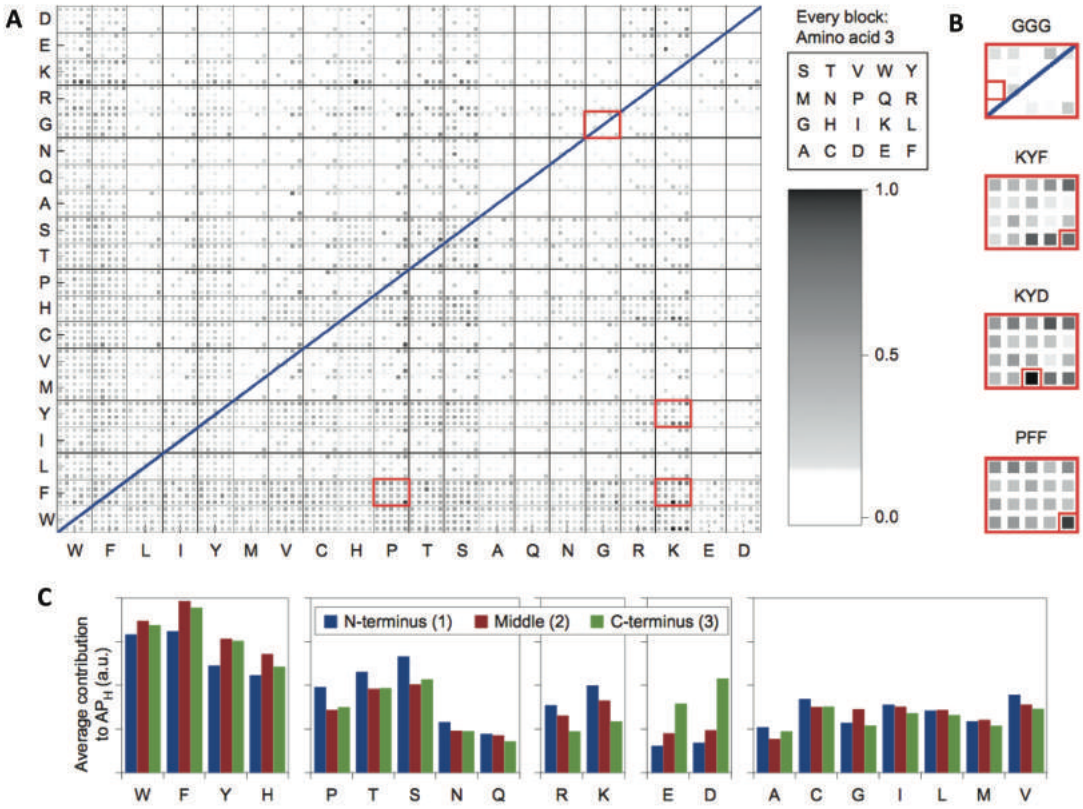

Figure 2.1: Tripeptide Aggregation propensities for all 8,000 tripeptides (darker the square, the greater the aggregation) B) Highlighted aggregations for 4 different tripeptides C) Design Rules for amino acid position indicating the most favored position for amino acids. Image adopted with permission from Ref. 124

Compiling all the data from simulations resulted in the determination of design rules. These rules indicate the amino acid sequence position that is most favourable for peptide aggregation (Figure 2.1). A cumulative analysis was carried out, where for each amino acid at each position; the AP_H value for peptides where the amino acid resides at the same location is summed. For example, for every tripeptide that has W at the N-terminal position, all the corresponding AP_H values are summed together to give the total AP_H value for W at that position. This process is repeated for every amino acid at the three positions within the tripeptide backbone. This analysis gave rise to several interesting observations, which led to the proposed design rules.

As expected, the strongest aggregating peptides were found to contain aromatic side chains. As the hydrophobic effect is a main driving force in aggregation, it is therefore expected that large hydrophobic groups tend to aggregate. Secondly, positively charged groups appear to show increased aggregation when situated at the N-terminus. Finally, negatively charged side chains appear to prefer the C-terminus. It has not been fully understood as to why these charge groups have a preference to adopt these positions; reasoning behind these observations are that this 'double' charge promotes the formation of salt bridges either intramolecular or intermolecular, which have shown to be important in a self-assembling structure. In all cases, the aromatic side group is preferred in the middle position of the tripeptide chain, in addition two sequential aromatic groups promotes aggregation because the conformation of the backbone and aromatic interactions promote the aggregation of the peptide. So, peptides prone to assembly are sequences such as KYF, FFD, *etc*. The peptide that were chosen in this study showed a high level of aggregation whilst the AP_H score were high which indicated promising results for the formation of hydrogels.

This chapter will explore the differences in the nanostructures formed using the design rules laid out using both computational and experimental methods.

The aims can be categorized by the following:

1. Confirm the design rules and use them to predict which peptides have the ability to form hydrogels.
2. Examine tripeptides, which obey design rules but do not form hydrogels.
3. Use computational methods to understand the interactions and conformations of these peptides.

2.2 Fibrous Peptide Assemblies

2.2.1 Experimental Characterization of Fibrous Peptide Assemblies

The formation of nanostructured hydrogels by peptide self-assembly is the main aim for this project. This would firstly involve predicting how short tripeptide molecules can interact, followed by experimental assessment to verify formation of nanofibers, which, in turn, can potentially give rise to formation of hydrogels. Using aggregation propensity data acquired from Frederix *et al.*, three peptides were chosen which obeyed the proposed design rules. The three peptides chosen were KYF, KYW and KFF (Figure 2.2). All peptides followed the design rules explained in the previous section (paired aromatics and paired charges), gave rise to a peptide aggregation score that was greater than 1.8, which was set as the benchmark for good aggregation. This value was set as it was the limit the aggregation based on the top 400 systems that aggregated. Furthermore, to understand how the design rules affect the assembly of these peptides, control peptides were selected in order to examine this behavior. The peptides chosen were FYK and KLL. Examination of FYK will identify the importance of the situating the positively charge amino acids at the N-terminal position, whereas KLL will examine the effectiveness of having aromatic amino acids instead of aliphatic amino acids.

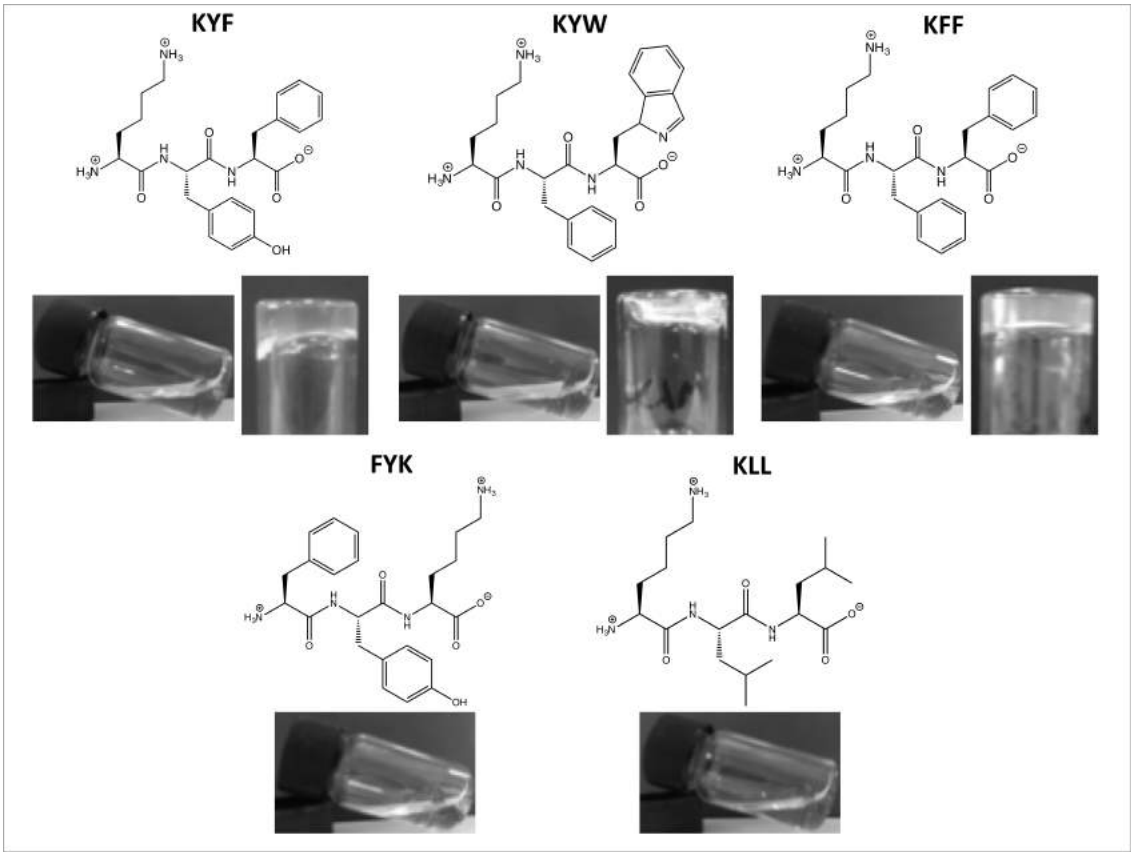

Figure 2.2: Structures of chosen tripeptides with macroscopic images after direct dissolution of the peptide in water and after pH adjustment to 7.4

All peptides are soluble directly in water at a peptide concentration of 40 mM, giving a clear solution with an initial pH approx. 5.1. At this pH, it is expected that both the lysine chain and the N-terminus amine will be in the protonated state. In addition, the C-terminus carboxylate will be in the deprotonated state. It is expected that the lack of formation of nanofibers is due to the repulsive electrostatic interactions between the opposite ends of the peptide chain. Upon pH adjustment to pH 7.4 using 0.5 M NaOH, terminal amines start to become deprotonated (pKa ~8.1) and therefore the overall charge within the peptide becomes neutral and zwitterionic. Therefore, KYF, KYW and KFF will be able to interact allowing for the formation of nanostructures. Although the same amino acids are found in the control peptides, the position of the amino acid is shown to be important with the observation that FYK does not form a hydrogel. Furthermore, exchanging aromatic amino acids to aliphatic prevents the peptide forming a hydrogel, as seen in KLL.

2.2.1.1 Fourier Transform Infrared Spectroscopy

Analysis by spectroscopic techniques allows for the determination of the molecular level interactions that occur during the self-assembly process. As such, the use of FTIR focusing on the amide I region allows examination of hydrogen bonding systems. For the presence of hydrogen bonding structures, the amide I region around 1650 cm^{-1} is examined. In this region, we expect to see the carbonyl stretch on the amide backbone. Changes in this peak either by the appearance of additional peaks (splitting) or changes in intensity indicate that there is an interaction between the carbonyl and another atom as well as possible resonance in vibration between multiple bonds, resulting in a change in vibration frequency and intensity.

The FTIR analysis of the self-assembled nanostructures shows the presence of several intense peaks allowing the determination of the crucial interactions present within the nanostructure (Figure 2.3). At pH 7.5, it is expected that the free carboxylate group situated at the C-terminus would be in the deprotonated state. This deprotonated carboxylate is indicated with the broad peak generally around 1580 cm^{-1}. On inspection of the FTIR from KYF and KYW, it is evident that this carboxylate peak has shifted to a lower wavenumber, which is associated with a decrease in the energy. It is suggested that this observation is related to the formation of a salt bridge.[125] The orientation of the salt bridge cannot be derived directly from FTIR spectra, but there are three possibilities that could result in the observed shift of this peak. The carboxylate could interact with the N-terminal amine of another peptide, or the lysine side chain on the same or different peptide (discussed in more detail in Section 2.2.2). KFF does not show a similar intense peak as KYF and KYW, suggesting a poor salt bridge formation of peptide. Although, a splitting of the peak is observed, the broadness and low intensity of this peak suggest that there are no strong interactions formed. The observation of this salt bridge peak coincides with the strength of the hydrogel formed. The lack of this salt bridge interaction seen in KFF can be directly linked with the weakness of the KFF hydrogel (discussed further in Section 2.2.1.4). Two additional peaks are observed within all three peptide hydrogels. These peaks indicate the hydrogen-bonding network of the peptide hydrogels. The intense peak at 1650 cm-

[1] is related to the C=O stretch on the backbone. In proteins, this peak is typically associated with a random coil secondary structure. However, these findings are extrapolated from data observed in proteins.[126-127] In terms of results obtained from short peptide assembly, it is difficult to compare data from proteins to short peptides. It can be assumed that the presence of peaks within the amide I region indicate a level of order in the assembled structures; however, it cannot be fully extrapolated from observations in protein chemistry. Similarly, in proteins, the presence of the peak at 1625 cm^{-1} indicates the formation of β-sheet structures, whereas is short peptide chemistry, this is associated with ordered hydrogen bonding from one of the amide modes found on the peptide backbone.[124]

To explain the differential assembly of KFF compared to KYF and KYW, the stronger electron density that is found between the phenyl rings in KFF; the hydrophobic effect has a greater effect on the aggregation behavior of this peptide. As a result, different packing occurs which disrupts the electrostatic interactions, thus a reorganizing of the peptides occurs. This reorganization prevents KFF from forming a hydrogel. As with KYF and KYW, the strength of the π-stacking is reduced in comparison with KFF thus aggregation is less driven by the hydrophobicity. As KYF and KYW have more hydrophilic aromatic rings, a reorganization of the side chain occurs allowing for a greater alignment. Examining the structural behavior of the two control peptides show significant changes in FTIR signals. The most noteworthy is the disappearance of the 1625 and 1649 cm^{-1} peaks. As these peaks are associated with the stabilization via hydrogen bonding, it can be determined alteration of the amino acid sequence alters the self-assembly ability of the peptide. The broad peak at 1580 cm^{-1} indicates the carbonyl stretch, of which there are no stabilizing interactions present. The intense peak situated at 1775 cm^{-1} is due to the presence of residual TFA from the deprotection step during synthesis. As TFA is strongly complexed to the positive charges found on the peptide, removal/exchange of the salt is difficult. The intensity of the peaks observed in the FTIR are due to the re-scaling process of the spectra which magnifies the TFA peak, whereas the intensity of the peaks found in the fibrous assemblies are too low to be observed in comparison with the new peaks.

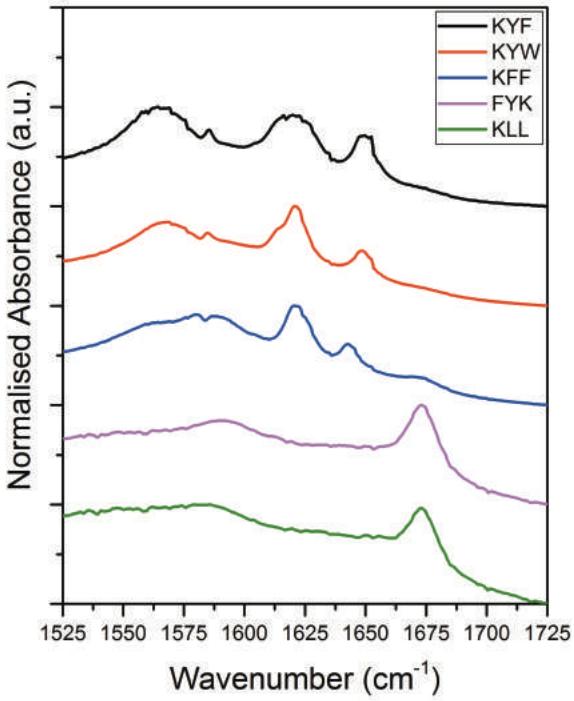

Figure 2.3: FTIR spectra of KYF, KYW, KFF, FYK and KLL indicating the differences in molecular interactions involved for each self-assembling system

2.2.1.2 Transmission Electron Microscopy

Electron microscopy was used to visualize the nanostructures formed upon hydrogelation (Figure 2.4). It is evident that KYF and KFF form similar types of nanostructures. Both of these peptide form nanofibrous networks, which is consistent with the hydrogelation observed. The size distributions of these structures are very similar, with KYF approx. 2.2 nm and KFF 3.3 nm in diameter, measured by averaging over 20 random structures. KYW forms different types of nanostructures. These structures are much greater in diameter approx. 20 nm in diameter but on close inspection these structures form short bundles (approx. 4.3 nm separation) that go in and out of focus creating intermittent section of the outer surface of the nanostructure. It is proposed, after discussion with a Cryo-TEM expert, Dr Amedee des Georges at the Advanced Science Research Center in New York, that this is due to the twisted nature of these structures indicating that these are not nanofibers but twisted microtubules. However, the formation of these nanostructures does not affect the formation of the hydrogel. It is proposed

that these microtubules must arrange themselves in order to create a network that is able to trap the water molecules.

The control peptides show two completely different assemblies. FYK forms spherical aggregates with a diameter of 30 nm. This assembly is consistent with the spectroscopic analysis, which does not show the presence of stabilizing interactions and results in the formation of amorphous aggregates. On the other hand, KLL forms supramolecular structures, which appear to be nanotubes (6-7 nm). These nanotubes appear to be uniform and interact together to form bundles. This suggests that these structures are unable to form the entangled network that is vital for the formation of hydrogels. Although, there is some ordering occurring, the orientation of the peptides upon formation into these tube-like structures must not form hydrogen-bonding interactions. This would suggest that the presence of aromatic groups is important to alter the packing of peptides driving fibrous assembly.

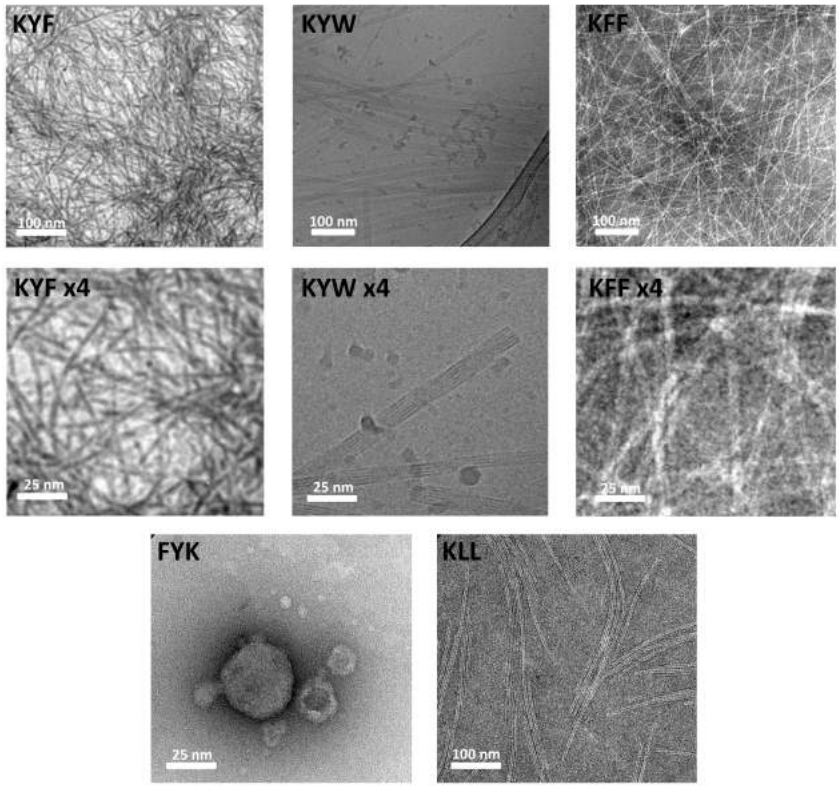

Figure 2.4: TEM images of all peptide assemblies showing the difference in supramolecular structures nanofibers, microtubules and amorphous aggregates.

2.2.1.3 Rheology

Rheological measurements were utilized to determine the mechanical properties of the hydrogels KYF, KYW and KFF, which were formed in order to examine the strength of each hydrogel. In order to do this, shear strain measurements must be carried out to identify the level of strain that can be associated with the hydrogel before the gel deforms. In each case, shear strain measurements were carried out on each of the samples and provided at shear strain of 0.5%, which was the point at which the strain began to deform the hydrogel.

Following shear strain measurements, frequency dependent measurements were carried out on all the hydrogels in triplicates. This is used to determine the viscoelastic strength of the hydrogel. Using the shear strain value measured, a frequency sweep between 0.1 and 100 Hz was applied to the hydrogel. Since in all cases the elastic modulus is greater than the loss modulus, each sample can be defined as a hydrogel. (Figure 2.5) Averaging of the values over the course of the linear section of the measurements give the relative strength of the hydrogel. Rheology measurements indicate that KYF is the strongest hydrogel of the three tripeptides with a strength of 8.7 ± 0.1 kPa, KYW is significantly weaker with a strength of 1.2 ± 0.3 kPa and KFF is the weakest hydrogel with a strength of 16 Pa. KFF is a very weak gel so the rheology measurements could only be taken once since the hydrogel collapsed. The sharp increase in both G' and G" at high frequency was due to the disruption of the hydrogel. At high frequencies, the probe moves at a greater intensity and this may damage the upper layer of the hydrogel resulting in loss of water molecules. As a result, sharp decreases or increases can be observed. These parts are not used for determination of the strength of the hydrogels. The strength of the KYF hydrogel is in line with most Fmoc based peptide gelators. (~10-15 kPa)[39] It has been widely studied that Fmoc gelators can form hydrogels, with changeable rheological properties depending on the concentration and additive that is used. Exploring the rheological properties of other known tripeptides, it was identified by Marchesan *et al*[76] that the formation of ^{D}VFF and ^{D}FFV formed hydrogels with a strength of ~10 kPa. Control experiments are not available due to the inability of FYK and KLL to form hydrogels.

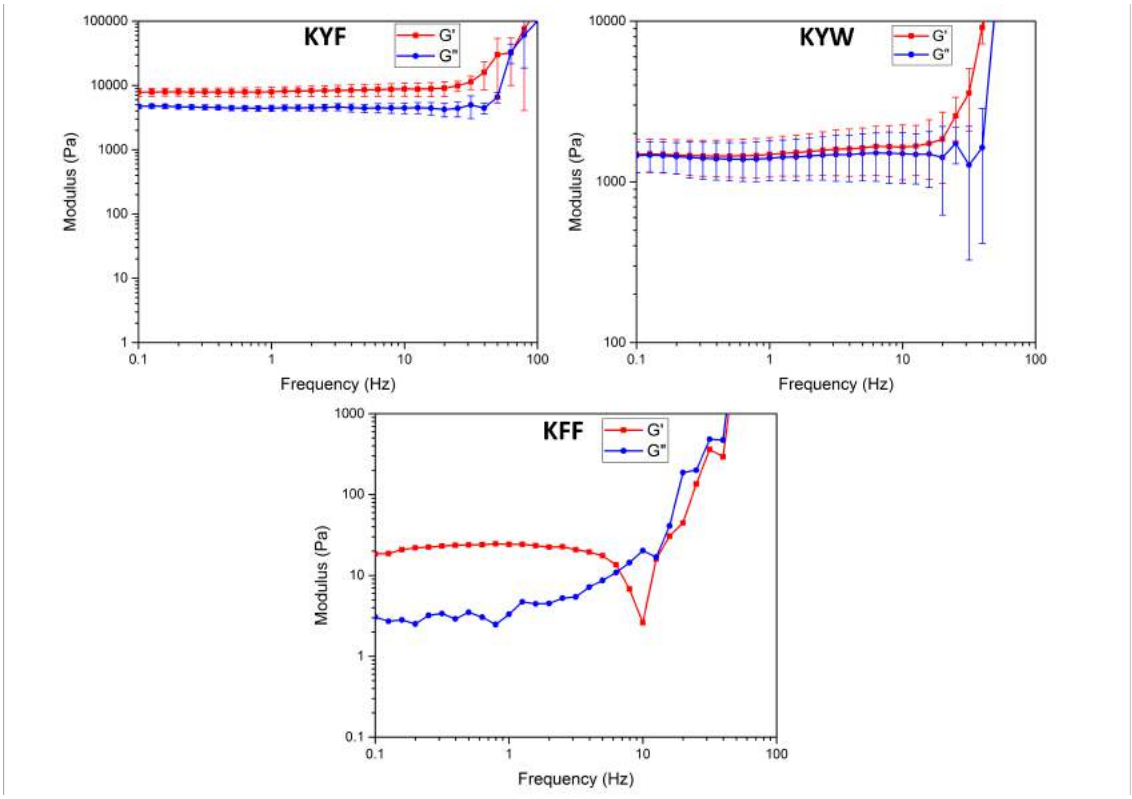

Figure 2.5: Rheology measurements of KYF, KYW and KFF showing the difference in G' and G"

2.2.2 Computational Analysis of Fibrous Peptide Assemblies

Computational methods were used in the screening process for the prediction of the aggregation propensities for all 8000 tripeptides. For the purpose of the screening process, simulations were run for a relatively short period of time at the coarse grain level (50 ns). To further identify how these nanostructures develop over time, longer simulations of these systems were carried out with stimulations running for 9.6 μs. (Figure 2.6) Over the course of the simulation snapshots were taken in order to identify the timescales for the development of nanostructure. It was evident that after 4.8 us that these systems had started to aggregate. By the end of the full simulation (9.6 μs) it was evident that peptide KYF, KYW and KFF adopted an elongated cylinder structure, indicative of a fiber formation with ionic groups predominantly positioned on the surface of the structure. On the other hand, FYK did not assemble into any highly ordered nanostructure. Starting from the random state, the peptide aggregate within the first microsecond to form an amorphous aggregate. KLL aggregates to some extent, the peptides start to form

small clusters, however, there is a high level of exchange between the peptides of different clusters. As a result, there is no stabilized structure observed. Consequently, the nanostructures observed from the CG MD simulations give good agreement with the experimental findings.

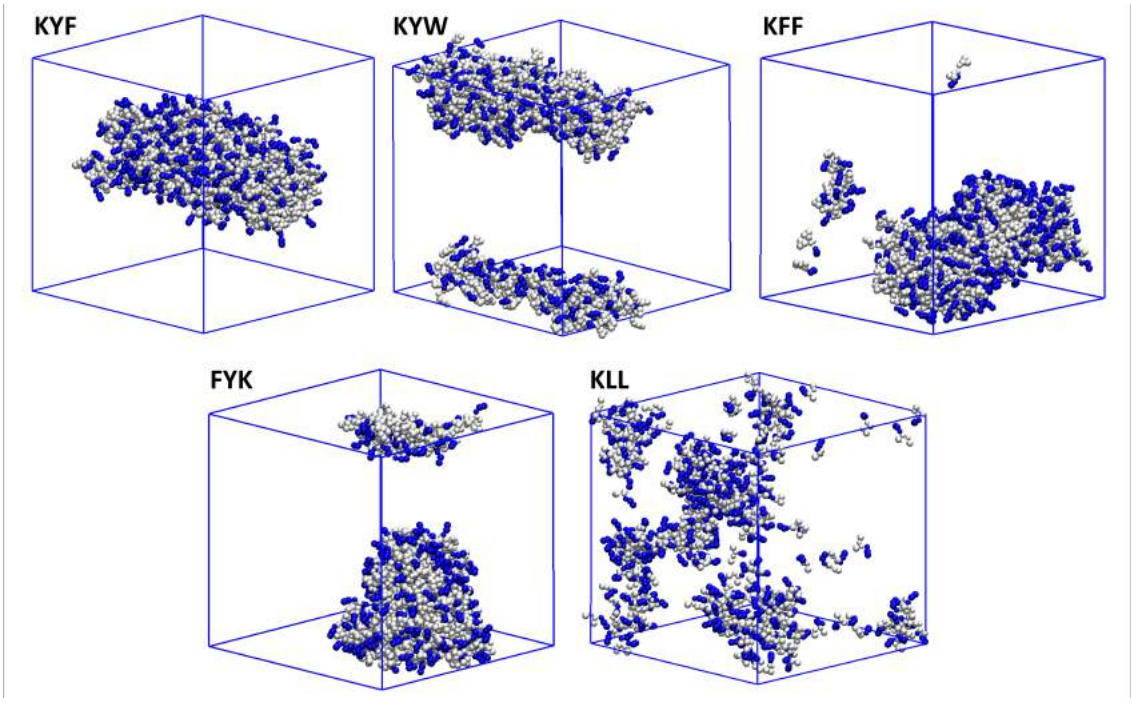

Figure 2.6: Coarse-grained molecular dynamics simulations of all peptide systems after a period of 9.6 μs showing the difference in molecular assemblies for each tripeptide structure

Although the use of CG MD has many advantages, such as examining simulations at large time scales, there are drawbacks to using these types of force fields. The loss of detail of specific interactions such as hydrogen bonding can prove to be an issue for understanding the molecular interactions involved. Experimentally it has been well documented that interactions such as hydrogen bonding are important for the directionality component of self-assembly.

To examine how the CG simulations map onto atomic simulations, for the MD structures of KYF, KYW, KFF, FYK and KLL further, back-mapping procedures were carried out. Using atomistic topologies, acquired from MARTINI, each system can be back-mapped from the CG representation to the all atom representation (Figure 2.7).

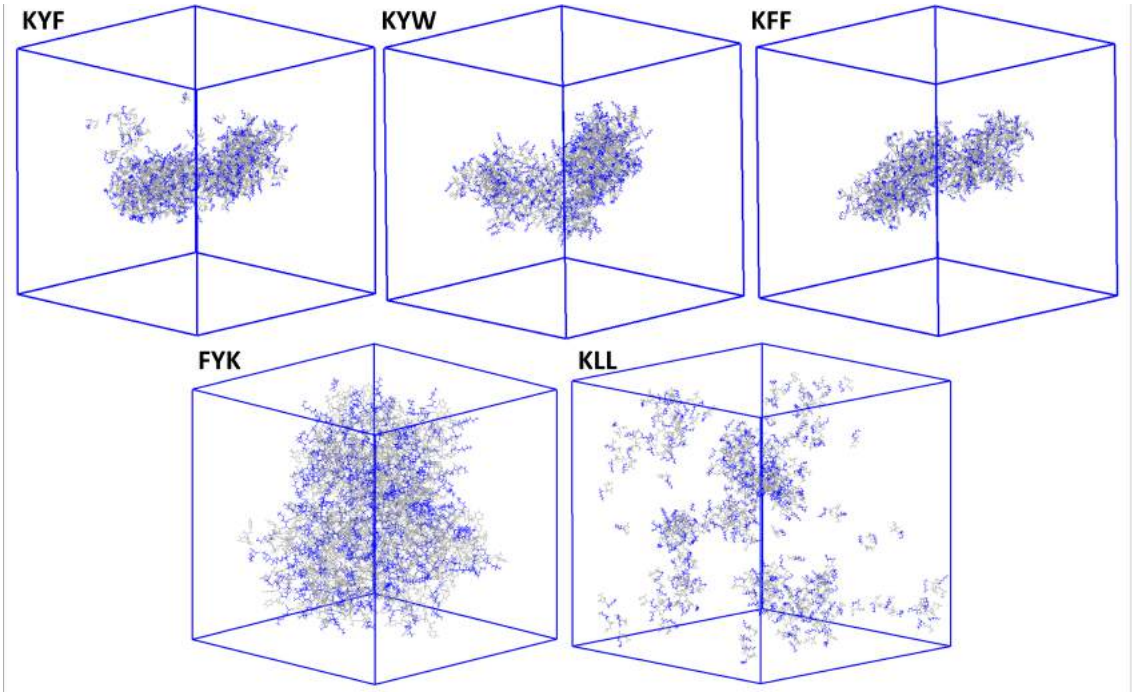

Figure 2.7: Initial backmapped structure from the final coarse-grain assembled structure after 9.6 μs

After the initial backmapping, has occurred, the structure was then subject to a 20 ns NVT (constant number of molecules, volume and temperature) simulation (Figure 2.8). During each of the simulations for KYF, KYW and KFF, it can explicitly be seen that the packed nanofiber structure begins to exchange peptide molecules. As a result, loss of definition of the fiber is observed over time. Although, in all cases after the 20ns simulation, there are remains of a fibrous structure suggesting that the coarse graining allows for a reasonable determination of the nanostructures, but the loss of finer interactions is integral to the stability of the assembled structure. For FYK, the structure of the spherical aggregate remains unchanged. This is potentially down to the lack of stabilizing interactions therefore the main driving force for this aggregation if the hydrophobic effect. Changes in the structure of KLL indicate that the KLL peptide molecules do not have an affinity to interact with each other. There remains a high degree of disorder between the peptides.

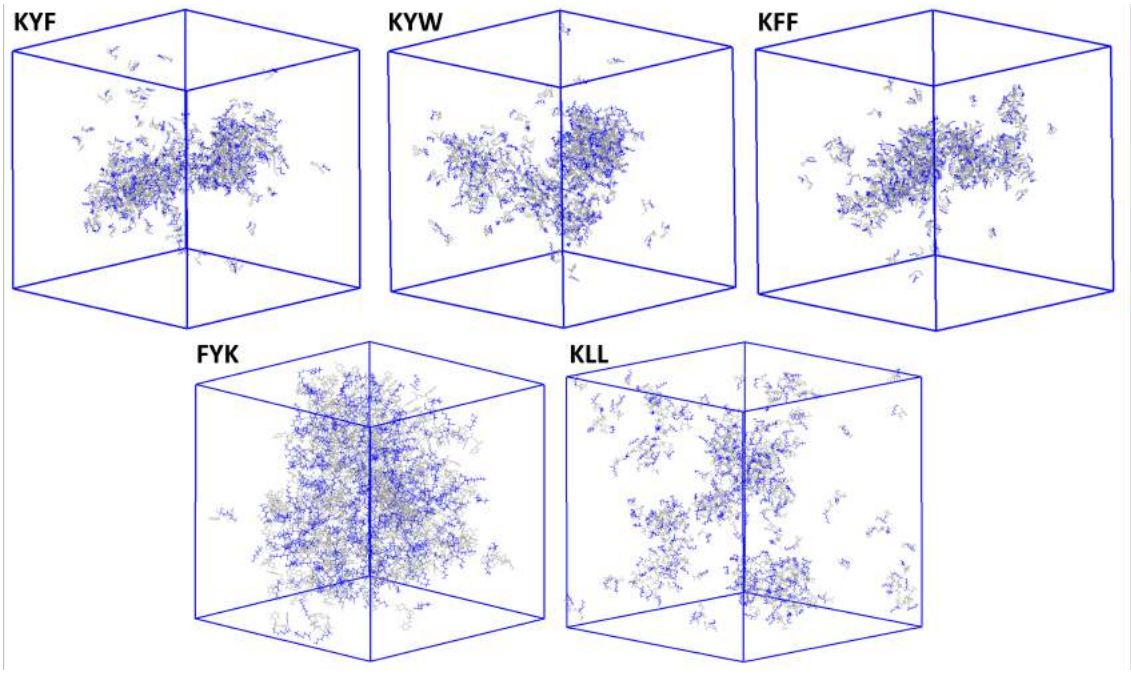

Figure 2.8: Atomistic simulations from the backmapped coarse-grained simulations after a 20 ns NVT simulation

Finally, in order to gain an insight into how these peptides change their conformations, analysis of a single molecule over a period of 50 ns was examined. In the case of a single monomeric unit of each peptide, no intermolecular interactions are present, therefore to understand the changes in conformation we focus on changes in dihedral angles. As we expect the hydrophobic effect to have a major influence in the self-assembly of the peptides, we primarily focus on CZ(Ar1)-CA(Ar1)-CA(Ar2)-CZ(Ar2) dihedral. Changes in the dihedral angle gives an indication on how the aromatic rings are situated in relation to each other. As shown in Figure 2.10A the distribution of the conformations differs depending on the chosen peptide. It is evident that from the populations there are two orientations that are preferred. At -135 degrees, the aromatic systems are extended on opposite sides of the peptide both, and therefore do not exhibit any type of intramolecular π-stacking (we refer to this as the *anti* confirmation) with each other whereas at 45 degrees, both aromatic systems are situated on the same side (*syn*) and can clearly adopt a π-stacking conformation. On comparison between the 3 systems, it is clear that KFF can adopt both *syn* and *anti* conformations in similar abundances. This might contribute to the observation

that KFF forms the weakest hydrogels as it is transitioning between two favored conformations, which result in less favored packing of the peptides, as more entropy would be lost upon assembly.

KYF shows less of an abundance to adopt the conformation at -135 degrees, with the most abundant population distributed between the -45 and 45 degree conformations. Therefore, KYF tends to adopt a *syn* conformation approximately 65% of time, which suggests this is a stronger conformation and therefore the resultant fiber formation (and consequently gelation) is favorable. KYW indicates a greater population in the *syn* conformation (~70%), which suggests that this could be an important parameter in determining if the peptide forms relatively stable fibers. This type of conformation was firstly observed in the observed crystal structures used by Gorbitz[62] (see Chapter 1, Figure 1.11). Later on, it was seen that by packing of FF examined by Gazit *et al*[7] showed similar conformations. In both cases, it was observed that the phenyl rings oriented into a *syn* conformation, where adjacent peptides interacted *via* π-stacking interactions. These conformations resulted in the backbone of the dipeptides orienting towards the core of the tubes. In addition, upon close examination of the favored conformations (Figure 2.9, Caption C) the lysine side chain rotates and interacts with the C-terminus. This suggests that the formation of the salt bridge that was observed in the FTIR is an intramolecular salt bridge. On inspection of the dihedral angles changes for FYK, it is clear that there is an affinity for the phenyl rings to adopt a similar *syn* conformation as seen with the previous peptides. However, the main difference observed for this peptide was the lack of the electrostatic interaction between the lysine and the C-terminus.

As the lysine side chain is situated at the amino acid position adjacent to the C-terminus. The lysine groups are unable to rotate effectively to interact. Therefore, this indicates why there is no presence of a salt bridge interaction in the FTIR. The lack of 'locking' the lysine group in place might suggest why a less ordered structure is observed. The positive charge on the lysine can freely rotate which can bring in steric implications as well as potential electrostatic repulsion. Measuring the dihedral angles between the leucine side chains for KLL indicate that KLL does

not have a preferential conformation. The peptide spends about 30% of its conformation time situated in different conformations. These observations indicate the importance of the presence of aromatic residues for peptide self-assembly.

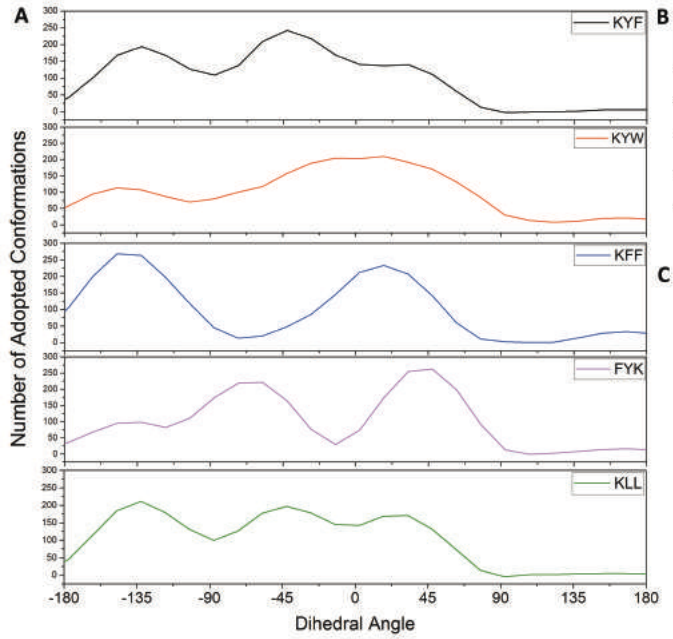

B

Dihedral Region	Percentage Abundance of Conformation (%)				
	KYF	KYW	KFF	FYK	KLL
-180 → -90	34.32	23.20	47.79	23.37	36.58
-90 → 0	44.01	36.48	17.78	33.46	37.64
0 → 90	21.11	36.34	30.59	41.03	25.08
90 → 180	0.56	3.98	3.84	2.14	0.70

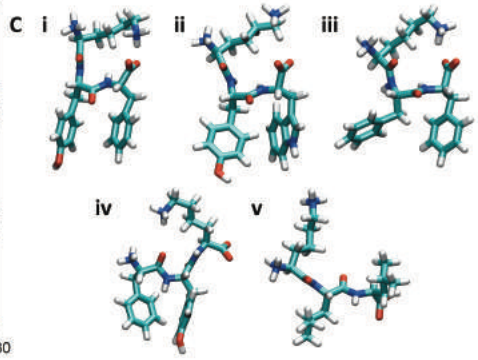

Figure 2.9: A) Graphical representation of the distribution of the aromatic-aromatic dihedral angle on a single peptide monomer. B) Percentage of area residing in 90° angles for each peptide C) most frequent found peptide conformation for i) KYF ii) KYW iii) KFF iv) FYK and v) KLL

2.2.3 Summary

In summary, a combination of experimental and computational techniques has lead to the discovery of the first report unmodified tripeptide capable of self-assembling into hydrogels in fully aqueous solvent. Using the design rules to predict which peptides have a high likelihood of hydrogelation. Analysis each of peptide has shown that changes in amino acid order and also the presence of aromatic residues are vital for the peptide ability to form supramolecular structures. Identification of key interactions, which promote the self-assembling process allowing these peptides to interact to form hydrogels, was vital. In addition, the use of computational methods, give a greater insight into examining the assemblies on the molecular level. CG MD has shown the self-assembly process at much greater timescales, with the use of backmapping procedures examine the

initial packing of the assembled structure Finally, analysis of a single molecule of each peptide has given insight into the conformational changes of the peptides. It has been identified that the π-stacking interaction is important but also the flexibility of the lysine to rotate and interact with the C-terminus is vital for promoting fibrous self-assembly.

2.3 Bilayer Peptide Assemblies

2.3.1 Experimental Analysis of Bilayer Tripeptide Assemblies

The design rules that were developed based on data obtained from Frederix *et al.*[124] indicated that aggregation propensity is enhanced in peptides with paired aromatics and paired charges. Thus, a subset of self-assembling peptides have negatively charge amino acids (D or E) located at the C-terminus combined with aromatic dyads. To explore this subset, the self-assembling properties of FFD, which follows these design rules, and the behavior of DFF, which does not, were investigated.

Upon dissolution of the peptide in water at a peptide concentration of 40 mM, it was evident that both peptides have poor solubility (Figure 2.10). Addition of 0.5 M NaOH to the undissolved peptide followed by constant vortexing and sonication for a period of 30 sec resulted in full dissolution of the peptide. Final pH measurement after dissolution gave a final pH of 7.4.

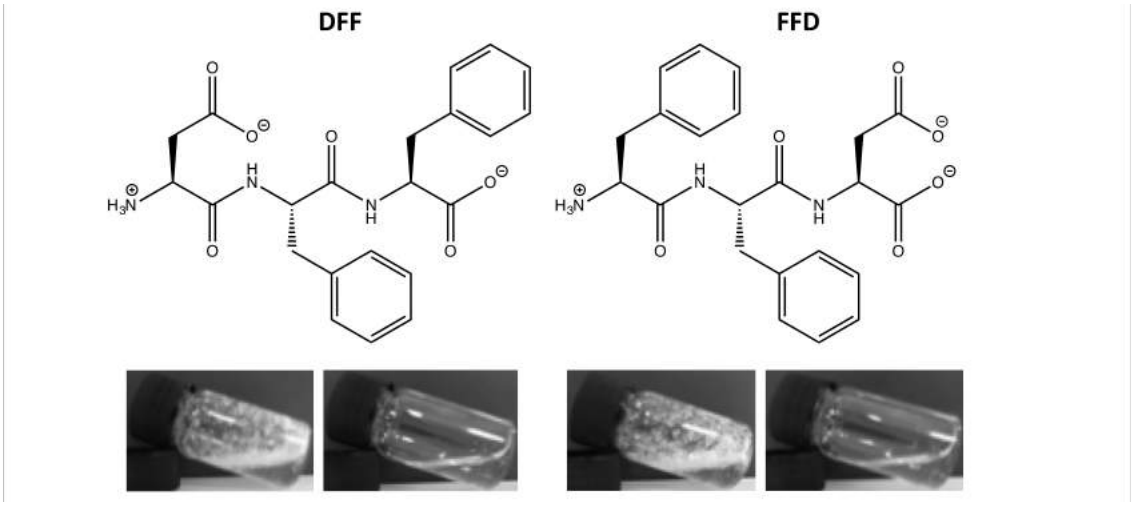

Figure 2.10: Structures of DFF and FFD and the macroscopic image upon dissolution in water and after pH adjustment to 7.4

2.3.1.1 Fourier Transform Infrared Spectroscopy

As both peptides were used at a final pH of 7.4, the final ionization of the peptide is expected to leave both aspartic acid side chain and the C-terminus deprotonated and the N-terminus protonated. To gain a better understanding of how the peptide interacts at this pH the resultant peptide solutions were examined *via* FTIR (Figure 2.11). Although there is no macroscopic difference between both DFF and FFD samples, small changes in FTIR spectra give an indication of the intermolecular interactions that are involved in the assembly of these peptides. Both peptides exhibit intense, broad peaks at 1580 cm^{-1}, which are associated with the deprotonated carboxylate. There is a slight difference in the intensity of the peaks between DFF and FFD. The sharpness of the peak that is observed in DFF could indicate formation of a salt bridge with the aspartic acid residue and the N-terminus. The most likely reason behind the presence of this peak is the proximity of the aspartic acid residue with the N-terminus. The C_β atom of the aspartic has the ability to rotate and freely interact with the N-terminus, without the presence of forming supramolecular nanostructures. The largest difference between these two peptides is seen within the amide I region. FFD exhibits a broad peak covering both 1625 and 1650 cm^{-1} regions. This suggests that there are no clear hydrogen bonded structures present within the FFD assemblies. On the other hand, for DFF the peak at 1649 cm^{-1} is more defined and therefore indicates that the carbonyl stretch on the backbone of the peptides induces some type of order. The presence of the peak at 1680cm^{-1} is due to residual TFA in the sample as a consequence of the synthesis procedure.

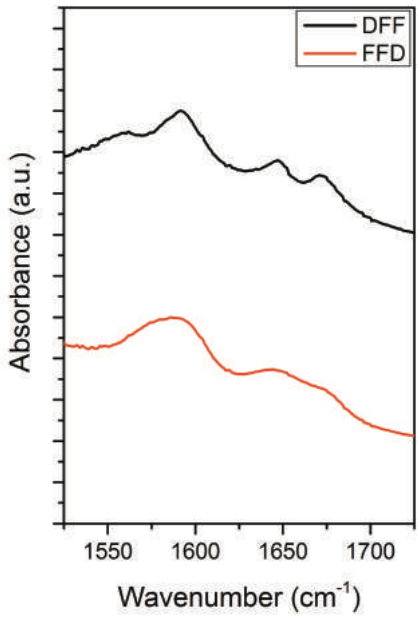

Figure 2.11: FTIR spectra of both FFD and DFF peptides in D_2O at pH 7.4

2.3.1.2 Transmission Electron Microscopy

Having determined the molecular self-assembling nature of the peptides, TEM is used to visually analyze the structures at the nanoscale. Upon visualization of the DFF, it was determined that a large amorphous aggregate was formed. This observation coincides with the spectroscopic techniques used as no define peaks are observed which indicate the presence of amorphous structures. On the other hand, FFD shows the formation of nanotubes. (Figure 2.12) These nanotubes can clearly be observed as the density of the structures change across the diameter of the tubes. These results do not fully compliment the spectroscopic results that have previously been mentioned as they form highly ordered structures. Upon the formation of these tubes, there is no hydrogen-bonding present within the nanotubes due to the lack of 1625 and 1649 cm^{-1} peaks in the FTIR. However, similar structures are observed for KLL with the FTIR spectra indicating the lack of ordered structures. This suggests that the main driving force for the formation of these structures is purely based on the hydrophobic effect. It would suggest that the phenyl rings of adjacent peptide interact via π-stacking. This creates a hydrophilic core to the nanotube with the backbone and the aspartic acid residues pointing into the core, similar to the observations found by Gazit and Gorbitz. However, differences observed from these assemblies are the rotation of the

aspartic acid groups to the center of the core. This assembly would not be seen by FTIR, as the peptides do not arrange themselves in a beta-sheet conformation so a random coil orientation is observed. The formation of the salt bridge is not observed as the aspartic acid residues will be directed out of the tube and unable to interact with the corresponding N-terminal amine so there can be no interaction.

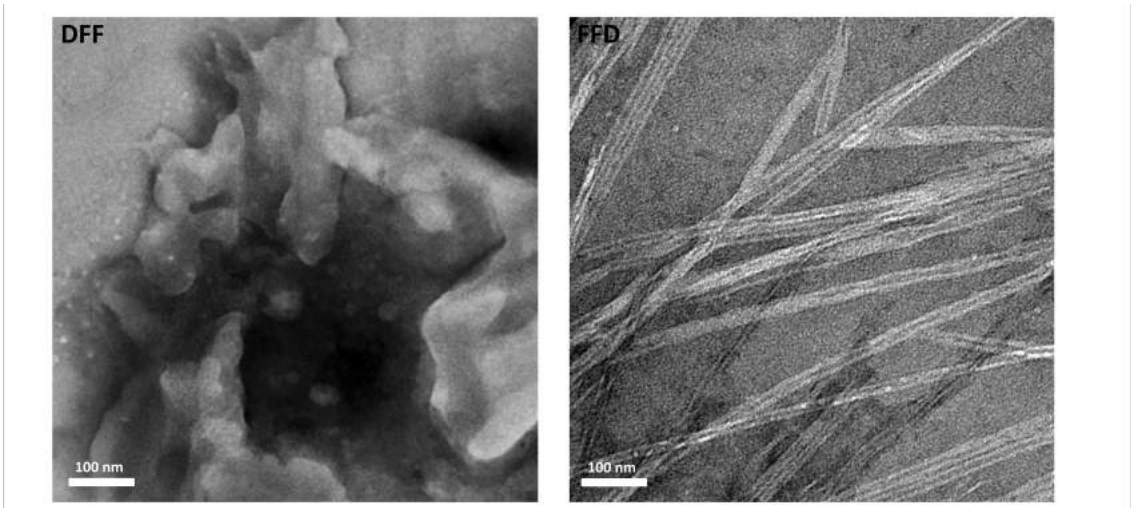

Figure 2.12: TEM images of DFF and FFD indicating and amorphous aggregate formed from DFF and nanotubes from FFD

2.3.2 Computational Analysis of Bilayer Forming Tripeptides

Similar to the approach that used in Section 2.2.2, extended coarse-grain MD simulations were employed to understand how these peptides assemble and what types of structures may be formed.

In this case, both peptides show similar nanostructures. Computationally, we observed the formation of bilayer-like structures (Figure 2.13). Similar to our hypothesis for the formation, the driving force is the hydrophobic effect where the phenyl rings aggregate together. As a result of the size limitations, the formation of nanotubes is not observed. These simulations are limited by the size of the simulation boxes and therefore extended systems would be difficult to achieve without the computational cost. In addition, the diameter of the tubes would be too

great to visualize without increasing the dimensions of the box, which increase the computational time and become more computationally expensive.

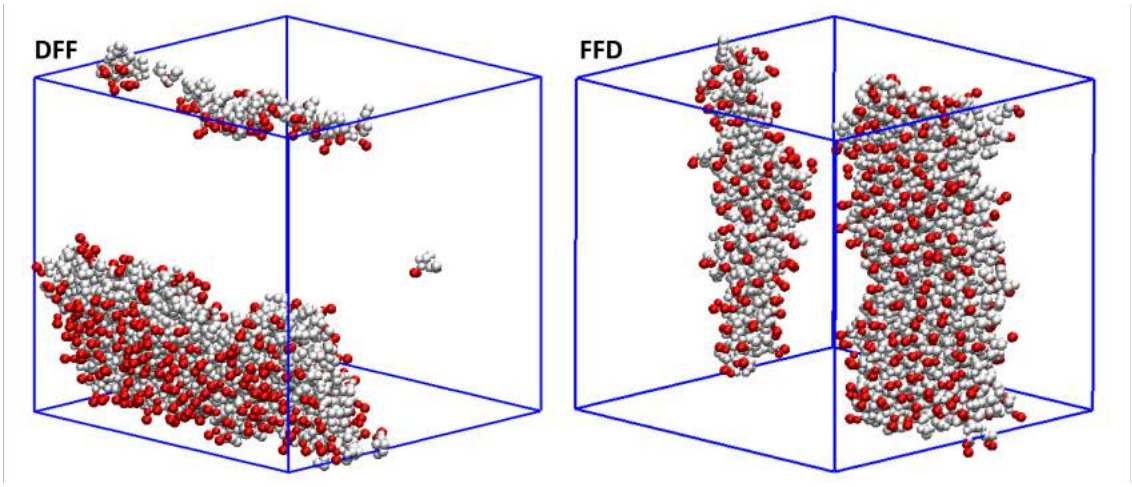

Figure 2.13: Coarse-grained molecular dynamic simulation of DFF and FFD showing the formation of bilayer-like structures after a period of 9.6 µs

Backmapping of these CG structures was carried to examine the stability of the peptides but also gain insight in the atomistic interactions. The assembled structures were successfully back-mapped to the atomistic representation and each structure was subject to a 20 ns NVT simulation.

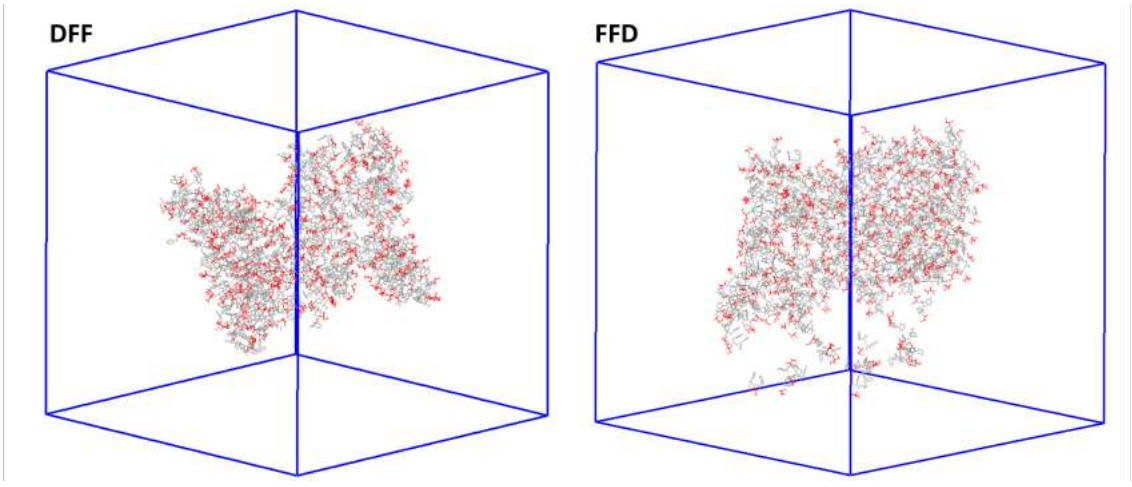

Figure 2.14: Initial backmapped structure of DFF and FFD from the final coarse-grain structure after 9.6 µs

It was evident that after the 20 ns NVT simulation the assembled were relatively stable indicated by the lack of disruption of the structure. (Figure 2.15) Although,

there is some exchange on peptides that occurs through the simulation the majority of the peptides remain undeterred. This is expected, as the spectroscopic analysis that was carried out showed no dependence on the hydrogen bonding interactions that peptides could undergo. The main driving force for each self-assembled structure was the hydrophobic effect and π-stacking. It can be clearly seen that the hydrophobic groups tend to still interact with each other *via* the π-stacking interaction, which is stabilizing the assembled structure.

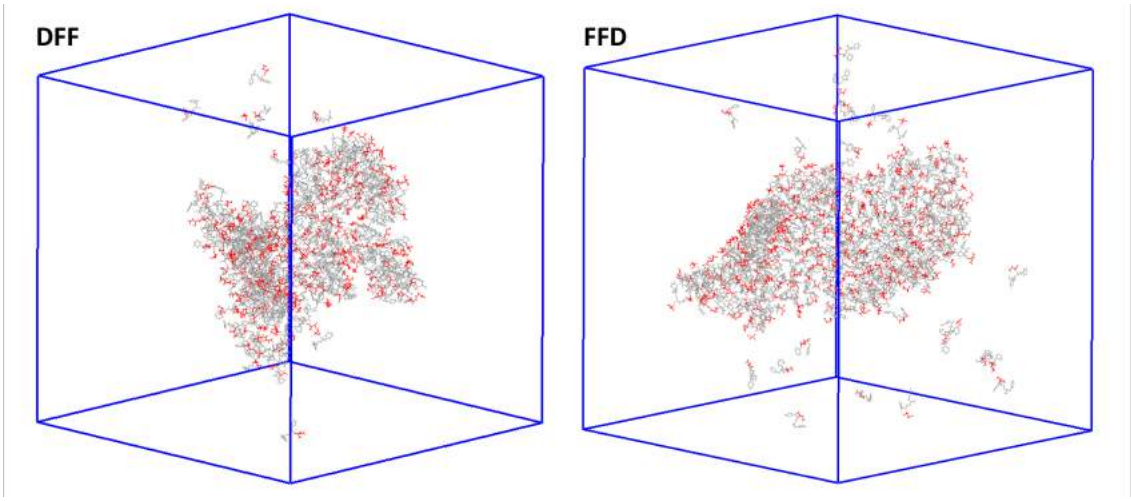

Figure 2.15:Atomistic simulations of the backmapped coarse grain structures of DFF and FFD for a period of 20 ns using the NVT ensemble

Finally, examination the conformational stability of a single monomeric unit of each of the peptide was measured. Focusing on a single monomer, the conformational changes that the peptide can go through can be identified and therefore a greater understanding of how the peptide side chains can pack together can be understood (Figure 2.16). In this case, we examine the dihedral angles between the phenyl rings. It is particularly significant in this case, as the hydrophobic effect drives the formation of these nanostructures therefore the positioning of the aromatic rings is crucial for the optimal packing of these peptides. It is clear that both peptides tend to adopt similar conformations where the dihedral angle between the two aromatic rings is in the region -45 to 45 degrees. This indicates that the peptide like to adopts the '*syn*' conformation that was similar to that observed for the fibrous assemblies (Section 2.2.3). As the

peptide adopt this *syn* conformation, this confirms the packing that was observed using the MARTINI force field. In addition, it is observed that there is a rotation of the side chain that has the aspartic acid. In the case of DFF, the aspartic acid rotates away from the core of the chain to reduce the negative repulsion that would be observed from interaction with the C-terminus. On the other hand, FFD rotates as to form a salt bridge with the N-terminus. These rotations may determine why one peptide assemblies into nanotubes whereas the other is an amorphous aggregate. The difference observed between the KXX peptides and DXX/XXD peptides is primarily down to the ionization state of the peptides. By altering the pH, changes in electrostatic interactions control the way the peptides can assemble, which results in the formation of fibers for KXX and tubes for XXD.

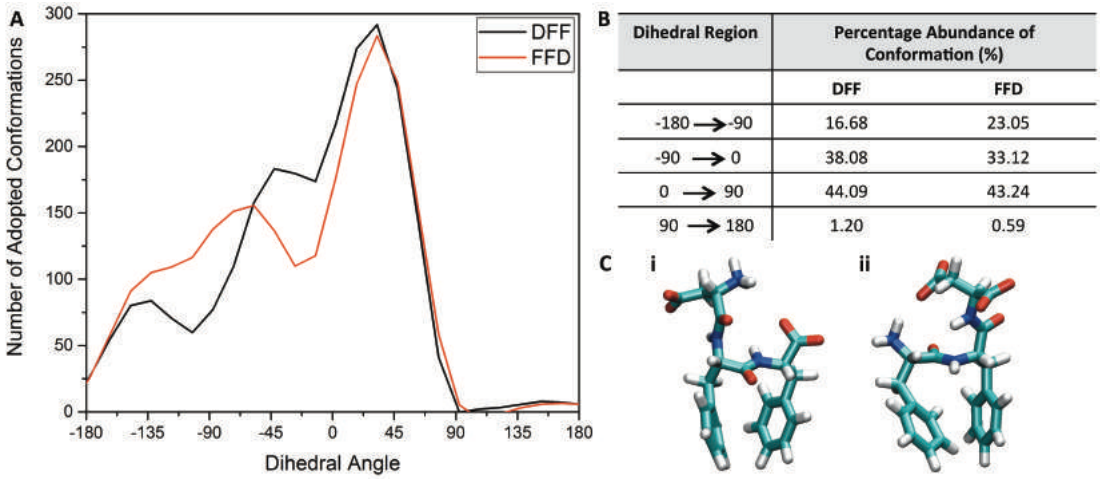

Dihedral Region	Percentage Abundance of Conformation (%)	
	DFF	FFD
-180 → -90	16.68	23.05
-90 → 0	38.08	33.12
0 → 90	44.09	43.24
90 → 180	1.20	0.59

Figure 2.16: Analysis of the single monomeric unit of the bilayer assembled nanostructures. A) Population of the number of times the peptide adopted a dihedral angle conformation B) percentage populations of dihedral angles in 90O sections C) most favored conformation for i) DFF and ii) FFD

2.3.3 Summary

In summary, we have shown that introduction of anionic amino acids in tripeptides can give different types of nanostructures compared to those observed for cationic amino acids. Although these peptides adopted similar structures as a single monomer, upon assembly in large nanostructures these peptides alter the conformation resulting in two different types of assemblies, amorphous aggregates and nanotubes. It is clear that although no spectroscopic evidence was available to see the differences in these nanostructures, the macroscopic evidence is there to

conclude that the design rules can determine how efficient the amino acid position is for the prediction of self-assembling nanostructures.

2.5 Conclusions

In conclusion, using the design rules that were stated in Frederix *et al.* we have identified the first reported unmodified tripeptides hydrogels. Using a combination of experimental and computational methods, we have been able to understand the conformation of the peptide is important for the peptide ability to assembled into it supramolecular structure. We have seen that the presence of aromatic groups is key for peptides to aggregation but also the additional interaction that is allowed with the use of aromatic rings enhances the peptide ability to assemble. The location of the charged amino acids has also been vital for the peptides ability to assemble. With the cationic amino acid situated at the N-terminal position hydrogelation is promoted with the lysine group interacting with the carboxylate. With the lysine groups situated at the C-terminal position, this interaction is not possible and therefore no hydrogelation is present. Furthermore, we also identify that anionic amino acids have a preferable position on the peptide chain. We determine that with anionic amino acids at the C-terminal position, the side chain can rotate and interact with the free amine similar to the cationic peptides. Although there is no hydrogelation observed for peptides with DXX/XXD ordering, the formation of different nanostructures allows us to enhance our understanding of the main driving forces for tripeptide self-assembling. The differences in structures obtained, allows us to exploit the different properties for each peptide, which can give rise to industrial applications, which are discussed further in Chapter 3.

2.6 Materials and Methods

2.6.1 Synthesis of Tripeptides

All samples were prepared using the solid phase peptides synthesis procedure. Preloaded wang resins were acquired from Novabiochem, now Merck Chemicals. Each synthesis carried out using 1g of preloaded resin. The resing were swollen for 15mins with DMF, 1mins DCM and 15 mins DMF. After the resin had been swollen, 20% piperidine in DMF was added for a 5min wash before a further 15mins to cleave the Fmoc protecting group. This stage was followed by solvent washes to remove any excess substrates. The addition of the first amino acid in DMF was carried out in three times excess. In addition, HBTU three times excess and DIPEA six times excess was added. The mixture was left on an orbital shaker for 3 hours. After this time, the sample was washed repeated using DMF and DCM to remove any unreacted substrates. This is followed by another 20%in DMF wash to cleave the Fmoc. The sample procedure is repeated until the target peptide is obtained. One the last coupling step has been achieved; the sample is washed with diethyl ether and left to dry overnight. The dry resin is transferred into a 50mL falcon tube and 95% TFA, 2.5% H_2O, 2.5% Triisopropylsilane (TIS) is added. The mixture is left on the orbital shaker for 3 hours to cleave the resin. Once cleaved, the mixture is filtered and the resultant solvent is removed under high vacuum to leave a sticky residue. Cold diethyl ether is then added to precipitate the target peptide, which is stored in the fridge.

2.6.2 Sample Preparation

Initial investigations of the self-assembling ability of the peptides were carried out using peptide synthesized in house. Further investigations were carried on the peptides using peptide purchased from Bachem Ltd. Each peptide was purchased at a purity of >98%.

Peptide samples were prepared at a peptide concentration of 40 mM. The dry peptide was weighed at placed in glass vial. To this vial, 1 mL of millipure water was added and the pH recorded. The pH of the peptide solution was adjusted using 0.5 M NaOH. After addition of NaOH, the vial was inverted three time before 10 sec

of bench top swirling. The peptide solutions were left in the fridge for a period of 24 hrs before analysis.

2.6.3 Fourier Transform Infra-red Spectroscopy (FTIR)

FTIR spectra were acquired using a Bruker Vertex70 spectrometer with a spectral resolution of 1 cm^{-1}. Spectra were obtained by averaging over 25 measurements for each sample. Measurements were performed using standard FTIR cuvettes (Harrink Scientific) where the sample was sandwiched between 2 CaF_2 discs (Crystran Ltd) separated by a 50 μm PTFE spacer.

For gel materials, a small amount of hydrogel was placed between two CaF_2 discs using a microspatula, separated with a 50 μm spacer. For free flowing samples, 100ul of the sample was pipetted directly onto the disc. D_2O was used as the solvent.

2.6.4 Transmission Electron Microscopy (TEM)

Carbon-coated copper grids (200 mesh) were glow discharged in air for approximately 30 secs. The grids were placed on the gel material of liquid solution before being blotted down using filter paper to remove the excess. 20 uL of negative stain was applied (1% aqueous methylamine vanadate obtained from Nanovan, Nanoprobes) prior to a further blotting using filter paper. Samples were then left to dry. The dried samples were then imaged using a LEO 912 energy filtering transmission election microscope operating at 120kV fitted with 14bit/2K Proscan CCD camera. TEM imaging was carried out at the University of Glasgow.

2.6.5 Rheology

Assessments of the mechanical properties were carried out on a strain-controlled rheometer (Bohlin C-CVO) using a parallel plate geometry (20mm) with a 0.5 cm gap. An integrated temperature controlled was using to maintain the temperature of the sample stage at 25°C. to ensure that measurements were carried out with the viscoelastic region, an amplitude strain sweep of the sample was carried out, which show no variation in elastic modulus up to a strain of 1%. The strength of

the hydrogels were measured as a frequency function, where the frequency sweep was carried out on a range between 0.1 to 100 Hz. These measurements were repeated at least three times to ensure repeatability. An average of the linear regions of the G' region was taken to give an approximate gel strength.

2.6.6 Coarse-Grain Molecular Dynamics

Molecular dynamics simulations were performed in GROMACs using the MARTINI force field version 4.5.3.

A single atomistic tripeptide molecule was converted to the coarse grain representation using the martinize.py script. 300 molecules of the chosen coarse-grained tripeptide was added to a box with the dimensions 12.5 x 12.5 x 12.5 nm using the genbox command. The simulation box was then solvated using standard CG water. Using the genion command in Gromacs, the system was neutralized with the addition of sodium or calcium ions. The MD system was then subject to a minimization for 5000 steps to ensure no overlap atoms. Once minimized, the system was subject to production run of 9.6 μs.

2.6.7 Atomistic Molecular Dynamics

A single peptide molecule is prepared using Avogadro and saved as a pdb file. The peptide molecule is then solvated in TIP3P water giving a box dimension where there is a minimum of 10 Å from the edge of the peptide to the side of water box. This is to ensure that the peptide does not interact abnormally. Ions are added to the water box to neutralize the charge. The simulation box is then subject to a short 1 ns NPT simulation to minimize back contacts between peptide and water. At this point the density of the water is check to ensure there are no void formed in the simulations box. The system was then subject to a 50 ns NVT production run.

3.

Tri-peptide Emulsions with sequence-encoded properties

* This work was published in part as: **G. G. Scott**, P. J. McKnight, T. Tuttle, R. V. Ulijn; Tripeptide Emulsifiers; *Adv. Mat.,* **2016**, *28*, 1381-1386

Declaration of contribution to published article: Any reproduced practical work from the aforementioned published article; I was solely responsible for, unless otherwise stated.

3.1 Introduction

3.1.1 Emulsions

Emulsions are defined as a dispersion of two immiscible liquids.[128] It is typical that one liquid is aqueous-based and the other is organic. The organic phase is normally referred to as the oil phase but this term is not generally correct, as it does not have to be oil in the conventional sense, other than it must be immiscible with the water phase. Two types of emulsions can be distinguished: oil-in-water and water-in-oil.[129-130] Oil-in-water emulsions are by far the most common types of emulsions and can be found in many different households or industrial applications such as paints, glues, agrochemical formulations, *etc*.[131-134] Examples of water–in-oil emulsions can be found in spreads, such as margarines.

In order to create stabilized emulsions, the presence of an emulsifier is required. An emulsifier is classified as a substance that reduces the interfacial tension created between two immiscible liquids to give a dispersion of droplets.[130] There are many different types of emulsifiers and each type can be utilized in various scenarios, depending on the outcome that is required. These emulsifiers range from traditional fatty acid based amphiphiles, polypeptides, copolymers to solid particles; they will be discussed in later sub chapters.

If oil is dispersed in a water solution without the presence of emulsifiers there are several outcomes that the emulsion can go through before full destabilization (Figure 3.1). Depending on the density of the oil, it can rise to the surface or sink to the bottom. These phenomena are called creaming and sedimentation.[129-130] Most common oil phases have a lower density compared with the aqueous phase; therefore the creaming mechanism is more common than sedimentation. Another scenario that may destabilize an emulsion is flocculation. This occurs as it is a secondary minimum state where the emulsions is energetically stable where the droplets can be close together without losing structural integrity.[129-130] All these processes are reversible mechanisms and the original state can be achieved with the application of high shear or application of heat. If either of these processes

occurs, the next stage of emulsion destabilization is coalescence. This is a destructive mechanism and involves the fusion of individual droplets into a single droplet, which is an irreversible process.[130]

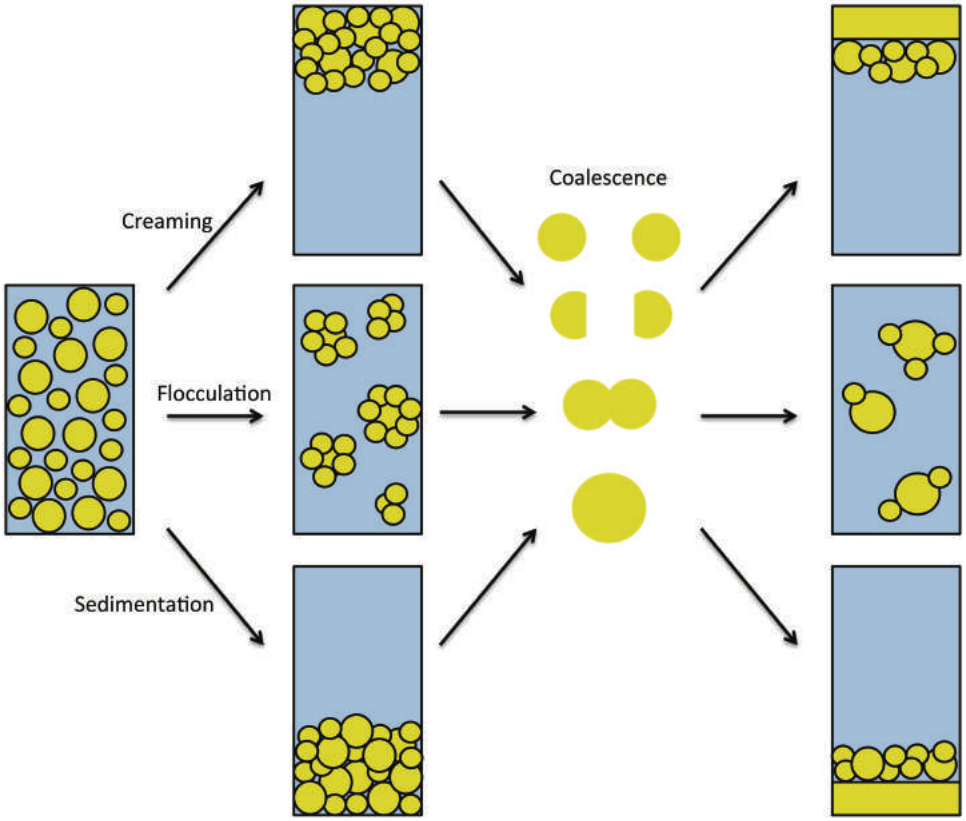

Figure 3.1: Schematic illustration of the mechanisms for destabilization of emulsions

3.1.2 Emulsifiers

Traditional, surfactant-based emulsions have applications in the food, cosmetic, encapsulation, and materials industries.[135-142] The majority of the surfactants that are currently in use are based on lipids that are extracted from natural sources. However, other surfactants, based on polypeptides, copolymers and solid particles (Pickering emulsions) all have applications (Figure 3.2). The process by which traditional amphiphilic surfactants stabilize biphasic mixtures by interfacial assembly and the consequent reduction of surface tension is well understood, as outlined in the previous section. Although these surfactants are well-suited to stabilize emulsions, they are not always biocompatible or biodegradable. In

addition, they may not have sufficient stability at elevated temperatures or extremes of pH,[143-147] which can limit their utility in a variety of applications. Therefore, it is desirable to identify a class of surfactants that can be tailored to match the application for which they are used.

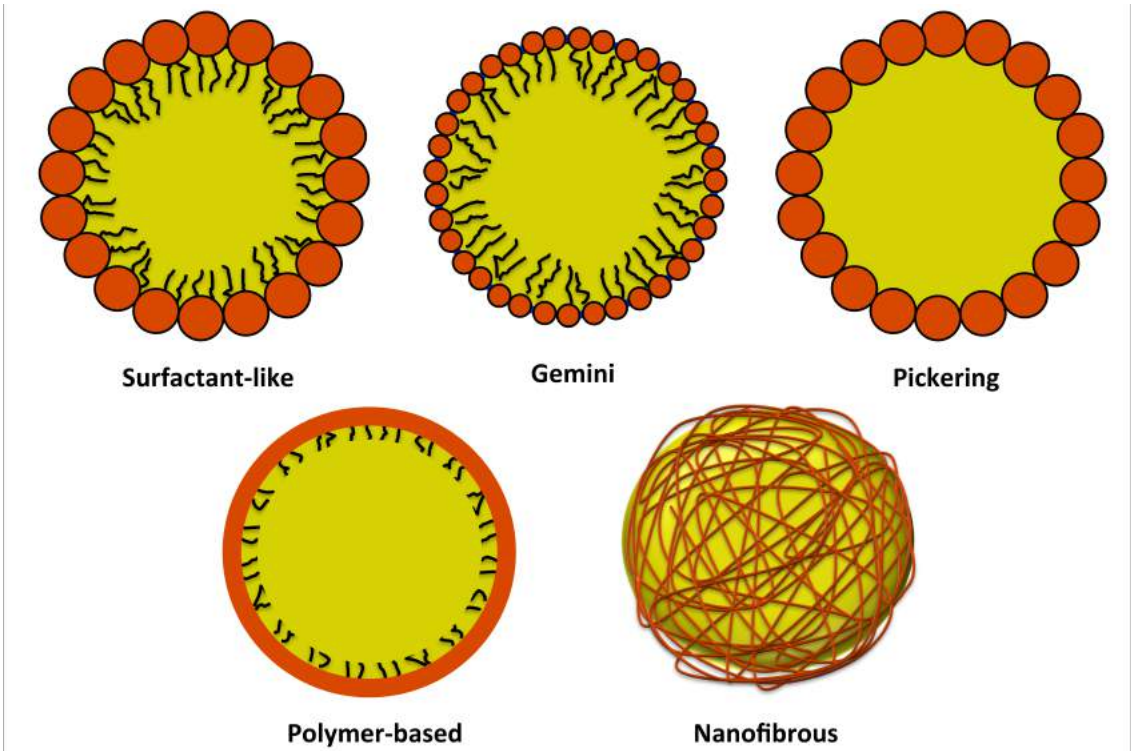

Figure 3.2: Emulsions based of different types of emulsifiers

Surfactant-like Emulsions

Traditional surfactants are primarily composed of a hydrophilic head group with one or more hydrophobic tail(s). In naturally occurring systems, the hydrophilic head is normally based around the structure of glycerol, the three branches allow for modification for the head groups as well as the tails. The tails consist of long chain aliphatics normally associated with fatty acids. Surfactants have the ability to diffuse through the solution and assemble at the interface between the water and oil (Figure 3.3, A). These types of surfactants can be derived from many different types of sources such as animals, plants, *etc*.

Gemini Surfactants

Gemini Surfactants are similar to traditional surfactant with the difference that there are 2 separate hydrophilic components to each of the surfactants. Each of these hydrophilic heads are joined by a linker group. The term 'Gemini' surfactant was first coined in 1993 by Menger *et al.,*[148-149] where they describe the importance of a rigid spacer between the two hydrophilic groups. The role of the spacer group is to provide a barrier between the hydrophilic groups. If this spacer was short and flexible, the rotation around the spacer would allow the chains to interact with each other leading to the typical miceller formation. This allows for different arrangements of these surfactants giving rise to a number of different types of emulsions. Concurrently, Rosen *et al*[150] demonstrated the use of the flexible spacers, which was shown to reduce the interfacial tension between the two phases by 3 orders of magnitude. This suggests that the double surfactant effect is substantial and has been associated to the distortion of the water structure by the two hydrophobic chains. Since the development of these Gemini surfactants interest has grown, allowing for the development of new emulsions.

Pickering Emulsions

The term 'Pickering Emulsion', refers to a type of emulsions described by S. U. Pickering[151] who reported a case of oil-in-water emulsions stabilized by solid articles absorbed at the interface. However, 4 years earlier, Ramsden[152] reported the ability of solid particles to adsorb to air-water interfaces. Pickering emulsions can stabilize both types of emulsions by the use of solid particles instead of surfactant-like molecules (Figure 3.2, C). The stabilization of emulsions by solid particles brings about specific properties in the emulsion. The strong adsorption of the solid particle to the interface creates a stronger emulsion. In addition, the use of solid particles has much improved qualities in industries such as pharmaceuticals and cosmetics as the surfactant free emulsion removes the adverse effects that the presence of ionic surfactants can have. It was deemed that these particles contributed to foaming and they could also be separated out giving a solid layer at the surface of water. Although, there was much discussion about the first discovery, these particles were classified as organic particles called 'proteids' and therefore are much softer than the particles used by Pickering.

There are many applications and reported cases of the use of Pickering emulsions.[153-160]

Polymer based Emulsions

Polymer based emulsifiers are primarily used in the cosmetic industry for industrial applications.[161-163] Block copolymers, which consist of alternating hydrophilic and hydrophobic blocks, behave in a similar fashion to that of low-molecular weight surfactants. Research based on this type of assembling systems was developed in the mid 1960s by work carried out by Molau *et al.*[164] in these publications it was identified that the colloidal aspects of these systems were important. This led to an increased research demand resulting in a number of new papers being published.[165-169] Reiss and Labbe[170] published an excellent review based on block copolymers for emulsion stabilization that examines the different types of copolymers and the substituents that change the emulsions' stability.

Peptide based Self- Assembly for Emulsification

Short peptides and derivatives thereof have also been explored as surfactants and emulsifiers. For example, Zhang *et al*.[171] first described short peptide sequences composed of block-like sequences of hydrophobic and hydrophilic amino acids, giving rise to designer peptide surfactants of approximately 6-8 amino acid groups long. Although, emulsifying capabilities were not sought the formation of amphiphilic peptides, which resembles surfactants, can be utilized for this purpose. Santoso *et al*[172-173] (Figure 3.3) examined further the behavior of hepta- and oct- peptides with the base sequence of 6 hydrophobic groups to 1/2 ionic. In this work, they examine how these peptides have the ability to assemble into nanotubes and nanovesicles arranging in a head-to-tail configuration, which is similar to the observations of surfactant based emulsifiers however with the potential for additional H-bonding between the peptide backbones to further stabilize these structures.

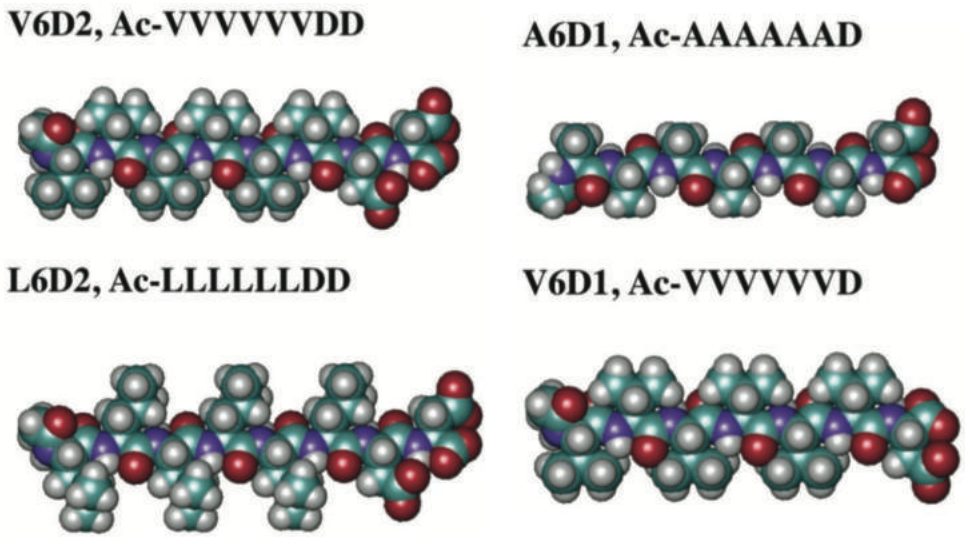

Figure 3.3: Structures of 4 different types of surfactant-like peptides. Adapted with permission form the National Academy of Science. Copyright (2001)[172]

Work in the Ulijn group recently demonstrated that aromatic peptide amphiphiles (Fmoc and pyrene peptides) are able to stabilize emulsions by the formation of nanofiber networks at the oil/water interface.[174] They demonstrated that these fiber networks are able to stabilize organic droplets (chloroform) within an aqueous solution formed upon brief shaking of the organic/water/peptide mixture by hand, showing enhanced stability compared to SDS.[175] The formation of interfacial nanofibrous networks, rather than a surfactant bilayer provides a distinctly different way to stabilize emulsions.

In this chapter, two types of self-assembling structures were focused on to determine the potential for short peptides to stabilize emulsions. Three peptides, which have shown fibrous morphologies (KYF, KYW and KFF) and two peptides, which show bilayer-like morphologies (FFD and DFF), were examined. In all cases, emulsions were formed using water and rapeseed oil, which is commonly used in the food industry. These emulsions were subject to 10 seconds of homogenization before a 24 hour period of rest before examination.

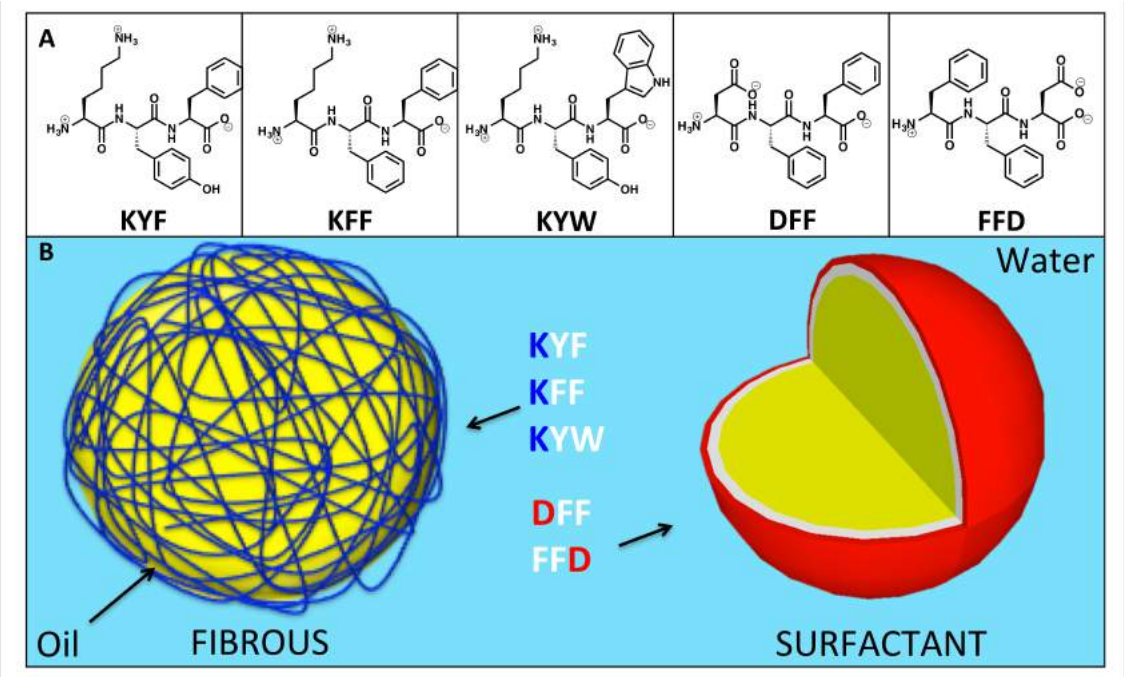

Figure 3.4: Overview of Tripeptide Emulsifiers

In order to clarify the main objectives that will be discussed in the this chapter, the following aims will be delivered:

1. Develop new emulsifiers based on unmodified tripeptides
2. Examine the structural and physical differences between fibrous and surfactant-like emulsifiers
3. Measure and compare the thermal stability between fibrous and surfactant-like emulsifiers

3.2 Fibrous Peptide Emulsifiers

3.2.1 Computational Predictions

As mentioned in Chapter 2.2, KYF, KYW and KFF have the ability to form fibrous nanostructures. An initial screening *via* computational methods was explored to determine the likelihood of peptide aggregation. Using these same methods, the introduction of 10% octane into similarly aqueous simulation was carried out to identify how the peptides interact between the two phases. Octane was used as the hydrophobic solvent instead of octanol, which is primarily used in atomistic simulations, as it gives a strong separation from water.

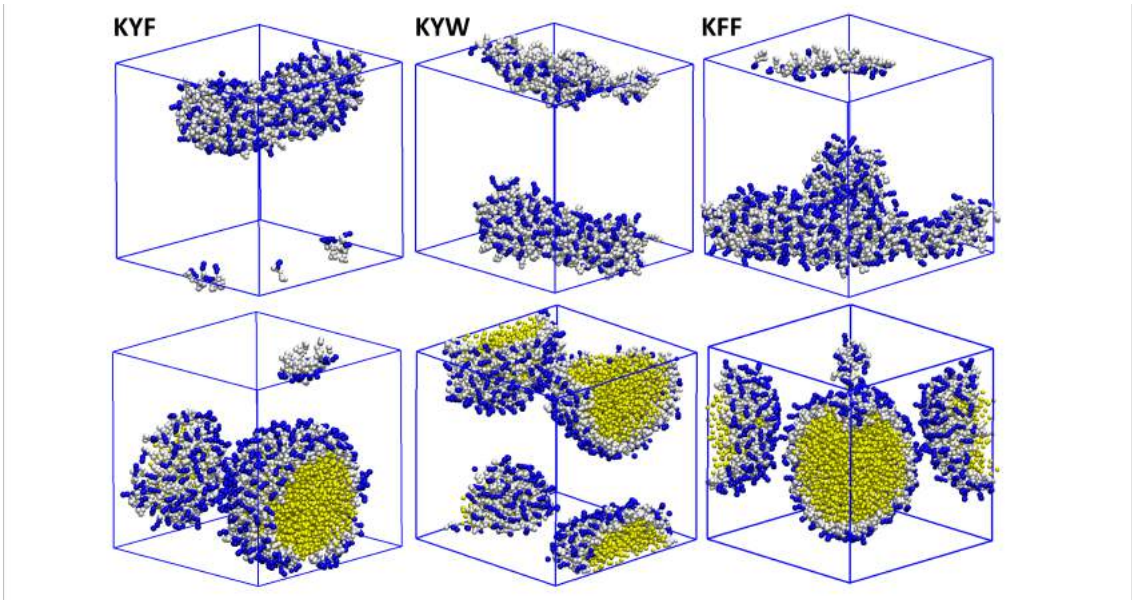

Figure 3.5: Coarse grained simulations of three chosen fibrous assemblies showing their self-assembled structures in aqueous media and their emulsified assembly

On commencement of the biphasic simulation, in all cases the octane aggregates into individual droplets. Peptide molecules are situated at the water/oil interface thus showing the amphiphilic nature of the peptides where they both contain hydrophobic and hydrophilic groups (Figure 3.5). The hydrophobic aromatic group, Tyr, Phe and Trp and located in the oil phase with the hydrophilic Lys groups on the surface of the water. As the simulation progress, the individual oil droplets coalesce into one larger droplet. This is expected, as due to the size

limitations of the box and concentration of peptide molecules the most stable state for the oil droplet to coalesce into is a single droplet. On inspection of the droplets formed, it is evident that each of the simulations produces approximately spherical oil droplets, which is evidence that the peptides have a strong interaction with the interface. To explore these systems further, we expand the dimension of the box to 25 nm^3 to examine how the introduction of more molecules can influence the emulsifying behavior, while keeping the concentrations constant.

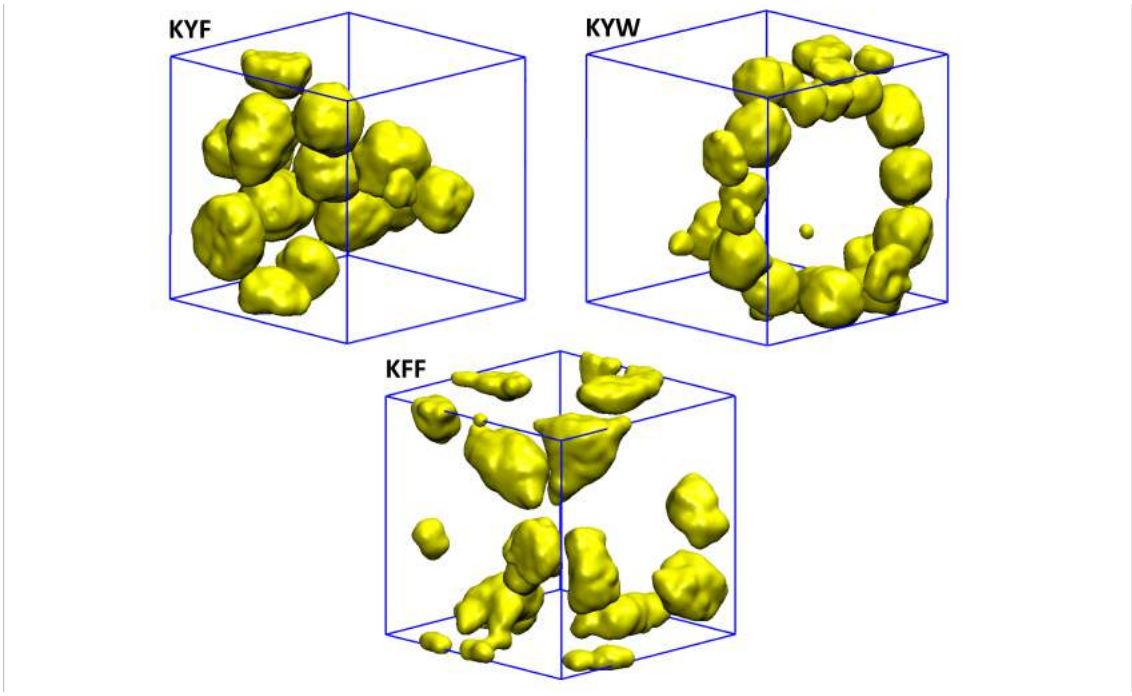

Figure 3.6: Larger coarse-grained simulations of fibrous peptide KYF, KYW and KFF indicating their stability of forming oil droplets. Peptide molecules removed from figure to give clearer image of the morphology of the oil droplets

Increasing box sizes allow for a closer examination of the formation of stabilized oil droplets. As can be seen from Figure 3.6, all simulations show an increased number of oil droplets. At the commencement of the simulation multiple oil droplet areas formed, and small droplets begin to coalesce into larger droplets. Early on in the simulations (*ca*. 1 μs) the simulations are stable and the droplets do not coalesce into larger droplets. This indicates that the peptides have created a stable barrier between the oil and the water and therefore, a stable emulsion is created. In addition, the simulations suggest that KYF is the most stable, followed

by KYW and finally KFF. This conclusion arises by focusing on the shape of the droplets. KYF droplets display a more homogenous size distribution where all droplets are approximately the same size and shape. Comparing these observations with KYW, the size distribution of the droplets has increased, and a further increase is observed with KFF. These observations led us to believe that KYF would provide the most stable emulsion, whereas KFF would be the weakest.

3.2.2 Experimental Validation

Succeeding the computational analysis of the fibrous peptides for emulsification, experimental techniques were used to validate the predictions. It was determined in Chapter 2 that the most suitable peptide concentration for the formation of nanostructures was 40 mM. 40 mM peptide solutions were prepared; the addition of 100-µL rapeseed oil followed by 10 secs of homogenization resulted in homogeneous emulsions (Figure 3.7). In order to examine the structural assemblies of the peptides at the molecular level situated the water/oil interface, FTIR was used to compare between aqueous and emulsion systems.

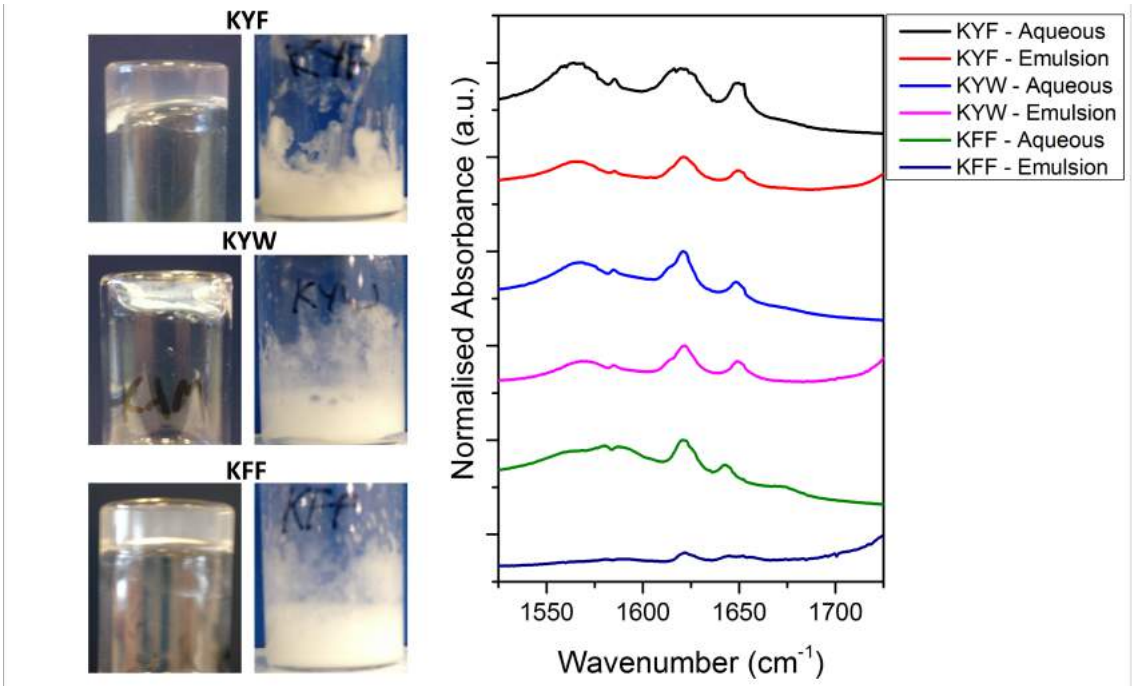

Figure 3.7: Macroscopic images of KYF, KYW and KFF in both the aqueous state and the emulsified state, In addition with the comparison of the FTRI between the two systems.

First impressions of the formed systems indicate that all three peptides form homogeneous emulsions. On inspection of the FTIR, similar FTIR spectra are observed on comparison with the aqueous assemblies. These suggest similar hydrogen bonding patterns are forming in the emulsified sample compared to the aqueous gels. Subtle changes in the FTIR spectra are observed, a dampening of all the peaks in the emulsion spectra are observed which can be associated with reduced relative concentration of the peptides due to the presence of the oil. KYF and KYW show near-identical traces between the aqueous and emulsion sample. Intense peaks at 1625 and 1649 cm^{-1} show hydrogen bonded structures are key in forming these nanostructures and therefore play a role in the stabilization of the emulsion. The similarities between the aqueous state and the emulsified state indicate that the similar structures (nanofibers) are formed.

KFF shows more significant changes with the intense hydrogen bonding peaks dissipating. This indicates the interactions involved in forming KFF are breaking up upon emulsification. A weaker emulsion is therefore observed. The lack of additional peaks on the FTIR spectra indicates that the former is most likely. For all emulsion samples an increase in absorbance is observed at higher wavenumbers ($\sim$1725cm^{-1}) this increase is due to the rapeseed oil itself, which does not interfere with any of the key areas within the amide I region.

In order to visualize emulsion droplets, microscopy techniques are applied. Fluorescence microscopy with an added dye is used to examine the droplets formed in the emulsification process. Two types of dye can be utilized for the visualization of emulsion droplets, FITC and Sudan II. FITC is a water-soluble dye, which causes illumination of the water phase upon excitation. Sudan II is an oil-soluble dye, which illuminates the oil phase upon excitation. In this work, as oil droplets are forming, the Sudan II dye was used.

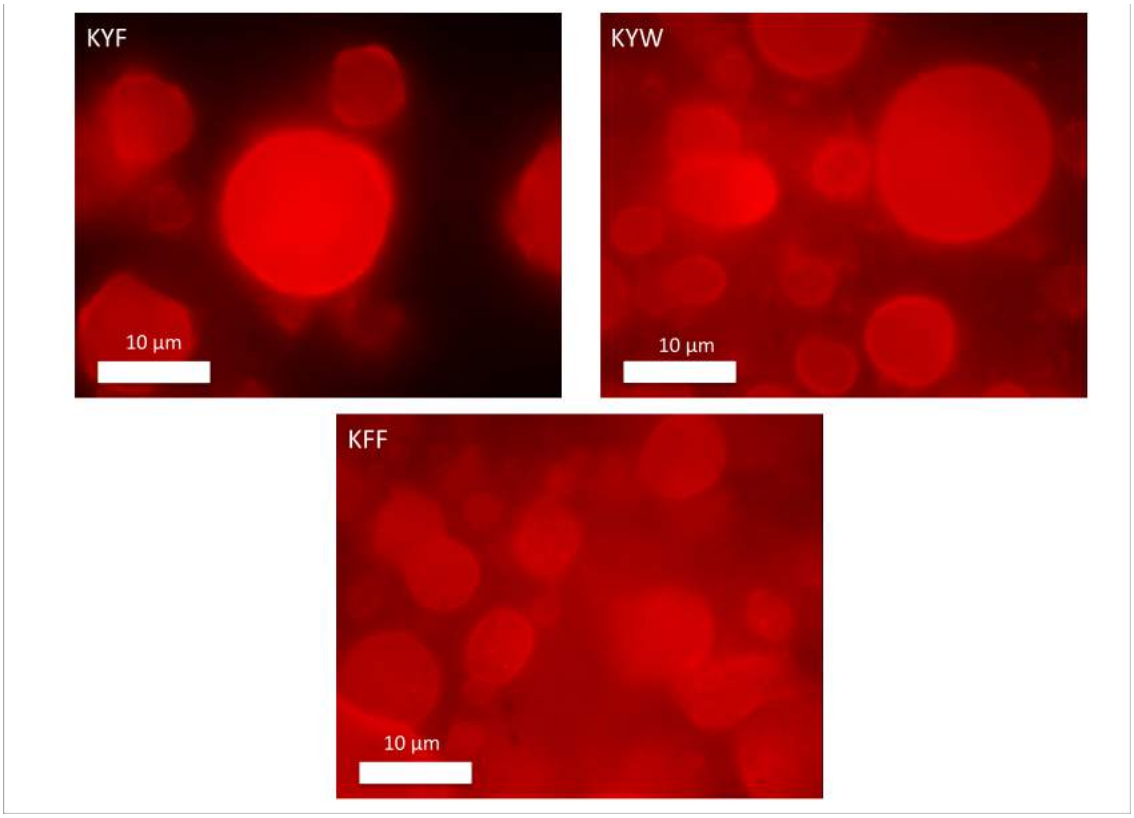

Figure 3.8: Fluorescence microscopy of emulsions stained with Sudan II dye

On excitation of the dye, stabilized oil droplets are observed. KYF shows large spherical droplets with an approximate size of 8 µm (Figure 3.8), compared with KFF (~5.8 µm) and KYW (~5.2 µm). For KFF, droplets are observed but the clarity of the droplets is poor with the oil phase leaching out of the emulsion droplets making it difficult to visualize. The leaching process occurs when the droplets are weakly stabilized and the droplets begin to coalesce. Leaching is observed in KYW but not to the same extent as KFF, with very little observed for KYF. As a result, these observations follow the hypothesis that KYF forms the most stabilized emulsions.

In addition, Thioflavin T staining can be used to examine the formation of β-sheet structures.[176-177] On the formation of β-sheets, there is an increase in fluorescence, which is not observed with any other assembly (Figure 3.9). The use of microscopy can determine the location of these assemblies and identify if the emulsions are stabilized by nanofibers.

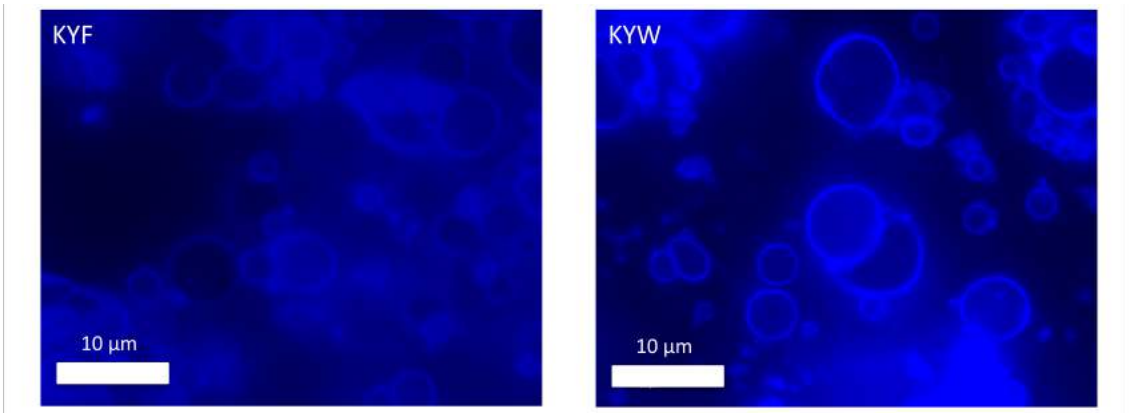

Figure 3.9: Fluorescence microscopy of emulsions stained with Thioflavin T

For both KYF (3-5 µm) and KYW (3-6 µm), Thioflavin T fluorescence is observed in both systems. . As the illumination of the Thioflavin T is localized to the water/oil interface, this indicates that we have the formations of β-sheet-like structures at the interface, suggesting the presence of nanofibers at the interface, which is therefore in fact stabilizing the emulsion. KFF did not show exhibit defined Thioflavin T signals indicating minimal β-sheet-like structures in this system. Therefore, the assembly of the nanofibrous networks when KFF is used is not significant, resulting in a weak emulsion.

Determining the thermal stability of emulsions is an important parameter for the manufacturing and processing of emulsions across a number of industries, especially within the food industry where a thermal annealing process is crucial for the creation of many products. Changes in temperature increase the total energy in the system. This increase in energy can cause molecules to vibrate and as a result key interactions, such as hydrogen bonding, weaken causing the breakdown of the nanostructures leading to de-emulsification. Strength of interaction differs between all three peptides. Therefore, the energy required to displace the peptides may not be observed until higher temperatures are reached (Figure 3.10). Therefore, both macroscopic images and temperature controlled FTIR was used to identify the structural changes observed upon heating.

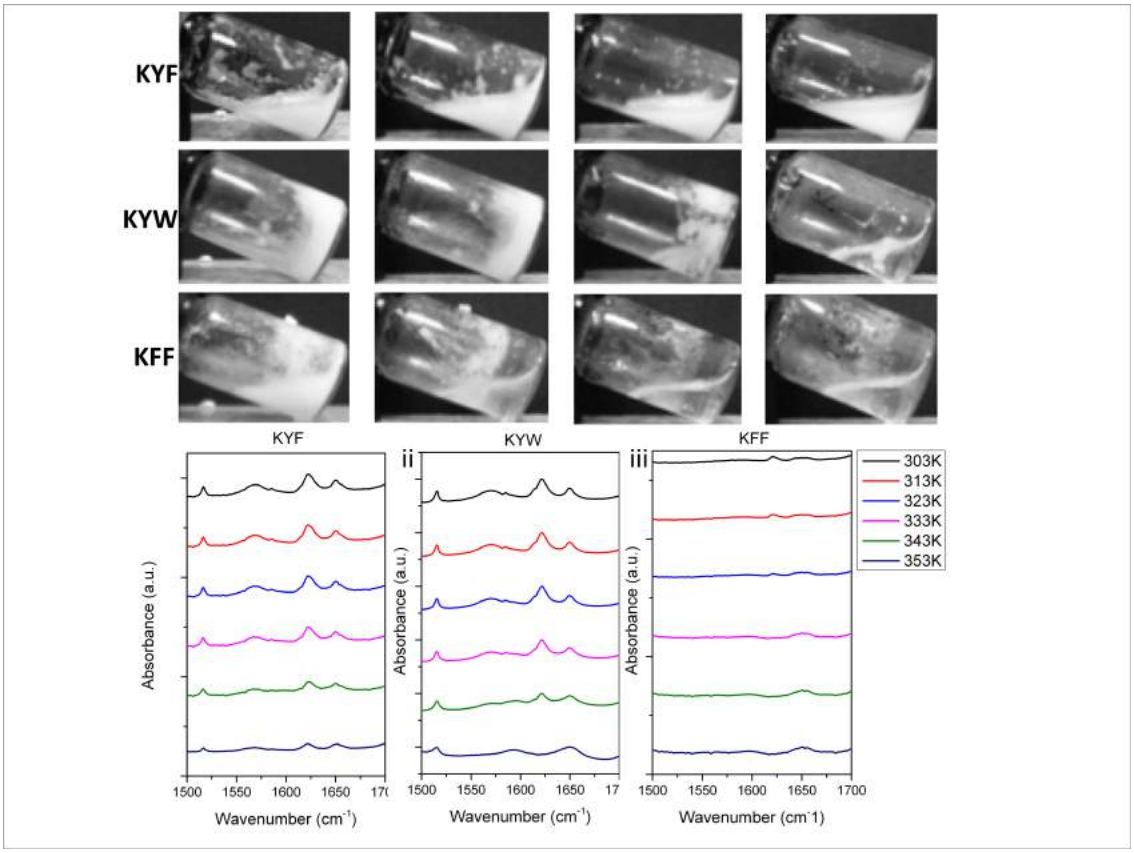

Figure 3.10: Thermal stability of peptide emulsions KYF, KYW and KFF. Macroscopic images of the destabilization of the emulsions with temperature controlled FTIR showing the critical temperature of de-emulsification for each peptide

Emulsions of KYF, KYW and KFF were produced and placed into an oil bath heated to 303 K. The samples were heated for 15 mins before being removed and photographed. The samples were returned and the temperature was increased in increments of 10°. This was carried out until a final temperature of 333 K. KFF showed the least stable emulsion at higher temperature. The breakdown of the emulsion into two immiscible layers was observed at 313 K. This satisfies the argument that KFF forms the weakest emulsions.

Thermal responses were further analyzed using the temperature controlled FTIR where the change in peaks observed in the amide I region indicated hydrogen bonded structure diminished rapidly upon heating. Peaks around 1625 and 1649 cm^{-1} have disappeared by 323 K resulting in no intense FTIR spectra peaks. This shows that the defining H-bonding interactions are removed and the energy in the system is high enough to cause the breakage of the interaction holding the

nanostructure together. KYW indicates the strength of the peptide is stronger than that of KFF. Signs of the KYW demulsifying occurs at 323K with full separation of the emulsion observed at 333K. Nanostructures observed using FTIR show diminished peaks upon heating of the sample. Although, peaks around 1635 and 1649 cm^{-1} are still present, the macroscopic morphology of the emulsions has destabilized. FTIR peaks are still present as there is still be some H-bonding interactions present in the solution but are not strong enough to stabilize the emulsions. At high temperatures such as 353K these peaks have disappeared and therefore the nanostructures have been dissembled into their monomeric units. KYF has the best stabilizing capability of the three-peptide chosen for fibrous peptide emulsion stabilization. KYF is able to stabilize emulsions up to temperatures of 333K where a free-flowing emulsion is still observed. At 333K, there are signs of de-emulsification where coagulation of the oil droplets is beginning to occur, although not to same extent as KYW and KFF. FTIR indicates at high temperatures the nanostructures are still present within the solution. This observation indicates that the total energy within the system is not high enough to fully disintegrate the nanofibers, therefore the peptide-peptide interactions are the strongest observed from the chosen samples.

3.2.3 Summary

In summary, three peptides were chosen (KYF, KYW and KFF) which showed formation of nanofibers in aqueous environment, to explore their potential as emulsification agents. It was hypothesized that the formation of nanofibers at the water/oil interface could have the potential to stabilize emulsions, as was previously demonstrated for aromatic peptide amphiphiles. Examination of the structural components of the three chosen peptides in the emulsified state and all three form stable emulsion, which are stabilized by an interfacial nanofibrous network was carried out. Stability examination has shown that subtle difference in amino acid choice can have a dramatic effect on the total stability of the emulsion. Stability analysis indicates KYF forms the strongest emulsion as examined *via* thermal annealing techniques, with KFF forming the weakest emulsions.

3.3 Surfactant Peptide Emulsifiers

3.3.1 Computational Screening

As seen in the previous section, short peptides can be used as emulsifiers *via* an interfacial self-assembling fibrous network. More typically, emulsifiers assemble at interfaces due to their hydrophilic head and hydrophobic tail morphologies. Tripeptide such as DFF and FFD have been chosen to examine their emulsifying capabilities due to their aqueous assembly of forming bilayers. The formation of bilayers suggests that there is a strong hydrophobic effect occurring resulting in the tight packing of the phenyl rings. Therefore, it was hypothesized that these peptides would stabilize emulsion *via* the more traditional surfactant-like assembly. Similar to the fibrous assemblies seen in the previous subchapter, coarse-grained molecular dynamics have been implored to examine how the peptides interact with the oil (Figure 3.11).

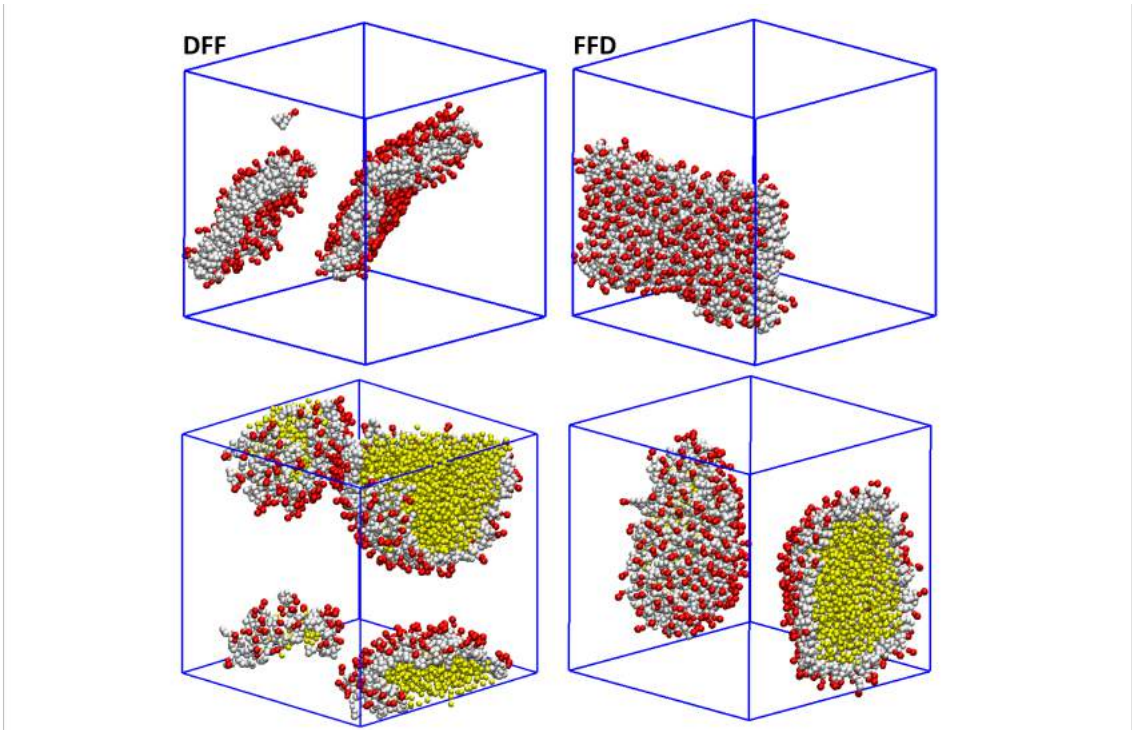

Figure 3.11: Coarse-grained simulation of DFF and FFD in both aqueous and biphasic states. Red = Asp, White = Phe, Yellow = Octane

Coarse-grained molecular dynamics indicate that, similar to fibrous peptide assemblies, the tripeptides have a strong affinity to localize themselves at the water/oil interface with the phenyl rings pointing into the oil and the aspartic acid residue in the water phase. Initial inspections of the coarse grained images suggest FFD is weaker than DFF. This is due to the shape of the stabilized droplet. The formation of the non-spherical structure observed in FFD indicates that the peptides are weakly bound to the surface of the oil droplet, allowing the changes in shape of the droplet. The droplet could potentially have fluid properties, which increases the probability of coalescence of the oil droplets, resulting in emulsion destabilization.

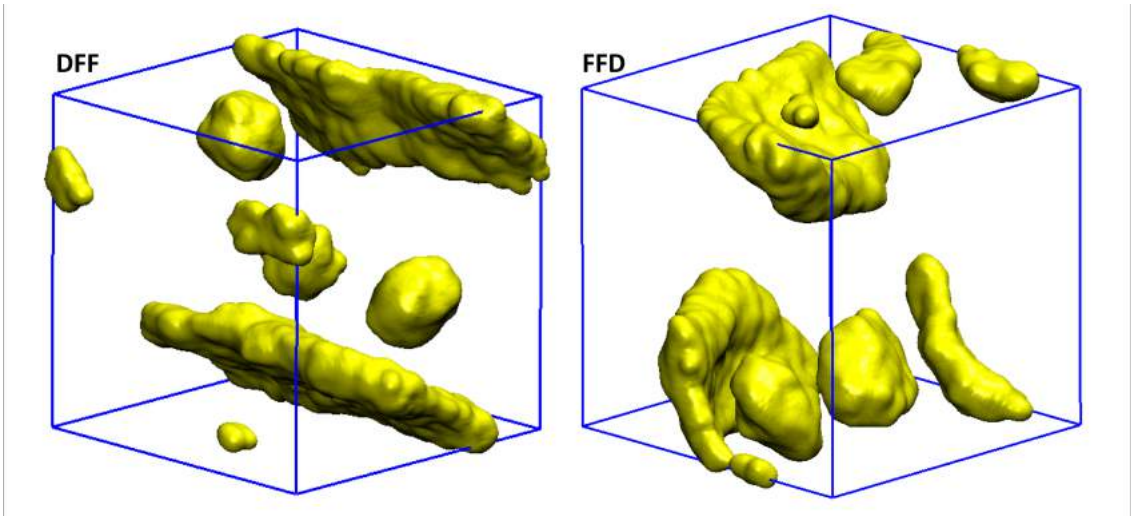

Figure 3.12: Larger coarse-grained simulation of DFF and FFD emulsions showing the coalesced of the octane in larger droplets. Peptide molecules have been removed for clarity

The stability of the emulsion was tested by increasing the box size in an analogous manner to that used for the fiber forming peptides (Section 3.2.1). This revealed that the surfactant-like emulsifiers (DFF and FFD) do not form stable emulsions (Figure 3.12). In both cases, initial interactions show several stabilized emulsion droplets. As simulation time progresses, these droplet begin to coalesce into large extended droplets. This suggests that the peptides are not as strongly bound to the interface, which allows the coagulation of the oil droplets. In addition, the extended sheet-like droplet indicates poor stabilization as this increases the oil/water interaction.

3.3.2 Experimental Validation

Progressing from computational analysis DFF and FFD were examined experimentally to ascertain the emulsifying behavior. In order for a direct comparison between the nanofibrous stabilized emulsions, all samples were prepared at 40mM peptide solution.

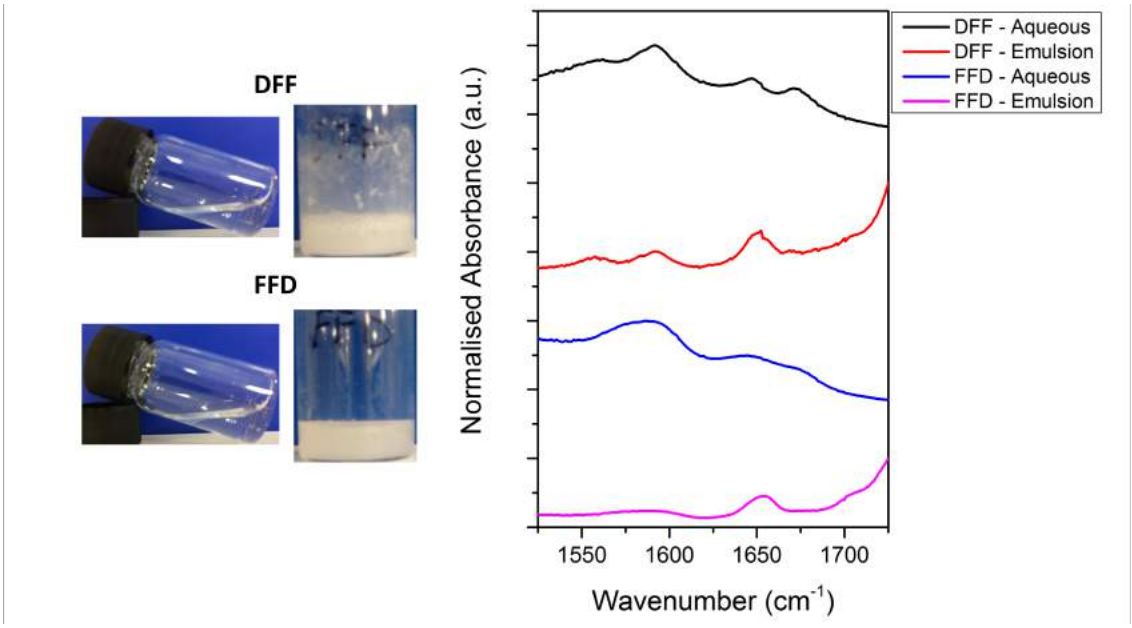

Figure 3.13: Macroscopic images of DFF and FFD in the aqueous and emulsified state with a comparison of the FTIR signals in both states

As previously seen, aqueous samples of DFF and FFD form clear solutions at pH 7.4. Upon emulsification with 100 uL rapeseed oil *via* homogenization, a cloudy solution appears. These emulsions begin to demulsify relatively quickly with emulsions disappearing after approximately 24 hrs (Figure 3.13). FTIR analysis shows several changes in the internal supramolecular structure of the emulsions. As expected, aqueous samples show a broad peak around 1580 cm^{-1}, indicative of a deprotonated carboxylate group. On emulsification, DFF shows signs of splitting of this peak, which suggests a salt bridge is forming. This splitting could be due to the close proximity of the aspartic acid residue and the n-terminus. Upon emulsification, the hydrophobic effect induces these molecules to become closer in the proximity; therefore, the forming of a salt bridge is seen, (see Section 2.3.2 for DFF conformation). This is not observed for FFD as the negatively charge head group is remote from the positive N-terminus, inhibiting salt-bridge formation. In

addition, there is a dramatic change in the hydrogen bonding of both peptides upon emulsification. The appearance of a peak around 1650 cm^{-1} in both samples indicates the emulsification process induces the formation of hydrogen bonding between peptides. This is primarily due to the hydrophobic effect, where the peptides are forced to be in close proximity to each other and therefore unordered hydrogen bonding can occur.

Visual determination of the stabilized emulsions was carried out via fluorescence microscopy using Sudan II dye.

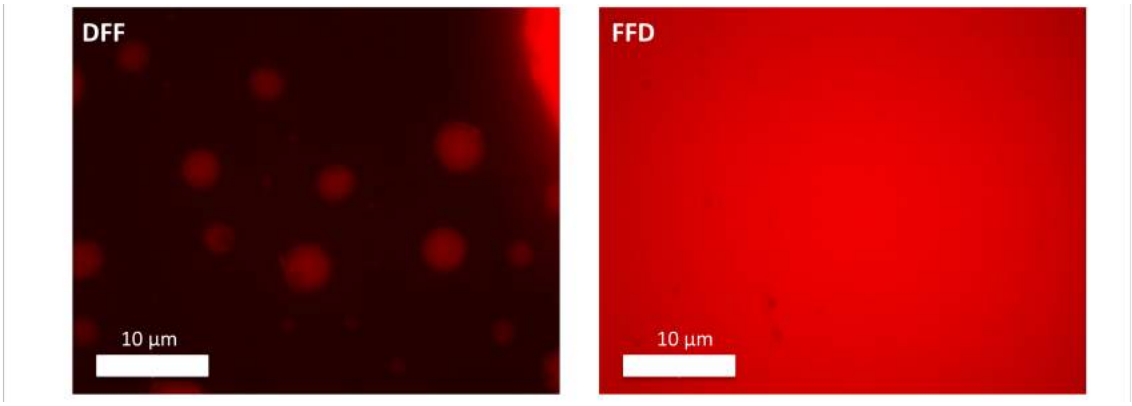

Figure 3.14: Fluorescence microscopy of DFF and FFD using Sudan II dye

Fluorescence microscopy of the DFF and FFD emulsion indicates the formation of weak emulsions. For DFF small and few droplets are observed where for FFD the de-emulsification process occurs at a quick rate therefore no stabilized droplets were visualized. (Figure 3.14) These results mean that the surfactant-like emulsions are very weak and the stabilization of the droplets is poor. No ThT signal can be detected as no beta-sheet structures are formed therefore no enhancement of the fluorescence signal can be observed.

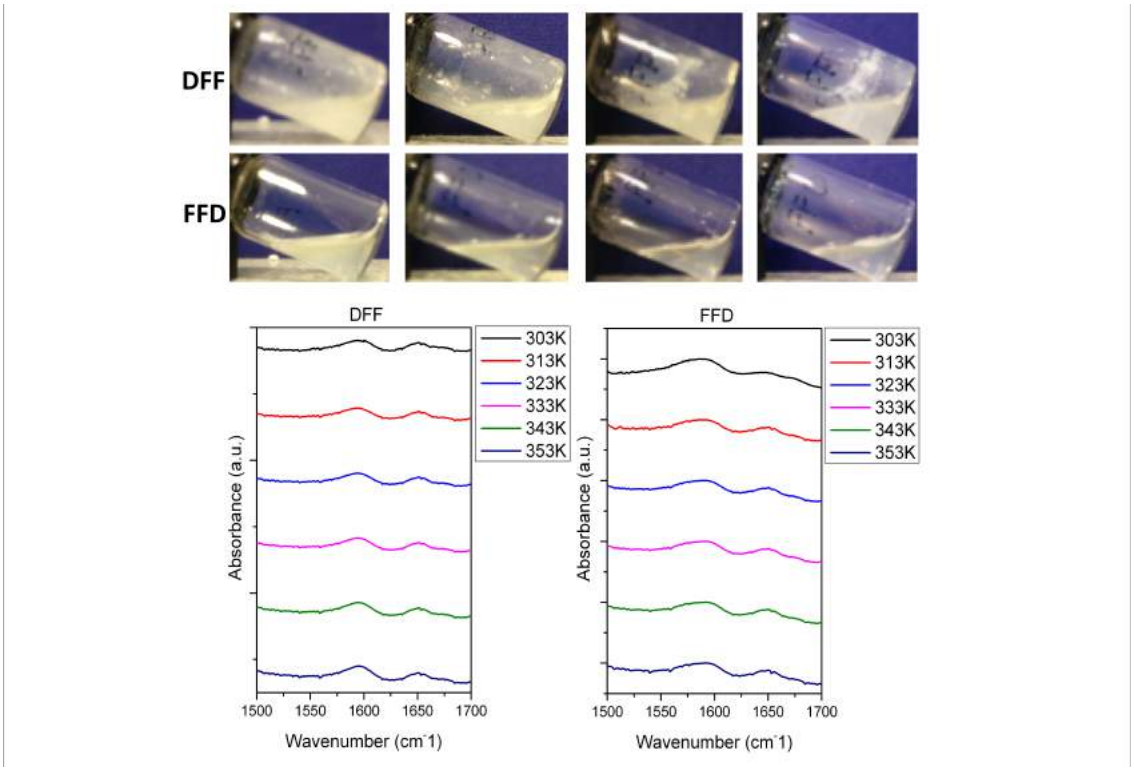

Figure 3.15: Temperature stability of surfactant-like peptide emulsions. DFF and FFD. Macroscopic images showing the de-emulsification of the emulsions with the temperature controlled FTIR indicating changes in molecular structure upon heating

Temperature-dependent studies of DFF and FFD emulsions indicate that the peptides are poor emulsifiers, resulting in de-emulsification of the peptides (Figure 3.15). Samples were stored in an oil bath and the temperature was increased in increments of 10° with images of the emulsions taken at each temperature point. It is clear that DFF samples demulsify at low temperature with clear indications at 303 K that the emulsions are breaking down with a noticeable second layer forming occurring at 313 K. In the case of FFD, two layers are noticeable from 303 K indicating that FFD does not have the interaction strength to stabilize the oil droplets for a great length of time. Temperature dependent FTIR shows little change as the temperature is increased.

3.3.3 Summary

In summary, emulsifying capabilities of DFF and FFD which were sought to form surfactant-like assemblies at water/oil interfaces were examined. Structural analysis of the systems, with comparison between aqueous and emulsion states, indicate that these peptides do not form fibrous assemblies at the interface. FTIR analysis showed subtle changes in hydrogen bonding structure but no beta-sheet stabilized structures were observed. These conclusions were verified by fluorescence microscopy, where Thioflavin T fluorescence was not observed. Therefore, as expected, these peptides form emulsions based on the traditional surfactant-like model. Identifying the stability of these emulsions, it has been indicated that these peptide do not form stable emulsion to the same extent as the fibrous emulsions seen previously. In both cases on increasing the temperature induces de-emulsification resulting in two separated layers.

3.4 Dipeptide Emulsifiers Screening

The concept of tripeptide emulsions was created as tripeptides have shown remarkable properties in creating a variety of different nanostructures that can have tunable properties. Although examination of tripeptide for emulsification processes has been explored in the previous section, dipeptide emulsifiers have not yet been explored. Previously, a screening process of all dipeptides for their aggregation propensities was calculated but Frederix *et al*.[124] These screening measurements indicated the likelihood of dipeptide aggregation and therefore the probability of the formation of nanostructures.

3.4.1 Screening Process

Using the same principles as in the aqueous screening process, all 400 dipeptide emulsions systems were examined for a period of 400 ns to determine how the dipeptides interact with the oil/water interface. For all systems, the solvent accessible surface area (SASA) was measured using vmd-scripting tools. This measures the degree of aggregation of the systems where it takes into account the amount of the molecule that is exposed to water. For example, a largely aggregated molecule will have a lower SASA value compared to a system that is poorly aggregated. The aggregation propensity (AP) of the system has been calculated as a ratio of the SASA from the starting (non-aggregated) structure with the SASA of the final structure (Equation 3.2).

$$AP = \frac{SASA_{initial}}{SASA_{final}} \qquad \text{Equation 3.2}$$

Table 3.1: AP scores of top 5 and lowest 5 dipeptide emulsions

Peptide	AP score	Peptide	AP Score
FW	1.72	NK	1.08
FW	1.68	RK	1.08
WW	1.67	KN	1.09
WF	1.63	RN	1.09
WY	1.61	DH	1.09

After calculation of all AP score for all 400 dipeptide emulsions, the data are normalized using Equation 3.3. This allows greater meaning of the data and allows a direct comparison between systems.

$$Normalised\ AP = \frac{AP_i - AP_{min}}{AP_{max} - AP_{min}} \qquad \text{Equation 3.3}$$

After normalization, results were plotted as a scatter grid using the mathematical software Matlab.[178]

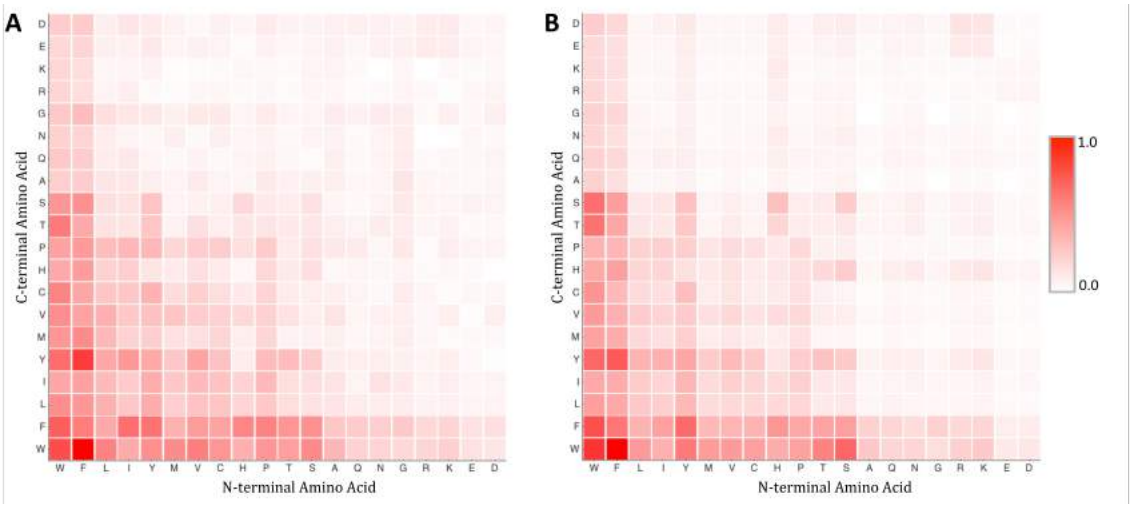

Figure 3.16: Coarse-grained computational screening of dipeptide emulsifiers. A) Aggregation propensities of the total system and B) aggregation propensities of the dipeptides.

Dipeptide emulsions have shown a variety of different aggregation behaviors. Figure 3.16 can be read by finding the amino acid found at the N-terminus (x-axis) and matching it with the correct C-terminal group (y-axis). All results have been

normalized therefore the sections with the greater density indicates dipeptide emulsion system with higher aggregation. Focusing on the aggregation propensities of the total system, it is clear that the presence of aromatic groups is a driving force for the aggregation the peptides. This is expected, as previously, it has been mentioned that the strong hydrophobic effect with the addition of the π-stacking can make these peptides aggregate more than typical hydrophobic peptides. Conversely, peptides that contain charged groups with no hydrophobic groups do not aggregate as much. The reasoning behind this is that peptides need to have some affinity to adsorb to the interface. The lack of hydrophobic groups does not allow the hydrophobic effect to drive the peptides to the interface. In addition, the close proximity of charged groups increases the energy in the system. The strong repulsive interactions between the peptide do not allow the peptides to pack as close as they need to be. This results in poor stabilization. Aggregation of the dipeptides shows that there is very little difference for the peptides themselves to aggregate. Therefore, the main driving force observed in the comparison between the full system and the purely peptidic system was the driving force for the peptide to interact with the octane.

Identification of the aggregation propensity for each amino acid at the two positions available on the dipeptide backbone was explored by a cumulative process by the addition of the aggregation propensity for each amino acid at the at position. (Figure 3.17)

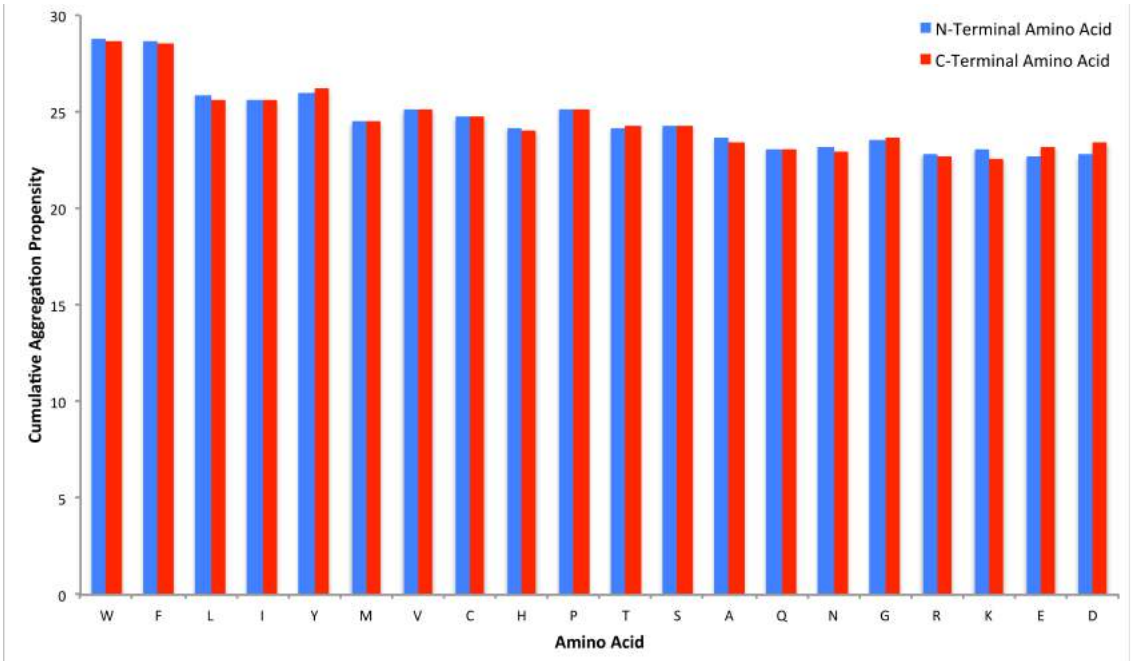

Figure 3.17: Distribution of aggregation propensity based on amino acid position within the dipeptide chain.

Positional effects for amino acids within the dipeptide chain show similar observation that was first introduced in Frederix *et al.*[124] The majority of the aggregation behavior is determined by the presence of aromatic groups on the chain. Hydrophobic residues have slightly better aggregation than others. Choice of the N-terminal over C-terminal on the dipeptide is shown to have less of an effect on the dipeptides ability to aggregation as an emulsified system, possibly due to the large influence the octane will have on the aggregation. For the charged amino acids, there are slight preferences for anionic amino acids to prefer the C-terminal position with the cationic amino acid preferring the N-terminal position.

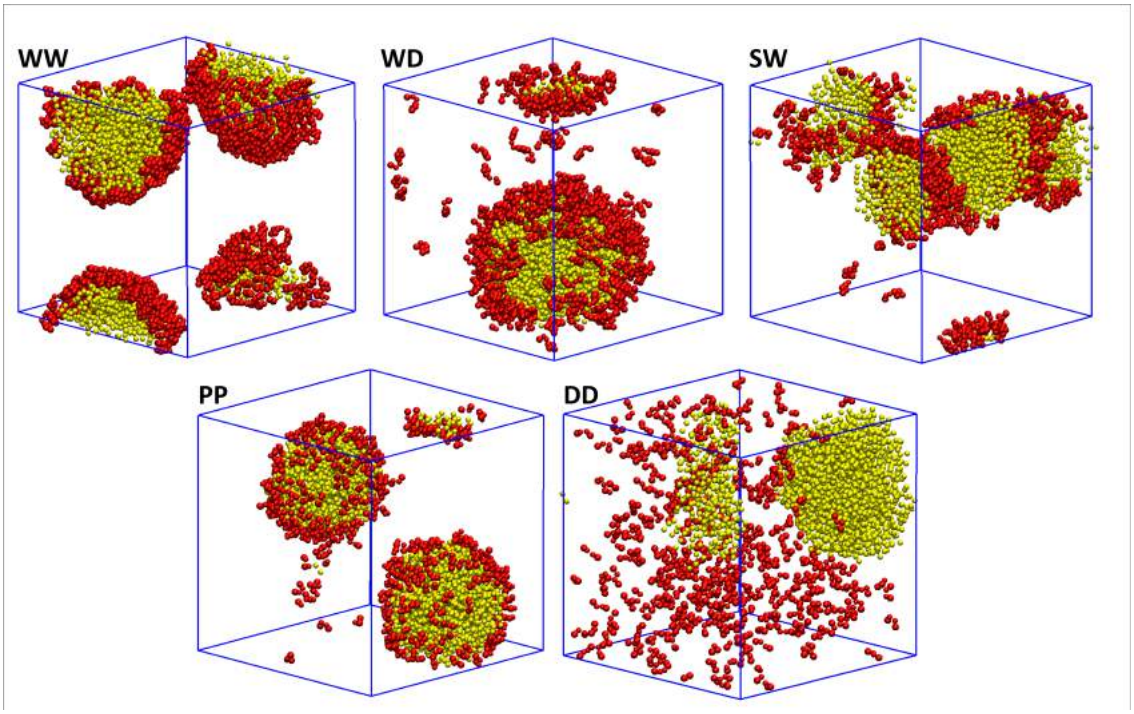

Figure 3.18: Coarse-grained molecular dynamics screening of dipeptide emulsions WW, WD, SW, PP and DD

Major differences are observed depending on the type of dipeptide chosen. WW, one of the most strongly aggregating dipeptides, shows strong binding to the water/oil interface. (Figure 3.18) This results in a stable spherical oil droplet being produced. On comparison with WD and SW, which contain a hydrophilic amino acid in place of a tryptophan, amino acid shows the different morphologies for the emulsion aggregation. Although WD shows major aggregation at the interface, peptide molecules are seen exchanging and can free moved from different parts of the oil droplet. This suggests the binding for WD is not as strong and therefore a lesser-stabilized droplet would be observed. Similarly, SW shows binding to the interface, but two individual oil droplets are observed, implying that the balance between the hydrophobic and hydrophilic groups is favourable resulting in a stable emulsion droplet. In addition, PP shows some affinity for the peptides to bind to the surface of the oil. Due to the mapping in the MARTINI model, results with proline are questionable as changes in the structure of the peptide often differ with what is observed experimentally.[116, 124] DD does not interact with the oil. As the DD is very hydrophilic it remains well solvated.

Table 3.2: Total AP score, AP(total), and AP score of dipeptide, AP(dipep) of chosen dipeptide emulsions

Peptide	AP(total)	AP(dipep)
WW	1.66	1.86
WD	1.31	1.27
SW	1.53	1.74
PP	1.31	1.19
DD	1.13	0.96

Comparison of the total AP scores with the AP scores of the dipeptides, indicate how the peptides performed and if they have a good binding to the surface. As the AP score for WW and SW are greater than the total AP score, it suggests that these would be suitable candidates for testing dipeptide emulsions. However, these results are only computational predictions of dipeptide emulsifiers and no experimental results are currently available.

3.4.2 Summary

In summary, we have computationally predicted how well dipeptides can aggregate in a biphasic system. Overall, we identify similar observations that were seen in the case of tripeptides. The presence of aromatic groups is essential for the formation of emulsions and without these groups, dipeptide will not form stable emulsions.

3.5 Conclusions

Emulsifiers are widely used in the food, cosmetic, and biomedical industries for different applications. Most currently used emulsifiers are derived from animal of plant products but the extraction methods can be long processes. We have shown that manipulation of the natural process of peptide interaction and controlling the self-assembling mechanisms provides a route to a range of peptide emulsifiers with tunable stability.

In this chapter, two different types of peptide emulsifiers have been examined where peptides that have the tendency to form fibrous nanostructures can be utilized to stabilize emulsion by interfacial nanofibrous networks. These emulsions withstand greater temperatures and are overall more stable in comparison with surfactant-based emulsifiers. The other type of emulsifiers examined was the utilization of tripeptides that have the ability to form bilayers and therefore can arrange themselves into surfactant-like emulsions. Due to the poor binding of these emulsifiers, weak emulsions were prepared.

Finally, using computational methods all possible dipeptides were screened to identify if dipeptides have the ability to assemble at the water oil interface and act as emulsifiers. It was determined that the presence of aromatic groups is a driving force for the aggregation of the peptides at the interface, although, a balance of hydrophobicity and hydrophilicity is important for dipeptides to form stabilized emulsions.

3.6 Materials and Methods

3.6.1 Sample Preparation

Peptides were purchased from Bachem Ltd. All peptides were purchased with a purity > 98%.

All emulsions were prepared at a peptide concentration of 40 mM. the peptides were dissolved in 900 µL millipure water and the pH was adjusted to 7.4. 100 µL of rapeseed oil was added to the peptide solution. Each peptide system was then subjected to 10 secs of homogenization using a bench top homogenizer. The samples were then left at room temperature for a period of 24 hours before analysis.

3.6.2 Fourier Transform Infra-red Spectroscopy (FTIR)

FTIR spectra were acquired using a Bruker Vertex70 spectrometer with a spectral resolution of 1 cm^{-1}. Spectra were obtained by averaging over 25 measurements for each sample. Measurements were performed using standard FTIR cuvettes (Harrink Scientific) where the sample was sandwiched between 2 CaF_2 discs (Crystran Ltd) separated by a 50 µm PTFE spacer. For gel materials, a small amount of material was placed between two CaF_2 discs using a microspatula. For free flowing samples, 100 µL of the sample was pipetted directly onto the disc. D_2O was used as the solvent.

3.6.3 Transmission Electron Microscopy (TEM)

Carbon-coated copper grids (200 mesh) were glow discharged in air for approximately 30 secs. The grids were placed on the gel material of liquid solution before being blotted down using filter paper to remove the excess. 20 uL of negative stain was applied (1% aqueous methylamine vanadate obtained from Nanovan, Nanoprobes) prior to a further blotting using filter paper. Samples were then left to dry. The dried samples were then imaged using a LEO 912 energy filtering transmission election microscope operating at 120kV fitted with 14bit/2K Proscan CCD camera. TEM imaging was carried out at the University of Glasgow.

3.6.4 Fluorescence Microscopy

Fluorescence microscopy was carried out on a Nikon Eclipse E600 upright fluorescent microscope at x1000 magnification. Samples were prepared by placing the sample on a glass slide with a glass cover slip placed on top. A drop of silca oil was placed in the sample to allow for a lubricated surface.

3.6.5 Temperature Dependent FTIR

FTIR spectra were acquired using a Bruker Vertex70 spectrometer with a spectral resolution of 1 cm^{-1}. Spectra were obtained by averaging over 25 measurements for each sample. Measurements were performed using standard FTIR cuvettes (Harrink Scientific) where the sample was sandwiched between 2 CaF_2 discs (Crystran Ltd) separated by a 50 um PTFE spacer.

For emulsions, a small amount of material was placed between two CaF_2 discs using a microspatula. The CaF2 discs were placed into a temperature controlled Harrink cell. The cell was allowed to equilibrate for 10 mins before measurement was taken. Directly proceeding the measurement, the temperature was adjusted followed by another 10min incubation period to allow the increased temperature to penetrate the sample. This process was repeated for until all temperature points were measured D_2O was used as the solvent.

3.6.6 Coarse-Grain Molecular Dynamics

Molecular dynamics simulations were performed in GROMACs using the MARTINI force field version 4.5.3.

A single atomistic tripeptide molecule was converted to the coarse grain representation using the martinize.py script. 300 molecules of the chosen coarse-grained tripeptide was added to a box with the dimensions 12.5 x 12.5 x 12.5 nm using the genbox command. The simulation box was then solvated using standard CG water. Addition of 10% of octane was carried out. This process inserted the octane molecules randomly to simulate the homogenization process. Using the

genion command in Gromacs, the system was neutralized with the addition of sodium or calcium ions. The MD system was then subject to a minimization for 5000 steps to ensure no overlap atoms. Once minimized, the system was subject to production run of 9.6 μs.

4.

Trapping Tripeptide Nanostructures in Kinetically Controlled Biocatalytic Self-Assembly

Declaration of contribution to published article: Any reproduced practical work from the aforementioned published article; I was solely responsible for, unless otherwise stated.

4.1 Introduction

Given that tripeptides are potentially useful as emulsifiers and gelators, there is a need for methods to scale up their synthesis and reduce cost. Enzymatic approaches to peptide synthesis may be of use in this context. Proteolytic enzymes can be utilized in the direct synthesis of short peptides from activated amino acids, enabling facile synthesis of self-assembling peptides in aqueous solution.[179-181] However, in cases where target peptides do not represent those preferentially formed at equilibrium, hydrolysis eventually takes over, giving rise to low yields at equilibrium.[182] In this chapter we compare means of controlling physiological conditions such as temperature and pH to allow trapping of a transiently formed peptide in the highest yield, self-assembled state, thereby providing a means of producing self-assembled tripeptides.

As detailed in previous chapters, short self-assembling peptides have numerous potential applications in a range of multi-disciplined industries, such as the food, cosmetic and biomedical industries, due to their versatility.[7, 86, 183-187] Thus, the emergence of the first reported self-assembling tripeptides based purely on unprotected alpha amino acids by computationally predicting their aggregation propensities gained these industries' atention.[124] A diverse range of nanostructures obtained from altering amino acid position allows the creation of different properties of short self-assembling systems. Such systems have arisen to give viable applications such as drug delivery vehicles; emulsifiers and cosmetics products. In addition, amino acids are cheap and readily available, allowing for a vast range of tripeptides to be synthesized, with sequence-tunable characteristics.[183, 188-189]

Although synthesis of tripeptides can be achieved with relative ease, by using solid-phase peptide synthesis, such methods are not easily scaled and can introduce harmful salts and solvents into the final product, which can be difficult to remove, an issue which is problematic for certain applications.[190-191] Enzyme-catalyzed synthesis of short peptides, using proteolytic enzymes has been extensively studied as a 'green' synthetic route for the synthesis of short

peptides.[181, 192-196] As the peptide products of these processes typically lie away from the chemical equilibrium (i.e., hydrolysis, rather than condensation is thermodynamically preferred in aqueous media), there is a need to promote peptide bond formation and suppress hydrolysis.[197]

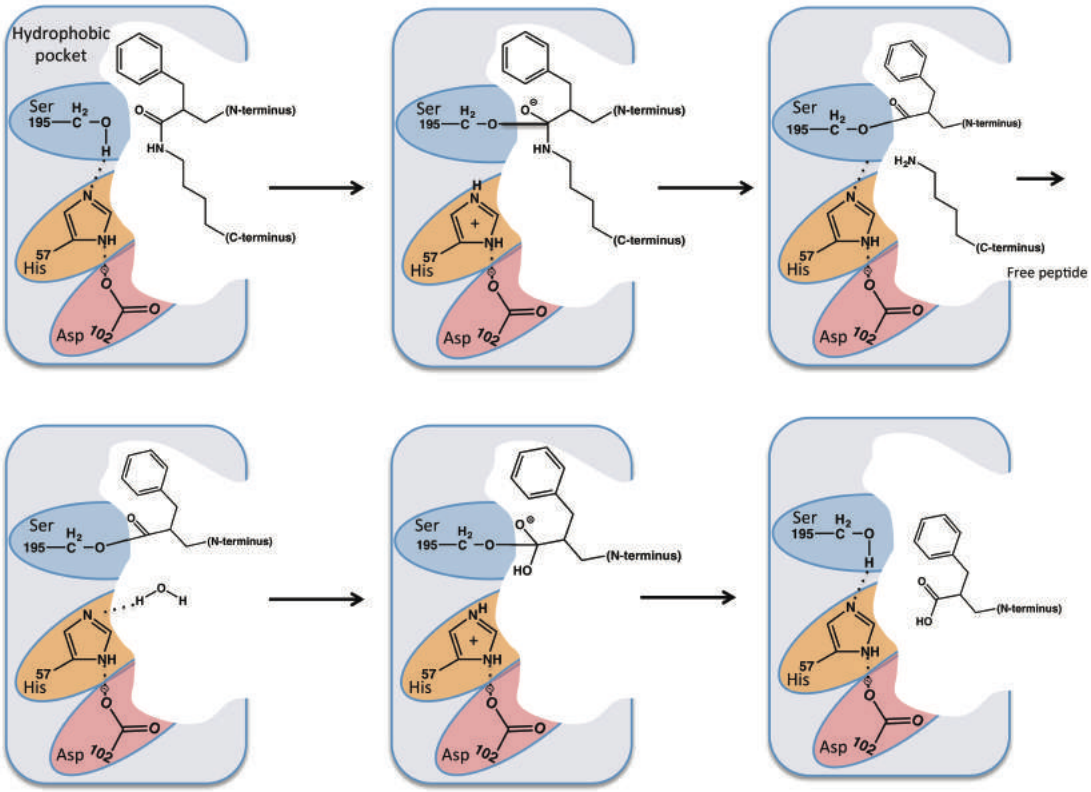

Figure 4.1: Schematic representing the hydrolysis of a peptide bond within the active site of α-chymotrypsin

Reaction conditions have to be controlled to allow for the shift in equilibrium to promote the condensation reaction over hydrolysis. Changing conditions, including the introduction of organic co-solvents or the use of highly concentrated suspensions, where reaction products precipitate, can both be used to shift the equilibrium in the desired direction, although both methods have drawbacks.[198-199]. The presence of the organic solvents introduces a less 'green' approach.[200-203] The presence of precipitation-driven (or solid-to-solid) methods also has its drawbacks, namely, that the peptides may not be the thermodynamically favored product, which can affect selectively on trapping the target compound.[204] In situations where the peptide products are not thermodynamically favored, the kinetically favored (desired) product may form transiently, before hydrolyzing to

form the thermodynamically preferred product (typically dipeptides, amino acids). Therefore, examining methods for the capture of non-thermodynamically favored product, which possess important self-assembling properties is of significant importance.[205]

A wide variety of enzymes are currently used in industrial applications ranging from the manufacture of household items, such as detergent, to biomedical applications.[206-210] Enzymes are can be derived from animal, plant, bacterial, fungal and yeast sources (Table 4.1) and have well-defined optimum operating conditions.[211-214] Digressing from these optimal conditions reduces activity of the enzymes due to poor binding between substrate and enzyme. Two main conditions that allow for manipulation of the enzyme activity are temperature and pH.[215-219]

Table 4.1: Table indicting different enzymes food form different source and the industrial application

Enzyme	EC Number	Source		Industrial Application
Catalase	1.11.1.6	Animal	Liver	Food
Chymotrypsin	3.4.21.1	Animal	Pancreas	Leather
Rennet	3.4.23.4	Animal	Abomasum	Cheese
Actinidin	3.4.22.14	Plant	Kiwi Fruit	Food
α-Amylase	3.2.1.1	Plant	Malted Barley	Brewing
Asparaginase	3.5.1.1	Bacterial	*Escherichia coli*	Health
Penicillin Amidase	3.5.1.11	Bacterial	*Bacillus*	Pharmaceutical
Pectin Lyase	4.2.2.10	Fungal	*Aspergillus*	Drinks
Cellulase	3.2.1.4	Fungal	*Trichoderma*	Waste
Invertase	3.2.1.26	Yeast	*Saccharomyces*	Confectionary

Thermal conditions can affect enzyme function in two ways: enzyme structural stability and the ability of the system to overcome its activation energy. With increasing temperature, the structural stability of the enzyme decreases, which may result in the deformation of the binding site and eventually in the denaturation of the enzyme. In addition, elevated temperatures increase the amount of energy present in the system therefore the activation barrier is easily

achieved for the substrate-enzyme binding causing an increase in collisions. For lower temperatures, the reverse is apparent where there is less energy available to overcome the activation barrier in order for the reaction to occur.

Enzymes are complex proteins, made up of a collection of ionisable groups, the isoelectric point (pI) and pK_a values are useful in determining the activity of an enzyme in different conditions.[220] Small changes in pH can affect the ionisable groups, which control the structural activity of the enzyme, especially within the binding site. In addition, movement towards/away from the pI of the enzymes, result in solubility and stability issues. In this chapter, the catalytic triad responsible for the reactivity of the enzyme is in the serine protease α-chymotrypsin and is formed by histidine (His), aspartic acid (Asp) and serine (Ser) amino acids (Figure 4.2).[221-222] The pK_a values for the side chains of these residues are 6.2, 3.9, and 13.0, respectively, although these values can shift substantially in folded 3D structures.[23] This indicates the susceptibility of enzymes at varying pH, as changes of the stabilizing ionisable groups can cause disruption to the conformation of the enzyme, which is integral for biocatalysis.[223]

Histidine is one of the most common residues for catalysis due to its variable protonation state within the biological pH regime. The residue can act as a proton shuttle between other residues, allowing for a stable intermediate states. This process is observed for α-chymotrypsin, a serine protease,[221-222] where the Ser is deprotonated by the His, which is stabilized by the negatively charged Asp. Since the pK_a of the imidazole ring on histidine is approximately 6, at a lower pH the residue is protonated, shutting down the reaction. At a higher pH, the basic nitrogen readily pulls off the proton on the serine so the reaction can happen at a greater rate.

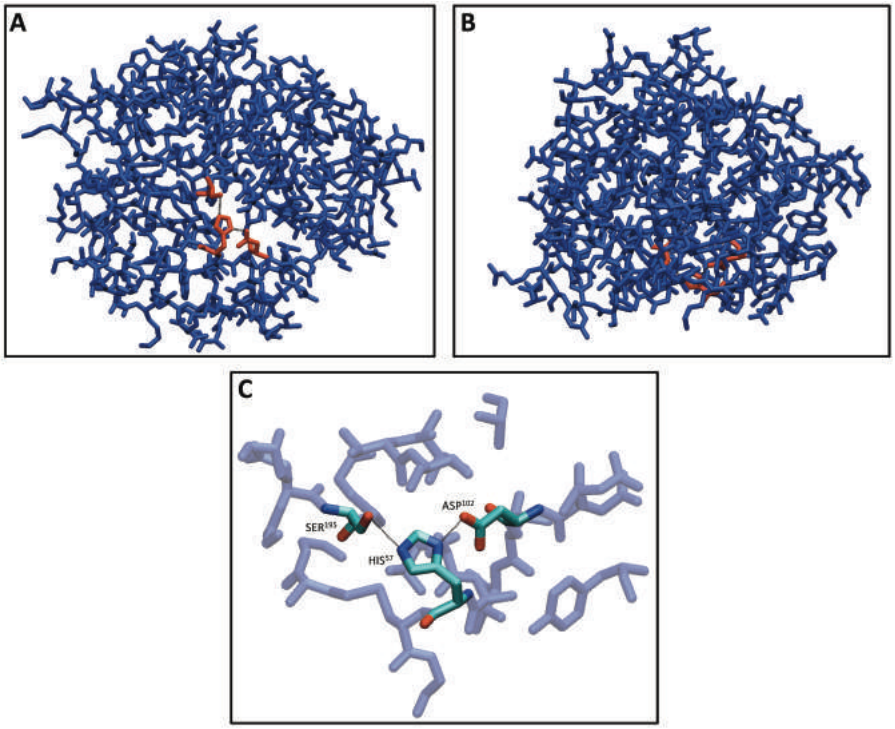

Figure 4.2: A) structure of α-chymotrypsin, active site (red) B) structure after a 90° rotation in the x-axis C) Active site emphasizing the catalytic triad. Protein taken from pdb databank (PDB ID: 4Q2K)

The first example of chemically fuelled, non-equilibrium systems was demonstrated by Boekhoven *et al*. who examined catalytic esterification to form gelators, with competing thermodynamically favoured hydrolysis.[224] (Figure 4.3)

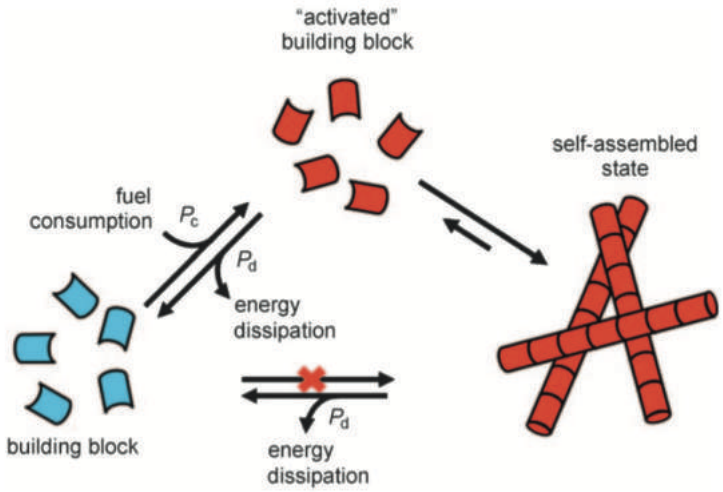

Figure 4.3 Schematic representing the fuel assisted assembly of monomeric units into supramolecular structures followed by the disassembly back to the starting monomeric units after fuel depletion. Adapted from Ref [224] with permissions of John Wiley & Sons, Inc. Copyright by John Wiley & Sons, Inc. (2001)

This work was continued further, by the same authors, where low molecular weight gelators were controlled using catalytic methods.[225]

Pappas *et al.*[226] successfully demonstrated the enzymatic formation of tripeptide-amides DYF-NH_2 and DFF-NH_2 from DF-OMe and F-NH2 and subsequent hydrolysis to DF-OH. The formation of DFF-NH_2 was carried out enzymatically *via* the transacylation reaction between DF-OMe (the common dipeptide sweetener aspartame), and the amidated amino acids F-NH_2 and Y-NH_2. In the presence of 1 mg/mL α-chymotrypsin (≥40 units per mg), the reaction goes to 100% completion for the formation of DFF-NH_2 in 5-10 mins, after which the competing hydrolysis reaction breaks down the tripeptide via two different routes. The HPLC data, in addition to the temporary shifts observed in the amide I region of the FTIR, show the relatively short lifetime of the tripeptides.[226] The formation of DFF-OH proceeds *via* the hydrolysis of the terminal amide linkage. DFF-OH then proceeds to a second hydrolysis reaction to DF-OH and free F. The second route (as observed previously) occurs via the hydrolysis of DFF-NH_2 to DF-OH. In both cases, the formation of the more favoured product DF-OH is formed.

Thus the aims of the work described in this chapter are::

1. Examine the behavior of α-Chymotrypsin in 4 different physical conditions
2. Show how these conditions can control the enzymatic degradation of peptides

4.2 α-Chymotrypsin Stability

In order to determine how the conditions under investigation affect the activity of the enzyme and therefore the outcome of the competing reactions taking place, a benchmark study of the enzyme activity with a known substrate, N-glutaryl L-phenylalanine-*p*-nitroanilide, under the associated conditions was carried out. Upon hydrolysis, the formation of *p*-nitroanaline induces the colorimetric change of the solution to yellow, which can be monitored *via* UV spectroscopy with an excitation wavelength of 400 nm. (Figure 4.4)

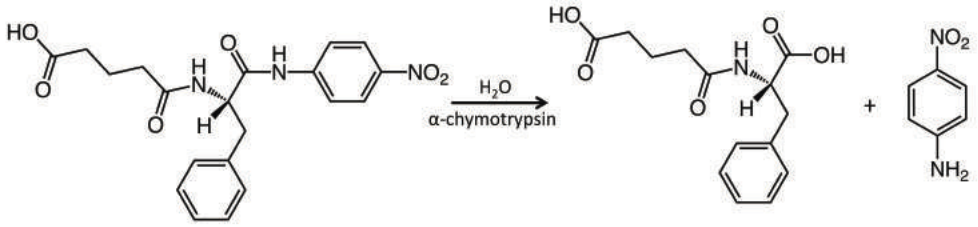

Figure 4.4: Enzymatic hydrolysis of N-Glutaryl L-phenylalanine-*p*-nitroanilide to form *p*-nitroanaline

In order to measure the effect of temperature on enzyme performance, a 1 mg/mL enzyme solution (activity ≥ 40 mg/mL) was placed in an oil bath for 5 mins at 80 °C to ensure the enzyme had been fully denatured.[227] Addition of 100 µL of substrate was followed by several vial inversions to ensure the substrate had been fully mixed. After heating to 80°C, no increase in the intensity of the *p*-nitroanaline is detected over time (Figure 4.5, green line). This is due to the denaturation of the enzyme, which deforms the active site and thus prevents hydrolysis from occurring.

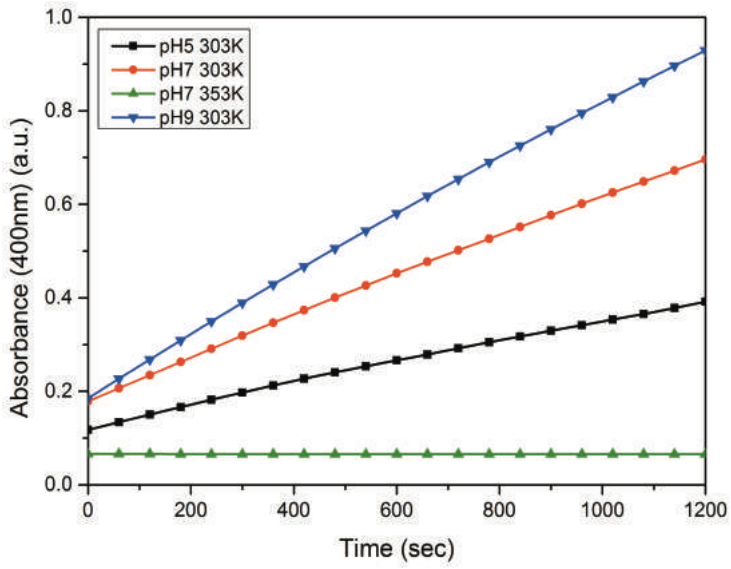

Figure 4.5: UV time course of the hydrolysis of N-glutaryl L-phenylalanine-p-nitroanalide measuring the rate of formation of *p*-nitroanaline

It has been shown that the maximal activity for α-chymotrypsin occurs at approximately pH 8.[228] At this pH, the protonation state of the enzyme's catalytic triad residues allows for the optimal rate of hydrolysis. Macroscopic evidence along with spectroscopic studies shows clear differences in the hydrolytic ability upon changing the pH. At pH 5, the α-chymotrypsin activity is lower due to denaturation of the active site as expected (Figure 4.5, black line). As the pH is increased to pH 7 (red line) and pH 9 (blue line), an increase in intensity of the *p*-nitroanaline is observed, indicating an enhancement of enzymatic activity (Figure 4.5). In addition to rate measurements, Circular Dichroism (CD) was used to determine the changes in structure of the enzyme at the different conditions.

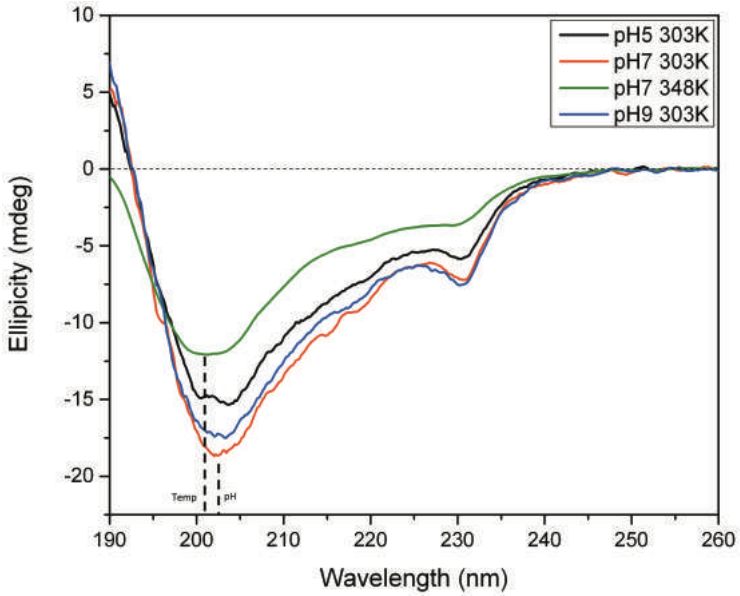

Figure 4.6: CD spectra for all 4 different physical systems indicating the changes in secondary structure exhibited by the enzyme.

CD measurements of α-chymotrypsin in aqueous media primarily give two peaks, at approximately 203 nm and 231 nm. The overall structure obtained from the CD measurements indicate a mixture of both alpha and beta type structures with approximately 15% α-helix, 26 % β-sheet, 20% turn, 39% random coil.[229] Upon changing pH, it was observed that the intensity of the 203 nm peak reduced with lower pH. At lower pH, the enzyme has a net positive charge (pI ~8.5), which can affect the intermolecular interactions vital for keeping the structure of the enzyme stable. As a result, the secondary structure of the enzyme begins to break down, as evidenced by the decrease in ellipticity (Figure 4.6). At pH 5, a decrease in intensity at 203 nm shows loss of secondary structure, in addition the peak begins to split with the appearance of an additional peak at lower wavelength. The presence of this peak suggests slight denaturing of the enzyme in comparison with the high temperature sample. The main peak has shifted from 203 nm to 201 nm, which is indicative of changes in secondary structure, leading to enzyme denaturation.[230] It is also observed that the minor peak around 235 nm reduces as the enzyme becomes denatured, further emphasizing the effect of temperature on the conformational stability. Therefore, altering pH and temperature give significant differences in CD spectra, where the decrease of intensity indicates loss of secondary structure whilst shifts in the peak indicate denaturation of the enzyme.

4.3 Changing Physiological Conditions to Control Tripeptide Formation/Hydrolysis

Examination of the reaction kinetics for the enzymatic degradation/transacylation of aspartame (DF-OMe, Figure 4.7, Structure 1) and F-NH_2 (Figure 4.7, Structure 2) was explored using a number of analytical techniques. Two reactions were followed. In the presence of α-chymotrypsin, aspartame and F-NH_2 rapidly react *via* a transacylation mechanism to form the tripeptide-amide product, DFF-NH_2 (Figure 4.7, Structure 3). The resultant product then undergoes enzymatic hydrolysis to DFF-OH (Figure 4.7, Structure 4) and finally to DF-OH (Figure 4.7, Structure 5).

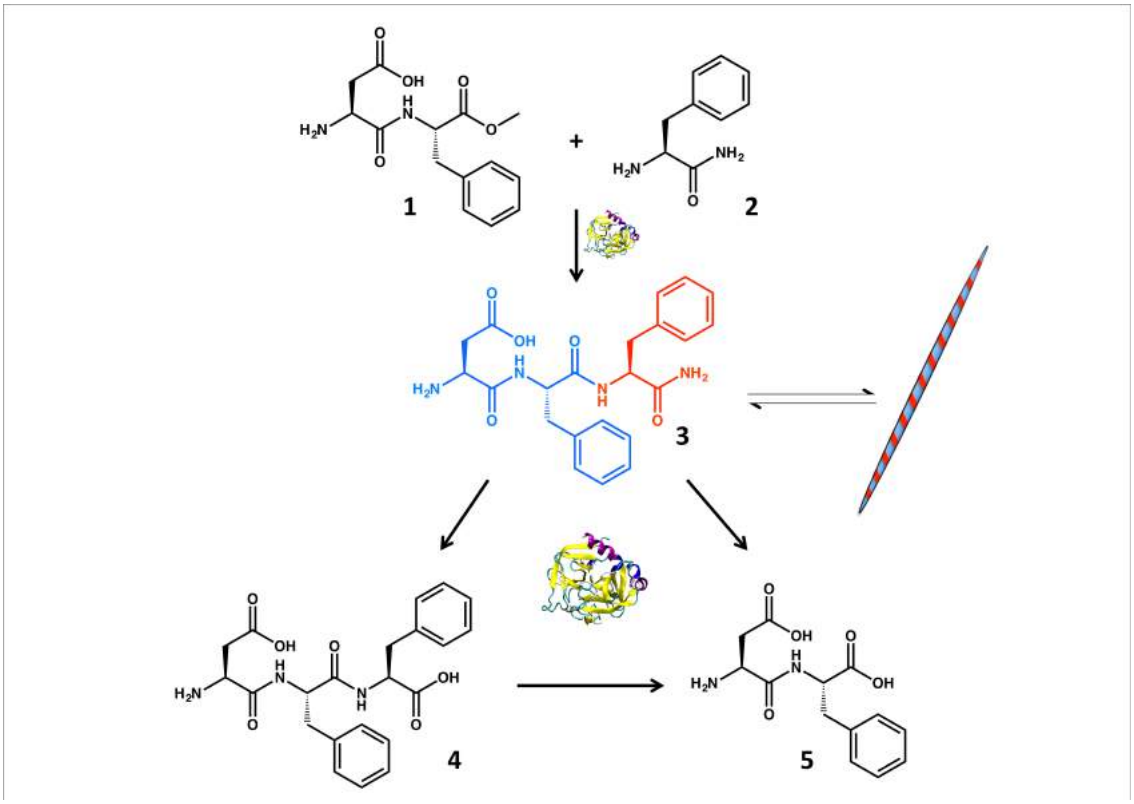

Figure 4.7: Schematic illustration the initial transacylation reaction to form DFF-NH_2. DFF-NH2 undergoes subsequent hydrolysis to DF-OH *via* two different pathways i) hydrolysis of the terminal amide followed by a second hydrolysis ii) direct hydrolysis of the FF amide linkage

4.3.1 LCMS Time Course

The initial transacylation reaction occurs with high yields ~70% of DFF-NH_2 after approximately 5 mins. At this point, the sample hydrogelates. Proceeding the transacylation reaction, the presence of the enzyme begins to hydrolyze the amide linkage between the two phenyl groups. The hydrolysis of DFF-NH_2, results in the formation of different peptides therefore supramolecular assemblies change and the hydrogel begins to disassemble. Investigation into the enzymatic kinetics[231-232] and formation of the different possible products depicted in Figure 4.7, were explored using a time dependent LCMS analysis examining the rate of formation of DF-OH, DFF-NH_2 and DFF-OH (Figure 4.8).

At all pH values tested, the formation of DF-OH is observed, albeit at different rates. At pH 5, the formation of DF-OH is much lower compared to pH 7 and pH 9. In addition, pH 9 gives rise to the highest enzymatic activity, we see the greatest yield of DF-OH formed. This shows that the enzyme is more active and hydrolyses the precursors to the dipeptide.

The formation of DFF-NH_2 is rapid at all pH values, but the rate at which the terminal amide is hydrolyzed depends on the conditions. At pH 9, the rate of hydrolysis is much quicker than at pH 7 and pH 5, which is consistent with the kinetic experiments. This is expected as, at pH 9, the conditions are more favorable for hydrolysis, as the ionization state of the catalytic site is fully active allowing for a high rate of catalysis. The lower rate of hydrolysis observed for pH 7 and 5 is in line with the observation from activity assays that alteration of the pH changes the effective activity of the enzyme. At lower pH, the ionization state of the active site changes where the histidine residue is fully protonated thus preventing hydrogen exchange, a process that retards the bio catalytic process. In addition, at lower pHs such as 3-5, the literature suggests that the enzyme begins to dimerise resulting in conformational changes and effectively reduces the chance for enzyme substrate binding.[223] The reverse trend is observed for the formation of DFF-OH where DFF-OH is formed in a higher yield at high pH.

At increased temperature (80°C) (Figure 4.8, C) an initial rapid formation of DF-OH is observed followed by a plateau. This initial formation of DF-OH is greater than at pH 5 and 7 due to the higher temperature of the sample. The increased temperature allows the activation barrier to be more readily overcome, therefore a higher observed product formation is seen before the enzyme becomes denatured. Similar observations are seen for the formation of DFF-NH_2 and DFF-OH where the hydrolysis is halted by the denaturation of the enzyme.

It is worth noting that at the condition pH 7 and pH 9 at 303 K, FF-OH was found as one of the products. It is unclear as to why this product was formed, as it does not follow the normal hydrolysis that would be expected.

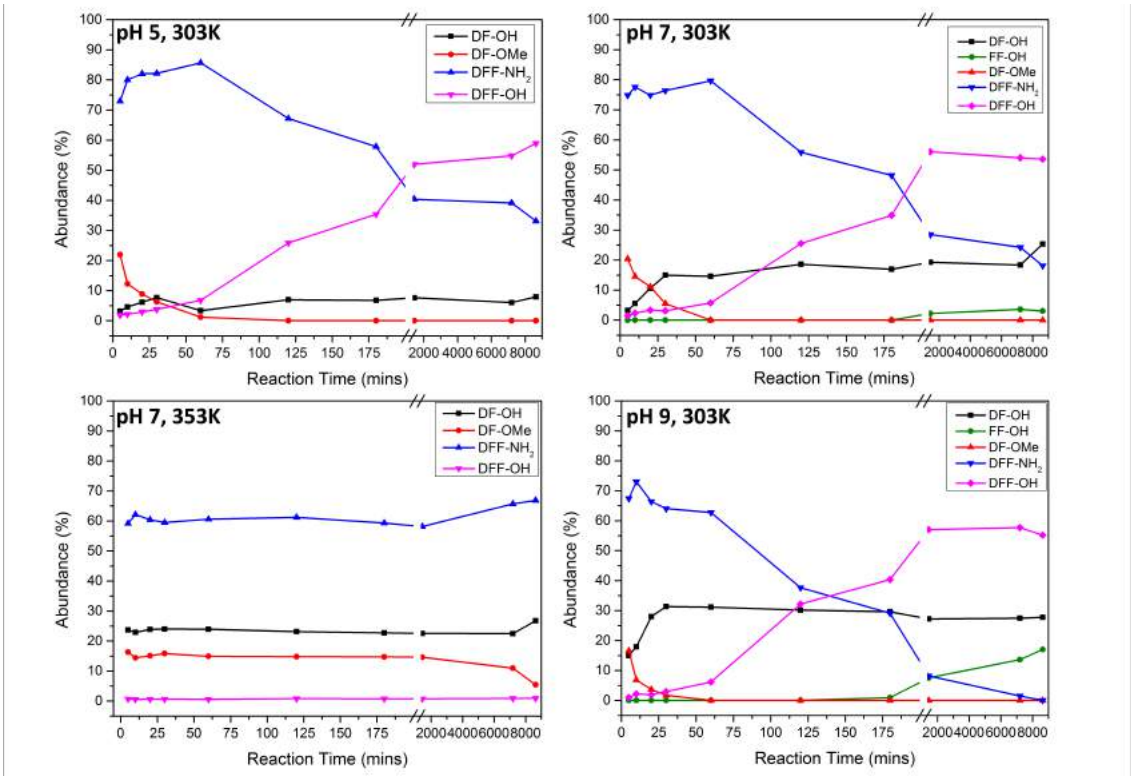

Figure 4.8: LCMS time course indicating the formation of different products for each of the systems at the defined condition

4.3.2 Fourier Transform Infrared Spectroscopy

FTIR studies have been carried out to identify hydrogen-bonding interactions as an indication of the self-assembly of the tripeptides formed. Significant peaks are

observed in the gel state due to the ordered hydrogen-bonding involved in forming nanostructures between corresponding peptides (Figure 4.9). Standards of DFF-NH_2 show clear peaks around 1650 cm^{-1}. In proteins, the presence of peaks around 1650 cm^{-1} indicates the carbonyl stretch of random coil. However, as discussed in Chapter 2, the presence of peaks at 1650 cm^{-1} indicate the formation of ordered nanostructures. There is a clear splitting of the peak suggesting two different types of hydrogen bonding. Previous research has shown similar observations have a significant role in the formation of a self-assembled fibers.[124] On comparison with DFF-OH, this peak is not present; therefore no strong, ordered hydrogen bonded interactions are formed in this peptide (Figure 4.9).

As expected with the heated sample, the peak at 1650 cm^{-1} remains unchanged over time showing the stable nanostructure formed by the peptide remains as the enzyme become inactivated. This is in contrast to the different pH samples; in the pH 9 sample, the 1650 cm^{-1} peak begins to diminish at a greater rate. This is due to a greater reaction rate as the enzyme is more active compared with the lower pH and as a result, greater effects are observed in the FTIR. At pH 7, the 1650 cm^{-1} peak show a slower reduction compared with the sample at pH 9, consistent with the view that the activity is slightly lower. At pH 5, the 1650 cm^{-1} peak remains relatively unchanged over the time course of the experiment, compared with the higher pH values, showing that the effect of hydrolysis is much slower at lower pH.

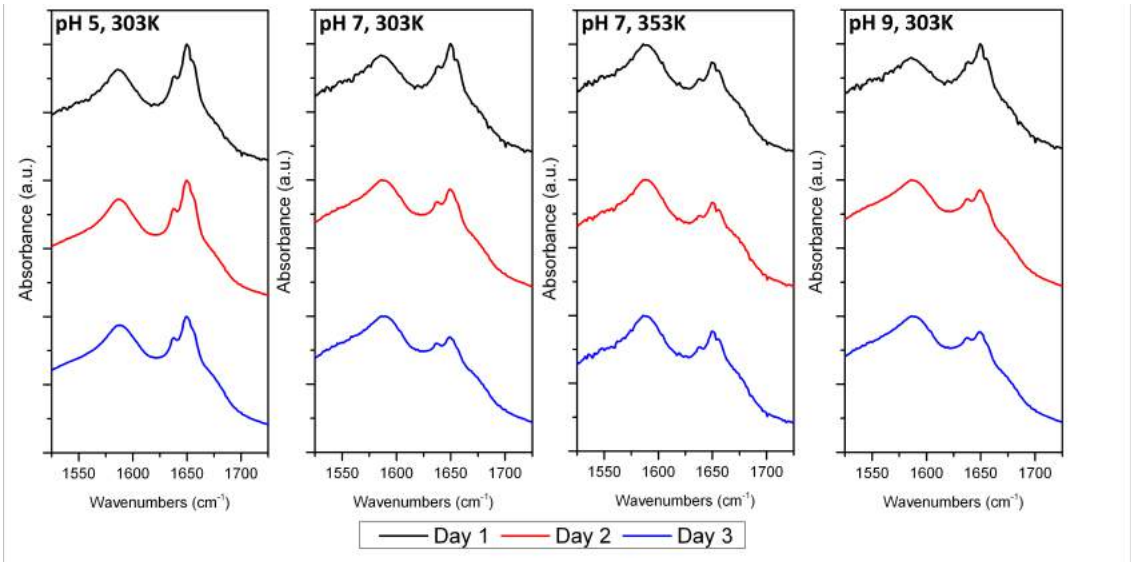

Figure 4.9: FTIR spectra over the course of 3 days, indicating the loss of supramolecular structure in each of the 4 conditions

4.3.3 Transmission Electron Microscopy

Corresponding TEM images were collected from each of the samples 1 day after the initiation of the reaction (Figure 4.10). As can be seen at pH 5, fibers are clearly observed (~30 nm in diameter). In contrast, as the pH increases to 7 these fibers become shorter, thicker (~100 nm) and less entangled. At pH 9, no definitive fibers are observed and small aggregates have formed (~20-40 nm). This is a result of the hydrolysis of DFF-NH_2. Loss of definition of the fibers has occurred and the structure begins to break down. When the reaction is carried out at elevated temperature, larger fibers (approximately 100 nm in diameter) are observed. The size distribution of the fibers on changing conditions is of note. On average, the distribution of peptide nanofibers range from 30-60 nm,[124, 233] taking into consideration N-protected and unprotected systems. At low pH, longer fibers are observed due to lack to hydrolysis of the DFF-NH_2. Upon increasing the pH to 7, the hydrolysis reaction occurs at a greater rate and therefore shorter fibers are observed. At pH 9, no fibers are observed due to the high levels of hydrolysis.

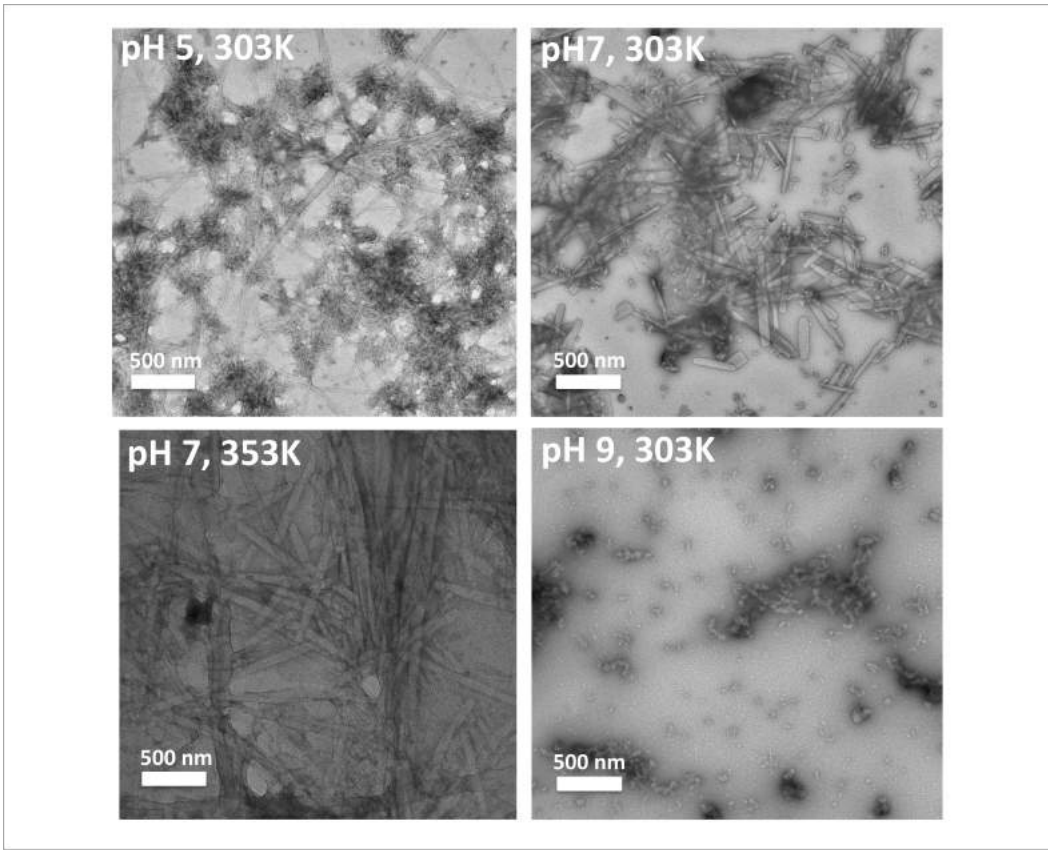

Figure 4.10 TEM images of the resultant assemblies for each of the peptide systems in their define conditions

4.3.4 Coarse-Grain Molecular Dynamics

As shown by LCMS, FTIR and TEM, as the hydrolysis process proceeds, structural changes of the resulting peptide nanostructure occur. Coarse-grained molecular dynamics simulations were carried out to visualize and identify how these structures change. On the formation of DFF-NH_2 (Figure 4.1) the peptide forms a tubular structure where the peptides arrange in a bilayer fashion where a cavity appears allowing for water to penetrate the core. Upon hydrolysis to DFF-OH, the three-dimensional tubular structures break down and give a sheet-like structure (Figure 4.11). This structure does not allow for the entrapment of water, which is consistent with the breakdown of the hydrogel at the macro scale. Further hydrolysis to DF-OH shows that very little aggregation occurs, resulting in clear solutions on the macroscale (Figure 4.11).

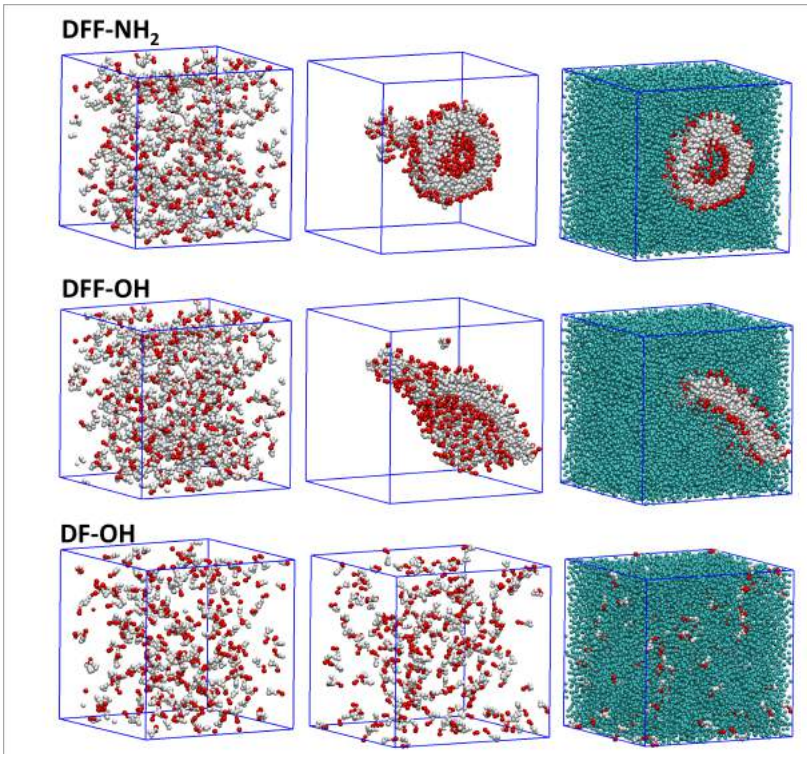

Figure 4.11 Coarse grained molecular dynamics simulations DFF-NH_2, DFF-OH and DF-OH indicating the differences in supramolecular structures from alteration of the certain groups.

4.4 Conclusions

In conclusion, it has been shown that alteration of the physical conditions such as temperature and pH, allows the control of peptide nanostructures by regulating the bio-catalytic ability of α-chymotrypsin. This enables control and isolation of different peptide products to >60% when competing pathways are present. Increasing the temperature allows for prevention of continuous hydrolysis by denaturation of the enzyme. This was shown to stop all process allowing for isolation of the target product. Alteration of the pH, changes reaction kinetics. At low pH, the rate of hydrolysis is reduced by changing the structure of the enzyme, whereas, at high pH the enzyme has a greater rate of hydrolysis. To further examine this work, using different starting methyl esters such as KY-OMe and KF-OMe, can fully investigate the benefits of using enzymatic procedures. Using these methyl esters, creation of tripeptides where self-assembling nanostructures are already observed can give a greater application for these systems. Furthermore, an investigation into small changes in physical conditions to fine tune these assemblies would be a great addition.

4.5 Materials and Methods

4.5.1 LCMS time course

LCMS data was acquired using an Agilent 6130 APCI LCMS and a Poroshell 120 EC-C18, 4.6 x 7.5 mm, 2.7 micron column. Flow rate 1 mL/min, injection 10 µL. Samples were solubilized in 50% acetonitrile in water with 0.1% TFA. The gradient for the measurements consisted of the following:

Time	Composition
0.00	95% water, 5% Acetonitrile
1.48	95% water, 5% Acetonitrile
8.50	0% water, 100% Acetonitrile
13.50	0% water, 100% Acetonitrile
16.50	95% water, 5% Acetonitrile
18.00	95% water, 5% Acetonitrile

50 µL aliquot of sample was removed at every time point and added to 950 µL of 50:50 acetonitrile/water mixture with 0.1 % TFA. The sample was then vortexed to ensure full dispersion of the sample in the HPLC vial. Each sample was then assessed via the LCMS method shown above.

4.5.2 Transmission Electron Microscopy (TEM)

Carbon-coated copper grids (200 mesh) were glow discharged in air for approximately 30 s. The grids were placed on the gel material of liquid solution before being blotted down using filter paper to remove the excess. 20 µL of negative stain was applied (1% aqueous methylamine vanadate obtained from Nanovan, Nanoprobes) prior to a further blotting using filter paper. Samples were then left to dry. The dried samples were then imaged using a LEO 912 energy filtering transmission election microscope operating at 120 kV fitted with 14 bit/2K Proscan CCD camera. TEM imaging was carried out at the University of Glasgow.

4.5.3 UV Spectroscopy

UV spectroscopy was carried out on a Jasco V-660 spectrophotometer using 1 cm path length measuring absorption at 400 nm. 800 mL of the chosen solvent system was pipetted into a glass vial. To the solvent, 100 µL of N-glutaryl L-phenylalanine-*p*-nitroanilide dissolved in methanol was added in addition with 100 µL of 1 mg/mL solution of α-chymotrypsin. Each sample was quickly inverted three times before being transferred to a UV cuvette for analysis.

4.5.4 Circular Dichrosim (CD)

CD measurements were performed using a Jasco J600 spectropolarimeter in a cylinder cell of 0.1 mm path length. Spectra were recorded with a step resolution of 1 nm, response of 1s, bandwidth of 1.0 nm and a scanning speed of 50 nm/min. CD spectra was recorded between 190 -250 nm to determine changes in secondary structure. Each sample was prepared by making solution of 0.1 mg/mL α-chymotrypsin in each corresponding buffer solution. For the heated sample, the sample was heated in an oil bath directly after the addition of the enzyme to the buffer solution. 100 µL of the sample was pipetted into a CD cell.

4.5.5 Fourier Transform Infra-red Spectroscopy (FTIR)

FTIR spectra were acquired using a Bruker Vertex70 spectrometer with a spectral resolution of 1 cm^{-1}. Spectra were obtained by averaging over 25 measurements for each sample. Measurements were performed using standard FTIR cuvettes (Harrink Scientific) where the sample was sandwiched between 2 CaF_2 discs (Crystran Ltd) separated by a 50 µm PTFE spacer. For gel materials, a small amount of small was placed in the CaF_2 discs using a microspatula. For free flowing samples, 100ul of the sample was pipetted directly onto the disc. D_2O was used as the solvent.

4.5.6 Coarse-Grain Molecular Dynamics

Molecular dynamics simulations were performed in GROMACs using the MARTINI force field version 4.5.3.

300 molecules of the chosen tripeptide was added to a box with the dimensions 12.5 x 12.5 x 12.5 nm. For DFF-NH_2, the C-terminal bead type was changed from Qa bead type to Nda. This was to compensate for the loss in the terminal charge on the peptide. The simulation box was then solvated using standard CG water. The system was then neutralized with the addition of sodium or calcium ions. The system was then subject to a minimization for 5000 steps to ensure no overlap atoms. Once minimized, the system was subject to production run of 9.6 μs.

5.

Counter-Ion Effects on Tripeptide Nanostructures and Hydrogels

Declaration of contribution to published article: Any reproduced practical work from the aforementioned published article; I was solely responsible for, unless otherwise stated.

5.1 Introduction

Throughout this thesis, it has been shown that the versatility of peptides allows for the formation of different nanostructures, some of which have the tendency to form hydrogels. One of the main reasons why this is possible is the many different interactions that influence the self-assembly. Of the peptides that have been discussed, only the cationic peptide KYF, KYW and KFF have shown the ability to form hydrogels, whereas anionic peptides such as FFD and DFF form clear solutions, although these do form nanostructures. Reasoning behind the clear differences in assemblies is the repulsive electrostatic interactions between the negatively charged residues. The charged residues on peptides in some cases are important for the formation of salt bridges, which is a relatively strong interaction, however, the reverse repulsive interaction can also be present which can be detrimental to a self-assembling system resulting in the collapse of the supramolecular nanostructures. The presence of salts can greatly influence supramolecular interactions. Alteration of the ionic strength, reduces the repulsive interactions observed between peptides allowing them to interact to form ordered nanostructures.

5.1.1 Hofmeister Series

Ion effects are abundant in chemistry, in particular in aqueous media. More than a century ago, in 1888, Franz Hofmeister[234] ranked ions based on their ability of salting out proteins from solution. This ranking order gave rise to the Hofmeister series. The Hofmeister series was generally more pronounced for the determination of anionic effects on proteins, however cations have also been studied. The Hofmeister series can be split into two different regions: Kosmotropes and Chaotropes (Figure 5.1). These terms were originally denoted due to the anions ability to interact and alter the hydrogen-bonding network of water. Kosmotropes, which are water structure makers, are highly hydrated and have salting out ability on macromolecules, which stabilizes these macromolecules such as proteins. On the other hand chaotropes are said to be water structure breakers, as these anions tend to salt in macromolecules destabilizing proteins.

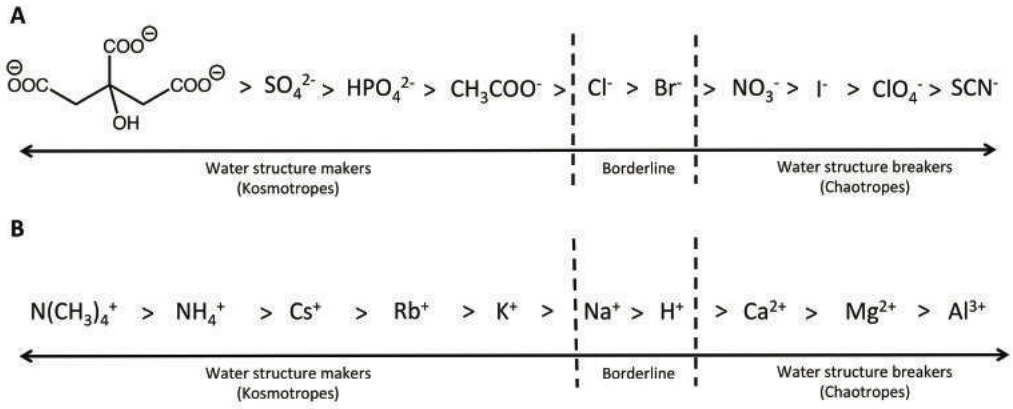

Figure 5.1: Hofmeister series of salts A) Anions C) Cations indicating the Kosmotropes and Chaotropes

In recent times, the understanding of the Hofmeister salts has started to become important due to growing relevance across a number of fields. It has been documented that the presence of these salts can affect protein stability[235-236], protein-protein interactions[237-239], enzyme activity,[240-246] etc.

5.1.2 Ionic Interactions Inducing Supramolecular Assembly

Understanding how salt affects supramolecular assembly is key for the development of new biomaterials as salts are clearly present in the aqueous media where these biomaterials are utilized. It is clear that ionic interactions are vital for peptides to assemble into highly ordered nanostructures.[124, 247] These ionic interactions are controlled by alteration of the physical conditions within the system.[248-249] The pH at which ionic groups can interact vary depending on the protonation state of these side chains. In soluble peptides, the protonation state of the amino acids is indicated by the pK_a values associated with each side chain. At physiological pH, 7.4, all carboxyl groups are deprotonated resulting in a negative charge. For the N-terminus, the pK_a is approximately 8.0 suggesting this terminus can be situated in a meta-stable state where both protonated and deprotonated states exist. On the other hand, for anionic amino acids such as aspartic acid, pK_a 4.1, the side chain will remain predominately in the deprotonated state.[250] These highly charge species results in a rearrangement of the peptides to form structures that are incapable of forming hydrogels.

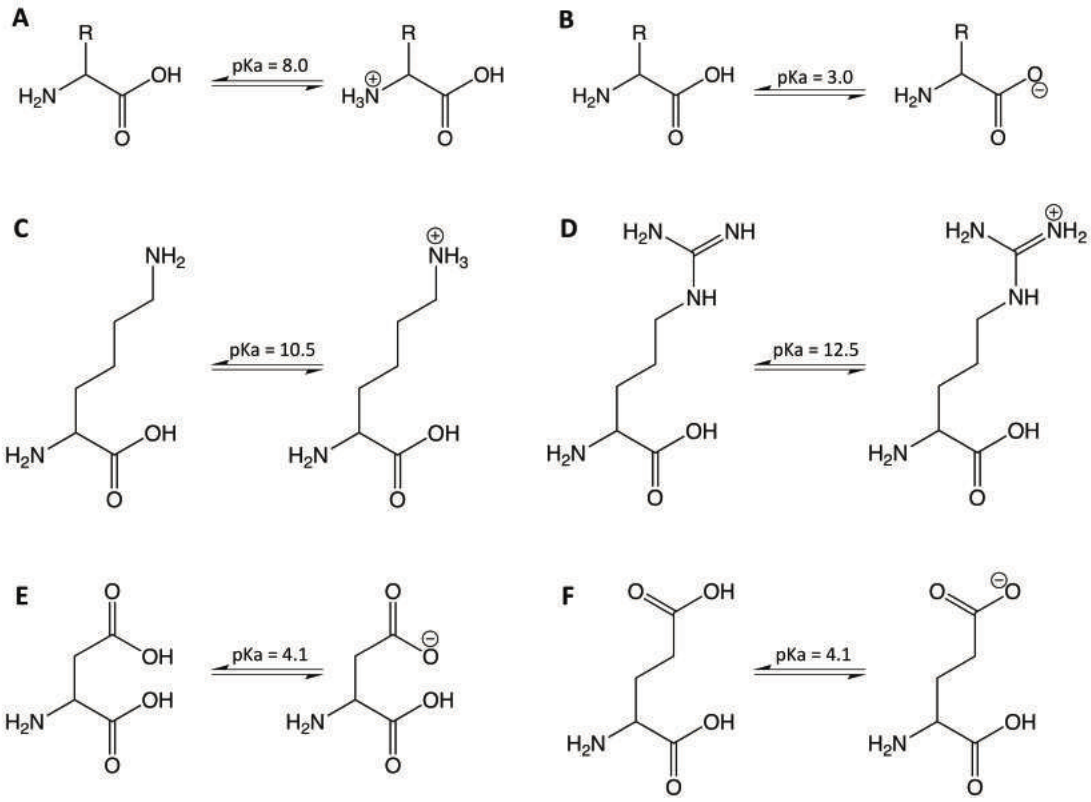

Figure 5.2: Resonance structures of ionizable amino acids A) N-terminus B) C-terminus C) Lysine D) Arginine E) Aspartic acid and F) Glutamic Acid with their associated pKa value

So far we have mentioned that one of the most influential supramolecular interactions is the electrostatic interaction between peptides. However, upon the formation of supramolecular nanostructures, different environments are created which can affect localized ionization. It is known that pK_a can shift in protein and peptide self-assembled systems due to the hydrophobic effect.[251-252] Shifts of up to 6.1 pKa units have been observed for aspartic acid based proteins in polymer-based pentapeptides.[253] In addition, pK_a shifts were observed in fatty acids such as palmitic acid.[254] Work carried out by Tang *et al.*,[23] examines the apparent pK_a shifts exhibit by Fmoc-FF at high concentrations. In this paper, the pK_a shift was followed *via* titrations at different concentration for Fmoc-FF with HCl. At low concentration such as 0.01, 0.1 and 1 mM, *i.e.*, below the critical aggregation concentration, it was evident that shifts in the apparent pK_a were not present. Upon increasing the peptide concentration to 5 and 10 mM it was clear that two apparent pK_a shifts were present. It was observed that there were dramatic pK_a shifts present at

approx. 9.5 and 6.5. pK_a[23] units where the normal N-protected nonpolar peptide have a pK_a at approximately 3.5.[255]

In addition to the titration of the peptides, 10 mM Fmoc-FF was subject to FTIR spectroscopy at pH values above and below each of the shifted pK_a values.[23] As the FTIR is used to determine changes in molecular structure of the assembled structures, it is clear that alteration of the pH affects the molecular interactions. At pH 10.5, the signal was low, however, there are peaks at 1625 cm^{-1}, suggesting formation of β-sheet structures. Upon lowering the pH below the first shift, the sample formed a translucent hydrogel, and indicated intense peaks at 1625 and 1687 cm^{-1} indicating the formation of an anti-parallel arrangement of β-sheets.[23] Further changing of the pH to the second pK_a shift, indicates similar amounts of ordered structure, however, as the pH passes to pH 4.2, further aggregation occurs followed by precipitation. At this point it is suggested that the terminal carboxylate has been protonated, which allows the peptide to aggregate further.[23]

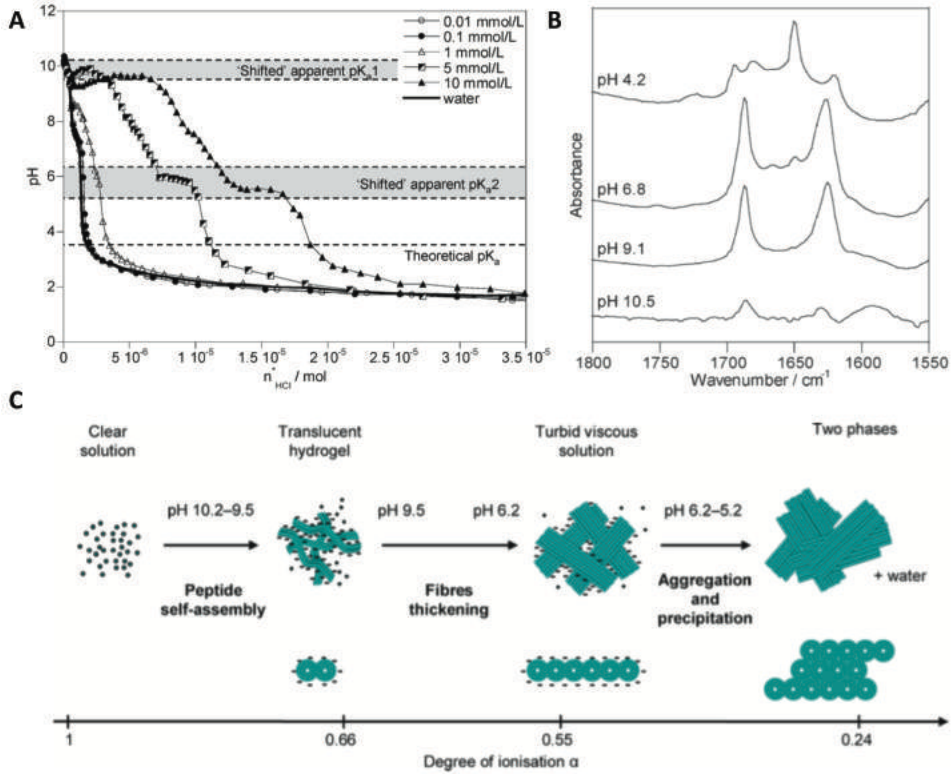

Figure 5.3: Apparent pK_a shifts of Fmoc-FF. A) Titration curved of Fmoc-FF at different concentration indicated shift pK_a values B) FTIR of Fmoc-FF at 10 mmol/L and C) Illustration of proposed mechanism associated with Fmoc-FF upon alteration of the pH. Image adapted with permission from Ref [23] Copyright (2009) American Chemical Society

This work was followed by examining the sequence dependence of Fmoc-dipeptides for their self-assembling ability upon changing pH.[256] In this case, a comparative study between Fmoc-FF, Fmoc-GG, Fmoc-GF and Fmoc-FG was carried out.[256] Initial titration experiments indicated a single apparent pK_a shift in Fmoc-GG/Fmoc-GF/Fmoc-FG peptides whereas in Fmoc-FF two shifts were observed. This was correlated to the hydrophobicity of the Fmoc-dipeptide molecules. In all cases, each peptide amphiphile self-assembled into nanostructures, however, Fmoc-GG and Fmoc-GF were only found to self-assemble below their apparent pK_a shift (which occurs at pH 4.8 and pH 7.6, respectively).[256] In contrast Fmoc-FG was observed to assemble above and below the pK_a shift, however, above the apparent pK_a shift, the sample forms twisted ribbons.[256] On comparison of different concentrations of the peptides, it is evident that higher peptide concentration increase the apparent pK_a shift for all samples.[256] The gelation behavior between the peptide amphiphiles changes from system to system. Fmoc-FG and Fmoc-GG both form hydrogels below the apparent pK_a shifts, which is in an agreement with the TEM analysis. Fmoc-GG formed similar structures to that observed in Fmoc-FF,[23] and Fmoc-FG was found to form hydrogels upon heating of the peptide. This process results in strong hydrogels where the storage modulus (G') decreases upon cooling. Fmoc-GF did not form hydrogels below the apparent pK_a shift, which is agreement with the TEM analysis where the peptide formed sheet–like structures. Overall, it has been observed that changing the amino acid residue from phenylalanine to glycine has a dramatic effect on the self-assembling ability of the Fmoc-dipeptide.[256] As all samples assemble into nanostructures, the hydrophobic effect and π-stacking interactions play a vital role in driving the peptides to self-assembly.[256] However, the location of the glycine residue alters the self-assembling ability of the peptide. Situating the glycine reside at the N-terminal position increases the flexibility along the dipeptide backbone. This reduces the backbone-backbone hydrogen bonding interactions, which are vital for assembly. The presence of phenylalanine at the N-terminal position makes the backbone more rigid allowing for a greater hydrogen-bonding interaction between the peptides.[256]

Although, changes in pH are important for understanding how peptides can interact and pack together, the presence of salts lower the effect of electrostatic repulsion and promotes self-assembly. Work by Roy *et al.*[257] examined the self-assembling behavior of different Fmoc-dipeptides under the influence of different salts. In this paper, they examine the dipeptide Fmoc-YL to establish the effects of changing the anion on the self-assembly of the peptide. As the formation of hydrogels is driven by the hydrophobic effect, with the structures formed further stabilized by π-stacking and hydrogen bonding interactions, the packing of the peptide can be monitored via fluorescence emission spectra (Figure 5.4, caption A). The peak at 320 nm, corresponds to the emission of the Fmoc group. The suppression of the intensity of the peak indicates the favoring of the stacking of the fluorenyl groups. This suppression follows the Hofmeister series, which indicates that kosmotropes promote the hydrophobic effect in the assembled states.[257] In addition, examination of the changes in secondary structures observed through CD also indicates that kosmotropes promote the formation of higher ordered structures (Figure 5.4, caption B). Upon, changing the salts from kosmotropes to chaotropes, it is evident that a decrease in CD occurs. This relates to loss of secondary structure of the assembled structures, suggesting that H-bonding interactions become less prominent.[257] This results in a morphological change, from highly ordered fibrous structures, observed for samples in phosphate, compared with spherical micellar aggregates in the presence of thiocyanate.[257]

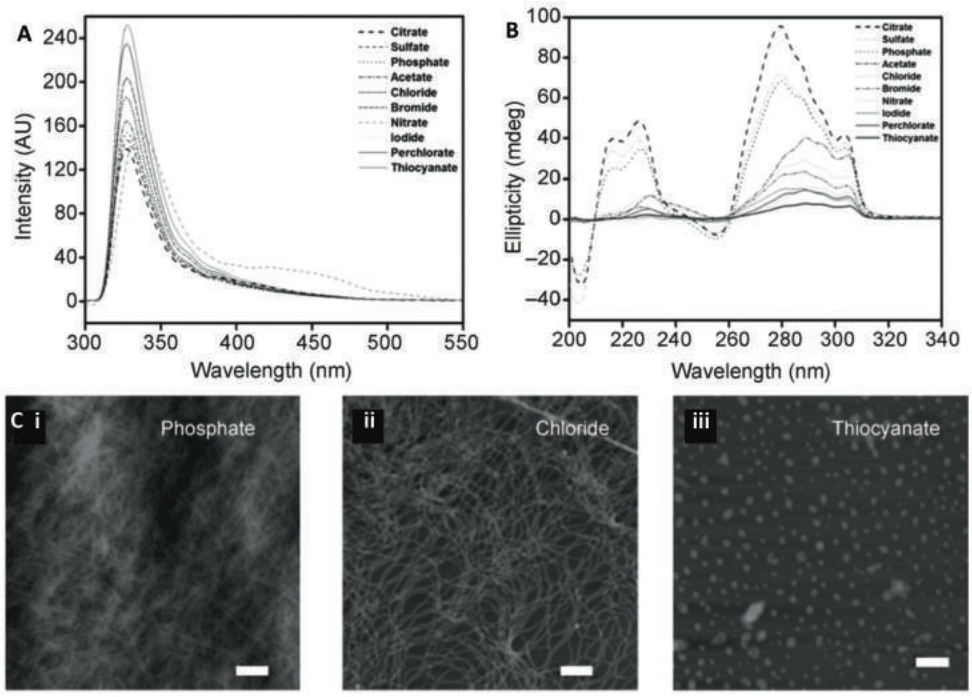

Figure 5.4: Analysis of Fmoc-YL in different salt solutions. A) Fluorescence emission spectroscopy B) CD C) AFM (scale bar 500nm). Image adapted with permission from Ref [257] and John Wiley & Sons, Inc. Copyright (2012) John Wiley & Sons. Inc

Nebot *et al*[258] then further built on this type of work, where they show the specific salt effects on the hydrogelation of a bolaamphiphilic peptide. In this case, they observed that in the presence of chaotropes the solubility of the of the peptide was high, thus the hydrophobic effect is disrupted not allowing the peptide to hydrogelate.[258] On moving to kosmotropic anions, the solubility decrease in such that the hydrogelator was soluble up to 3.3 mM, in the presence of sulphate, whereas in other salts the solubility was greater (thiocyanate – 10 mM, Chloride - 4 mM, no salt 9.3 mM).[258] In addition, upon increasing salt concentration, from 0 mM to 500 mM, kosmotropic salts lowered the solubility of the peptide. Rheological properties of the peptides were examined to ascertain the mechanical strength of the hydrogels. It was distinguished that the presence of Kosmotropes resulted in an increase of the G', as seen for both fluoride and sulphate anions.[258] Conversely, Chaotropes did not alter the rheological properties of the hydrogel to a great extent form the control experiments (no salt).[258] These results, in addition with those presented in Roy *et al*, confirm the importanrt role that salts can play in the process of peptide self-assembly.

Similar work was carried out by the Adams and co-workers[259-260] where they focused on the interactions of salts with Naphthalene protected dipeptides. In this publication, they examine that peptides such as Nap-FF and Nap-AV show highly viscous materials at high pH (~ 10.5).[259] However, in the presence of salts, there is a promotion of hydrogelation. Results indicate there is an affinity for the peptides to form stronger hydrogels in the presence of divalent cations such as Ca^{2+}. In addition, the choice of anionic counter ion affects the mechanical properties of the hydrogels. For example, the strengths of hydrogels vary for NaCl, $NaNO_3$ $CaCl_2$ and $Ca(NO_3)_2$ where, the mechanical properties (G') are 153, 182, 72,897 and 74,211 Pa respectively.[259] This indicates that calcium has a dramatic effect on the mechanical strength of the hydrogels while the anionic counter ions slightly alter the strength. This work was carried on further by altering the side chains with protecting groups.[260] Finally, in the papers that were previously discussed, researchers relied on the presence of Hofmeister salts to change the morphological and rheological properties of hydrogels by impacting on the hydrophobic effect. However, it has been well known that certain ions can also be specifically involved in gelation, for example, the presence of calcium ions can act as cross linkers in anionic peptides to promote self-assembly for peptides by masking the charges of the side chains. Work by Mart *et al.*[261] showed that the presence of $CaCl_2$ was able to trigger the sequence FEK into a structural rearrangement where the calcium ions are able to crosslink between the anionic amino acids. Indeed, calcuium has been shown to be a popular choice in the promotion of peptide self-assembly for a number of different applications. [262-263]

In this chapter, the behavior of the non-gelating tripeptide FFD was examined in the presence of chloride, sulphate, phosphate and citrate. In addition, an investigation into the difference between sodium and calcium ions in affecting the self-assembling ability of FFD will be carried out.

In order to examine this, the following aims were set:

1. Determine if the presence of cations can improve the self-assembling ability of the non-gelating tripeptide FFD to induce gelation at pH 7.4

2. Examine how anions affect the supramolecular packing of the peptides and identify if these alter the mechanical properties of any hydrogels.

5.2 Effect of Sodium of FFD Assemblies

As discussed in the introduction, the presence of counter ions can assist peptides' ability to assemble together. Ions can balance the strong repulsive charges that build up throughout the systems and can therefore promote cross-linking between peptide molecules. Cation selectively for promoting molecular interactions in addition with how the anionic counter ion can have a role in determining the packing and overall strength of the final self-assembled structures, is investigated. To this extent, it is observed that the role of the ions is three-fold, general electrostatic screening, specific interactions of divalent cations with carboxylates and impacting the hydrophobic effect.

FFD is an anionic tripeptide that at neutral pH assembles in nanotubes (see Section 2.3), but does not form a hydrogel. In this section we will examine the behavior of FFD in the presence of the different salts but more specifically we examine how the peptide interacts with the cation. It is well-known that the presence of calcium promotes crosslinking between peptides, therefore we compare the different structural effects sodium and calcium have on the peptides' ability to interact.

5.2.1 Macroscopic Analysis

All FFD samples are produced with a peptide concentration of 20 mM in water. In order to determine the effectiveness of the salts in the solutions, a macroscopic examination of the samples are performed at varying salt concentrations. To this end, the systems were examined at 2 mM, 20 mM and 200 mM salt concentration of sulphate, chloride, phosphate and citrate, whilst keeping peptide concentration constant. An investigation into salt assisted peptide self-assembly could be carried out at equimolar concentrations, however, it was determined that multiple peptides can be involved with a single cation. Therefore, an examination of both a 10-fold increase and decrease of the salt concentration, as well as equimolar (1:10; 1:1; 10:1) would allow for a fuller understanding of the role of the salts.

Upon dissolution of the peptide in the sodium salt solution (chloride, sulphate, phosphate and citrate), the samples were vortexed and sonicated to ensure full dissolution. The samples were then left for a period of 24 hours to allow for any nanostructures to form. After this period, it was apparent that there was no change in macroscopic appearance of the samples (Figure 5.5). This initially concludes that the presence of sodium anions with a range of different anions do not induce a gelation behavior of the peptides. However, a closer examination of the systems on the molecular level is required.

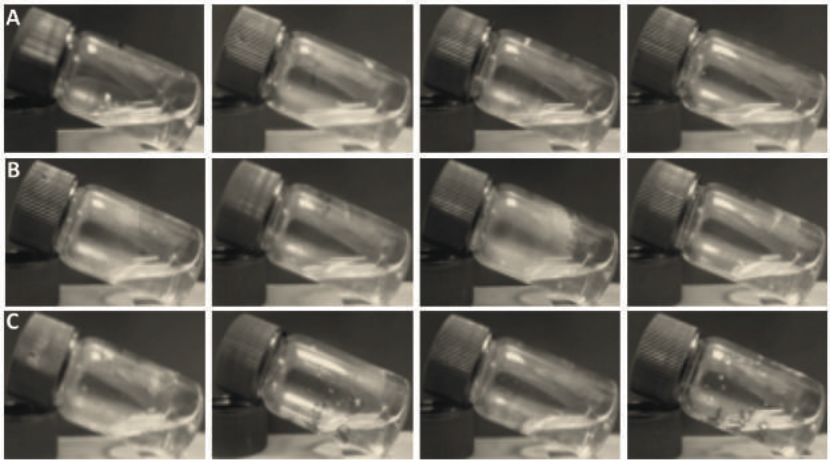

Figure 5.5: Digital images of the macroscopic assembly of FFD in different sodium salts (*left* to *right*, citrate, sulphate, phosphate, chloride) at A) 2 mM B) 20 mM C) 200 mM salt concentration

5.2.2 Fourier Transform Infrared Spectroscopy

As in previous chapters, FTIR can be used to aid the understanding of hydrogen-bonding interactions involved in the self-assembly process. Interestingly, on looking at the FTIR spectra obtained from each of the samples, it was evident that there was no change in supramolecular H-bonding apparent in the presence of these salts (Figure 5.6). Each sample show a large broad peak at 1580 cm^{-1} which indicated the presence of the carboxylate group. However, examination of the amide I region reveals no peaks which suggests ordered hydrogen-bonded structures are not present. Differences are observed in the samples containing sodium citrate due to the increased concentration of the citrate anion. The citrate anion consists of three C-O groups, which result in the increase in intensity of this peak.

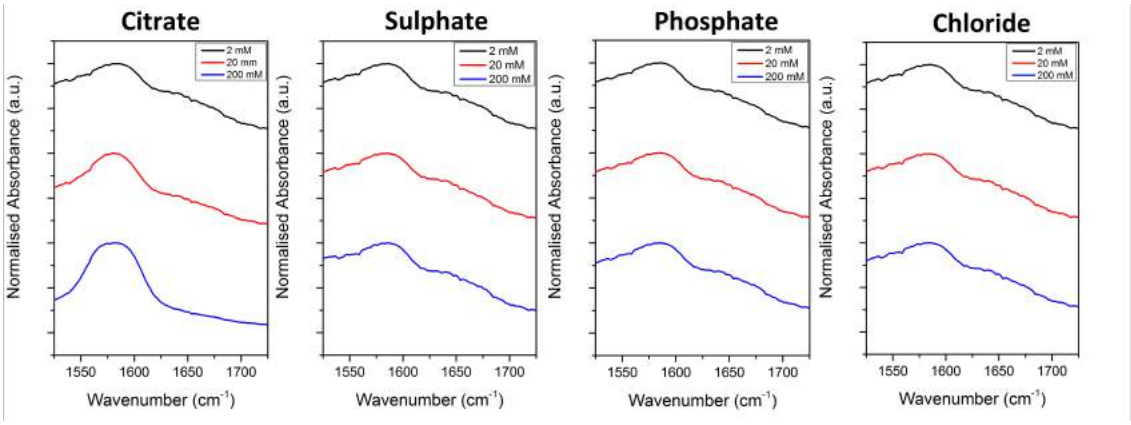

Figure 5.6: FTIR spectra of FFD in different sodium salts

5.2.3 Atomic Force Microscopy

Although the FTIR does not indicate the presence of ordered hydrogen-bonded structures, it is important to visualize these nanostructures in order to determine if the peptides are interacting. In this case atomic force microscopy (AFM) is used for samples at a concentration of 2 mM. In this technique a micro-sized tip is tapped across a surface, which gives an image of the surface, based on the cantilever deflection, for the visualization of any nanostructures that have formed. AFM results for all samples showed different types of assemblies depending on the salt (Figure 5.7). FFD in the presence of sodium citrate assembles into sheet-like structures that stack on top of each other. These structures vary in length, although the diameter of the stacks is relatively constant at *ca.* 300 nm. This is quite large compared with observed structures for hydrogels but due to the block-like nature of the structures and the inconsistent length, this give a probable reason for the inability to form hydrogels. However, the shape and size of these samples could indicate the presence of salt crystals due to the precipitation of the salt during the drying process. These structures are unable to entangle and trap water molecules thus they do not give rise to a hydrogel. Sodium sulphate, does form fibrous type structures however these structures are large, *ca*. 410 nm and are uniform in length which, similarly to citrate, would be unable to assemble into structure that are capable of form hydrogels. Sodium phosphate forms large aggregates and the chloride derivative form similar structures to that observed for sulphate. Although the choice of anionic counter ion does not induce any gelation

properties of the samples, there are clear differences in the shape of structures that are formed. Anions that tend to be more kosmotropic form more ordered structures. However, these structures doe not formed the required structures for hydrogelation.

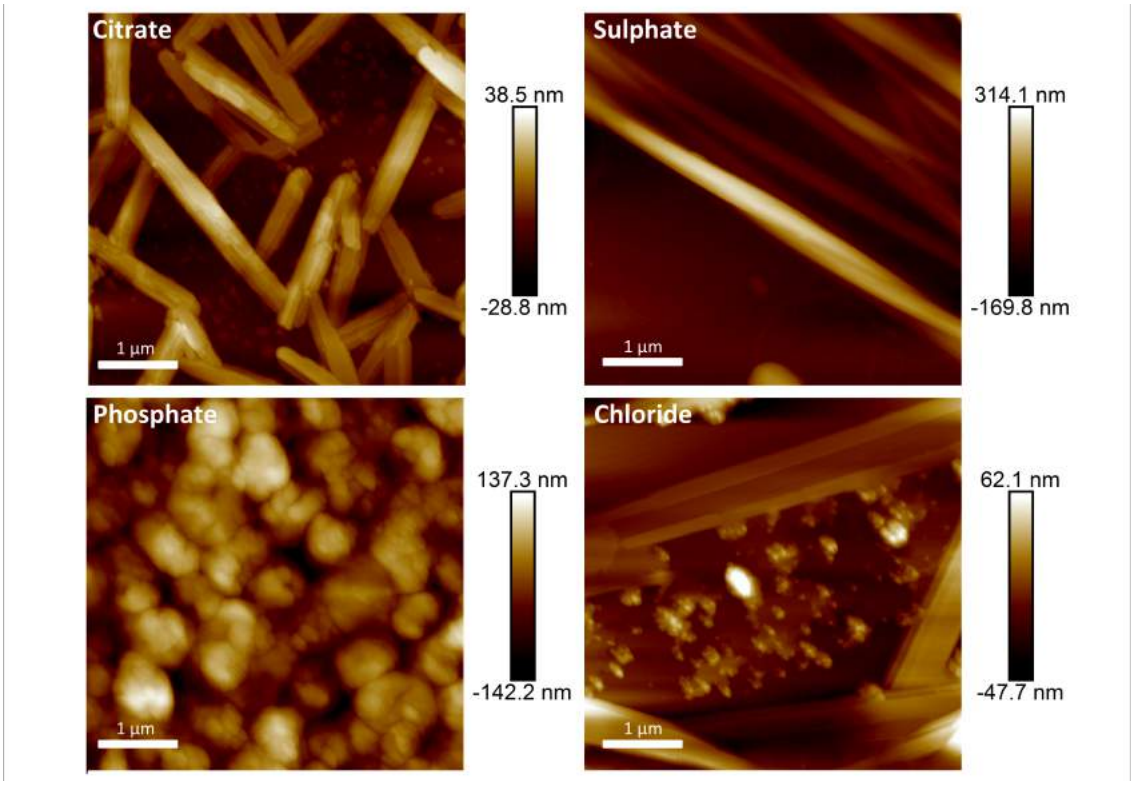

Figure 5.7: AFM images of FFD assembling in the presence of different sodium salts

5.2.4 Summary

In summary, the behavior of FFD in the presence of different sodium salts has been carried out. It is evident that sodium does not provide an adequate stabilizing ability to allow FFD to closely interact to form nanostructures capable of forming hydrogels. Through FTIR, there is no change in the interaction at a molecular level whilst macroscopically there are no nanostructures that are formed that would be capable of trapping water molecules. There are subtle differences in size and shape of the structures formed from different anions. However, these differences do not result in the formation of hydrogels.

5.3 Effect of Calcium Ions on FFD Assemblies

Calcium ions have shown benefits by the reported crosslinking of peptides, which help promote the self-assembly of the peptides. In this section we explore how the presence of calcium ions promote this behavior and can give rise to formation of hydrogels.

5.3.1 Macroscopic Analysis

Similar to the FFD/sodium salt systems, all samples are prepared at 20 mM peptide concentration with different salt concentration to determine how the salt interacts with the peptides. Due to the limited solubility of the calcium salts, high concentrations of these salts were unable to be analyzed (Figure 5.8). As a result, for calcium citrate the maximum salt concentration achievable was 1.66 mM, calcium sulphate was 15 mM and calcium phosphate was 85 mM. Upon dissolution of the peptides at pH 7.4, samples form a clear solution; repeated vortexing and sonication resulted in the formation of a turbid solution. After 30 secs of repeated vortexing and sonication, the samples were left for a period of 24 hrs. After this time, all samples showed gelation behavior at a salt concentration of 2 mM. Upon increasing of the salt concentration, each system starts to behave differently. 15 mM calcium sulphate does not form a homogeneous hydrogel, although there are clear signs of aggregation of the peptides. The formation of aggregated clumps of peptide suggests that the increase in salt concentration causes the peptide to interact at a much greater rate than at lower salt concentration. As a result, the hydrophobic effect is the main driving force for these peptides and the self-assembled structure begin to salt out resulting in the precipitation of the peptides. For calcium phosphate and chloride, this effect is similar although the samples do tend to hold their structure more efficiently. However, it is evident that upon increasing the salt concentration, this has a detrimental effect on the peptide ability to form a hydrogel.

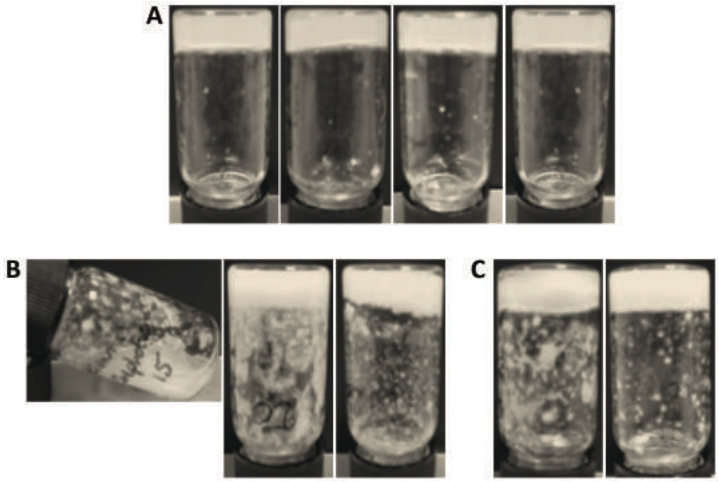

Figure 5.8: Digital images of FFD hydrogels in the presence of calcium salts (*Left* to *right* - citrate, sulphate, phosphate, chloride). A) 2 mM with exception of citrate which was 1.6 mMB) 20 mM with exception of sulphate which was 15 mM C) Calcium phosphate at 85 mM and calcium chloride at 200 mM.

5.3.2 Fourier Transform Infrared Spectroscopy

To understand the self-assembling ability of these gelating peptides, FTIR was used to determine the supramolecular interactions that play a pivotal role in these assemblies. Firstly, by comparison with sodium salts (see Section 5.2) it is quite clear that the presence of calcium has a stronger role in the self-assembly process, which is shown by the formation of hydrogels but also, the dramatic changes in FTIR signals (Figure 5.9).

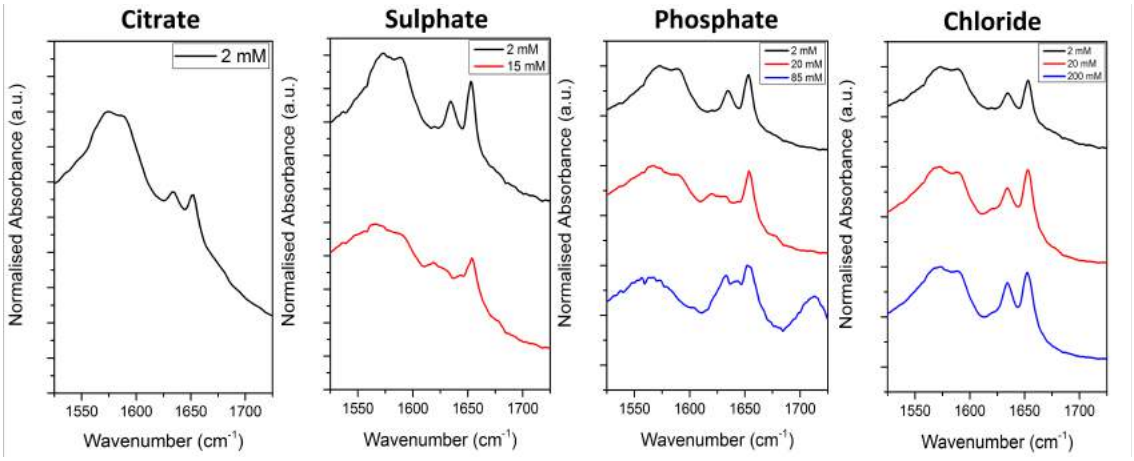

Figure 5.9: FTIR of FFD in the presence of calcium salts at different concentrations

For calcium citrate, the appearance of peaks at 1625 and 1649 cm^{-1} indicate the presence of hydrogen bonding environments. Unfortunately, due to the presence of citrate in the samples, this has lead to a strong signal at 1580 cm^{-1} where the carboxylate peak is located. Despite the strong carboxylate signal, it can be seen that there is a splitting of this peak, which suggest that the carboxylate is situated in two different environments, one of which is creating a salt bridge. Due to the pH of the systems, 7.4, it is likely that this is a cross-linked salt bridge between the peptide (COO^{-} ••• Ca^{2+} ••• COO^{-}) that is allowing the peptide to interact with each other. Similar observations are seen with all the systems; however, upon increasing of the salt concentration, different effects are observed.

For calcium sulphate, increasing the salt concentration results in loss of the ordered hydrogen-bonding peak. Loss of the 1625 cm^{-1} peak suggests that the beta-sheet formation is disrupted. This could potentially be due to the increase in calcium ions bringing the peptides closer together by electrostatic screening, resulting in the hydrophobic effect having a greater influence in the packing of the peptides. Additionally, the presence of the double negative charge of the sulphate groups could interfere with the peptides and increasing the concentration builds up this charge, which affects the packing. In addition, at 1580 cm^{-1}, this peak shifts to a lower wavenumber, indicating the greater tendency for the peptides to form salt bridges. Loss of this 1580 cm^{-1} peak suggest that the greater number of calcium ions results in a greater number of stabilized electrostatic interactions, thus, there a fewer free carboxylate groups present.

Changes are more evident in samples containing calcium phosphate. At low salt concentration, the splitting between the free carboxylate and the stable salt bridge is clear. Upon increasing the salt concentration the disappearance of the 1580 cm^{-1} peak results in a more pronounced peak at 1560 cm^{-1}. In addition, changes in the amide I region indicates that the presence of the salt disrupts the organization of the hydrogen bonding. At low concentrations, a typical FTIR spectrum is recorded for FFD assembling under the influence of calcium. Upon increasing the salt concentration, the peak associated with ordered hydrogen bonds have diminished and indicating the loss of ordered structures. However, upon increasing the

concentration to 85 mM, this peak begins to re-appear. A loss in definition between the two types of hydrogen bonding modes becomes apparent (peak broadening) the sample become much more aggregated. That is, there is less structure to the self-assembled peptides, which result in the broader signals.

Finally, on inspection of the FTIR spectra obtained from calcium chloride samples, it appears that this salt does not alter the molecular interactions to the same extent as observed with the other calcium-based salts. At 2 mM, 20 mM and 200 mM, peaks associated with the formation of a salt bridge (1560 cm^{-1}) and free carboxylate (1580 cm^{-1}) are both intense. However, on inspection within the amide I region there are subtle differences in peak intensity. It is observed that, as the salt concentration increased, the peaks associated with hydrogen bonding, both ordered (1625 cm^{-1}) and random (1649 cm^{-1}) become greater in intensity. This suggests that the salt promotes the formation of ordered structures when the concentrations are higher, an observation which does not follow the trend with the other peptides. Reasoning for this may lie within the role of the chloride ion. As this is a relatively small atom with a single negative charge, compared with both sulphate and phosphate where the anions have a greater charge and as such may not specifically interact to affect the packing of the residues. Therefore, the FFD peptides are able to get closer together allowing for stronger hydrogen bonding without the negative repulsion of the anionic counter-ions.

5.3.3 Atomic Force Microscopy

To further examine the effects of calcium salts on the self-assembling ability of FFD peptides, we look at the nanostructures formed by AFM. Similarly to the sodium salts, 50 μL of the assembled sample, is aliquoted onto a small piece of mica. This sample is left for a period of 48 hours to ensure the sample is fully dry. Each sample is measured on a fast scan AFM in tapping mode. On first inspection of all the samples, it is apparent that similar structures are formed for each of the samples. Each of the samples form fibril-like assemblies that appear to form networks. In order to gauge the size distribution of the fibrils, an average of 20 different sections from different fibers were taken. These results gave a range of

different distributions, however, the deviations in the sizes is relatively large. FFD in calcium phosphate gave the largest fibril diameter of approx. 299 ± 96 nm. Calcium citrate 248 ± 81 nm, calcium chloride 228 ± 73 nm and calcium sulphate 210 ± 45 nm (Figure 5.10). The larger size distribution of the calcium phosphate peptides may be a result of clustering of single nanofibers. On closer inspection of these images, it appears that the structures are composed of an amalgamation of several fibers in a twisted structure. This suggests that the packing of the peptides to form these fibrils result in orientating the side chains so that interaction between corresponding fibers is favorable. These observations are not seen in the other peptide assemblies.

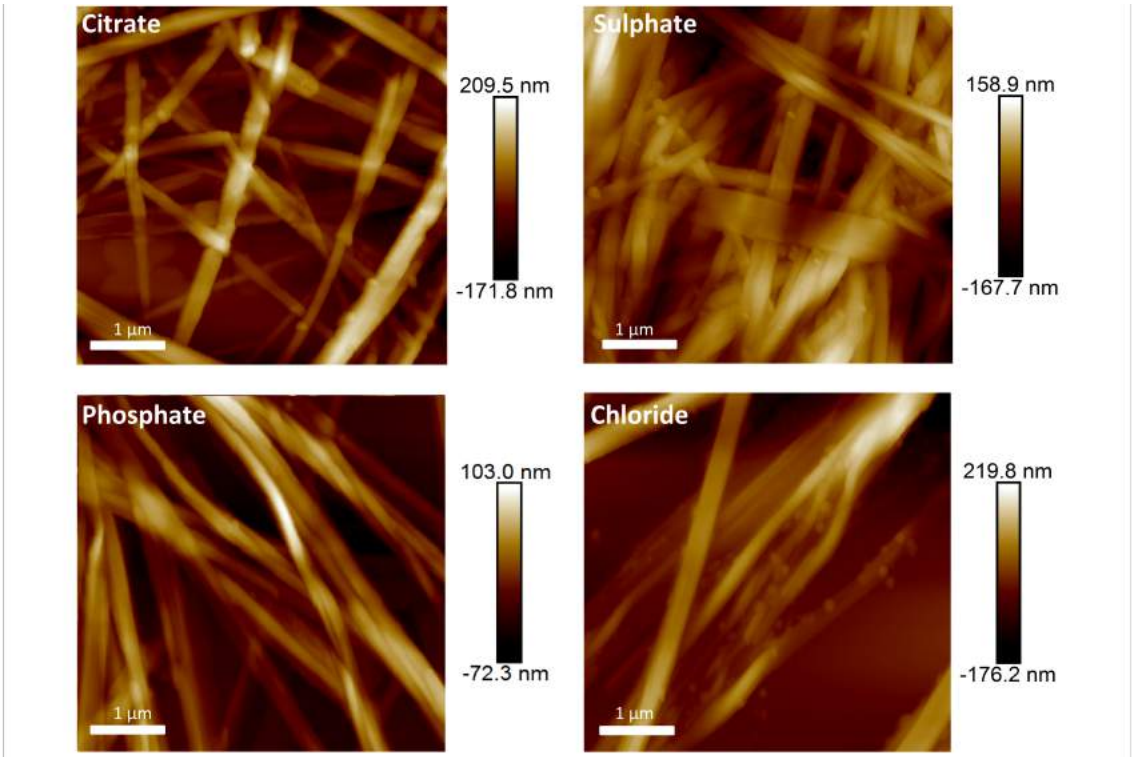

Figure 5.10: AFM images of FFD in different calcium salts. Note: Due to solubility issues all AFM images were taken at the lowest concentration measure (2 mM, 1.6mM citrate)

5.3.4 Rheology

The presence of calcium ions has altered the self-assembling ability of FFD. To determine how calcium (and its counter ion) has an effect on the properties of the formed hydrogels, analysis of the rheological properties of each hydrogel is carried

out. Measuring the mechanical properties of the hydrogel provides insights into the peptide interactions but also, and most importantly, how well the formed structures interact with water molecules to create a stable network. As previously mentioned in Chapter 2, in order for peptides to assemble and form hydrogels, there must be a balance between the hydrophobicity and hydrophilicity in order for the peptides to aggregate together and interact with water. The presence of calcium ions, promote the aggregation, however, the counter ion can affect the strength of the packing.

In all cases, a shear strain sweep was carried out on each peptide system prior to the frequency sweep. It was determined that the shear of the hydrogel was based at 0.5% for each sample as after this point the hydrogel begins to breakdown. Measurement of the frequency sweep, was used to determine the strength of the hydrogel. In all samples, it is clear that the storage modulus was greater than the loss modulus (Figure 5.11), which is indicative of the formation of hydrogels. However, the differences in strength of each of the hydrogels is interesting.

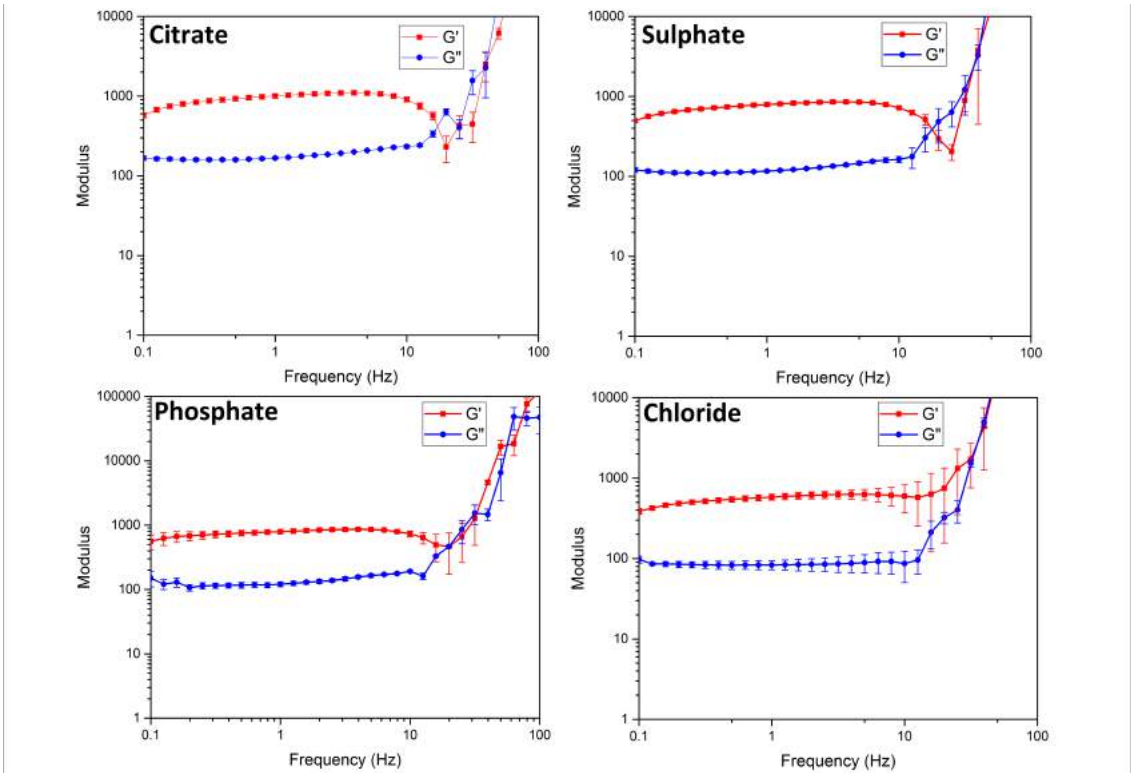

Figure 5.11: Rheology measurements of FFD hydrogels in different calcium salts. A) Calcium Citrate B) Calcium Sulphate C) Calcium Phosphate D) Calcium Chloride. Note: All measurements taken at in 2 mM salt concentration, 1.66 mM Calcium Citrate

The relative gel strength was taken as an average of the linear section of the G' modulus, from 0.1 to 10 Hz. After 10 Hz, the frequency of the plate becomes too great and as a result, the gel becomes damaged. The rheology measurements gave gel strengths of 942.5 Pa (citrate), 747.2 Pa (sulphate), 731.9 Pa (phosphate) and 561.5 Pa (chloride) (Figure 5.11). The first observation from these hydrogels is that they are weak (1 order of magnitude) compared with previous tripeptide hydrogelators introduced in Chapter 2. Interestingly, the gel strengths follow the order of the Hofmeister series (see Figure 5.1). This suggests that the presence of calcium is the main driving force for the assembly of the peptides; whereas the anionic counter ion has an affect on the packing of the fibers. The presence of kosmotropes provides an environment, which stabilizes the interaction of the water molecules in the fibrous network.

5.3.5 Summary

In summary, the presence of calcium with FFD dramatically changes the morphology of the assembled nanostructures. The divalent charge on the calcium situates itself between the anionic FFD. This enables the ion to crosslink the peptides. This crosslinking alters the structural morphology allow the peptide to form nanofibers. The presence of the nanofibrous network induces a gelation effect, a process that has not been observed for FFD. Furthermore, the anionic counter ions have been shown to affect the packing of the peptides, which results in a variation of the mechanical properties that follows the Hofmeister series. These findings demonstrate that hydrogels formed through short peptide assemblies can be finely tuned through the appropriate selection of different salts.

5.4 Conclusions

In this chapter, the difference in types of salts can affect the self-assembly ability of peptides. Initial examination of the self-assembly of FFD, indicated that the peptide did not form fibers and thus hydrogels at pH 7.4. Recent literature investigated how salt can interact with peptides to induce changes in supramolecular assemblies. The first part of this chapter demonstrated the cation dependence on forming new hydrogels. In the presence of calcium ions, FFD is able to self-assemble into hydrogels, an observation that has not been previously reported. The strong divalent nature and size of the calcium ion reduce the electrostatic repulsion that occurs at pH 7.4 allowing the FFD to arrange into nanofibrous networks. In addition, the difference in anionic counter ions is also important for determining the strength of the resultant hydrogel. Interestingly, the strength of the hydrogel follows the Hofmeister series, indicating the importance of understanding the salting-in and salting-out effect of the series.

5.5 Materials and Methods

5.5.1 Sample Preparation

FFD was purchased from Bachem Ltd at a purity >98%.

20 mM of FFD was dissolved in a salt solution of known concentration (2, 20, 200 mM) the pH was adjusted to 7.4 using 0.5 M NaOH. Each sample was then subject to repeated vortexing and sonication for 2 mins until a turbid viscous solution was formed. The samples were then stored in the fridge for a period of 24 hrs before analysis.

5.5.2 Fourier Transform Infra-red Spectroscopy (FTIR)

FTIR spectra were acquired using a Bruker Vertex70 spectrometer with a spectral resolution of 1 cm^{-1}. Spectra were obtained by averaging over 25 measurements for each sample. Measurements were performed using standard FTIR cuvettes (Harrink Scientific) where the sample was sandwiched between 2 CaF_2 discs (Crystran Ltd) separated by a 50 um PTFE spacer. For gel materials, a small amount of small was placed in the CaF_2 discs using a microspatula. For free flowing samples, 100ul of the sample was pipetted directly onto the disc. D_2O was used as the solvent.

5.5.3 Rheology

Assessments of the mechanical properties were carried out on a strain-controlled rheometer (Bohlin C-CVO) using a parallel plate geometry (20mm) with a 0.5 cm gap. An integrated temperature controlled was using to maintain the temperature of the sample stage at 25°C. to ensure that measurements were carried out with the viscoelastic region, an amplitude strain sweep of the sample was carried out, which show no variation in elastic modulus up to a strain of 1%. The strength of the hydrogels were measured as a frequency function, where the frequency sweep was carried out on a range between 0.1 to 100 Hz. These measurements were repeated at least three times to ensure repeatability. An average of the linear regions of the G' region was taken to give an approximate gel strength.

5.5.4 Atomic Force Microscopy (AFM)

AFM images were measured on a Bruker MultiMode 8 AFM. The operation was carried out on the fast scan tapping mode setting. Temperature was set at 25°C. Preparation of the samples were carried out 24hours prior to imaging. 50 μL of gel sample was placed onto a clean slice of mica. The samples was then left to air dry before a period of 24 hrs

6. Conclusions

In this thesis, the design, characterization and application of self-assembling tripeptides has been explored. The idea of peptide self-assembly has been around for about two decades with many publications based on N-protected-peptides and unmodified peptides containing 6-8 amino acids. The formation of materials from these systems has gained interest due to their industrial applications. However, developing new short peptide materials, which give rise to new materials with tunable properties, is of interest. New methods and predictions based on computational screening has predicted a number of different tripeptides capable of self-assembly.

The design of self-assembling tripeptides was carried out using a combination of computational and experimental techniques. An initial investigation into the self-assembling ability of tripeptides was examined through a screening process, where the aggregation propensity (AP) of all 8,000 tripeptides was determined to give an AP score of the tripeptide. After which, this was scaled with the Log*P* of the peptide to give the hydrophilicity weight AP_H. This value was used to determine how well the peptide aggregates but also how the peptide can interact with water, a key factor in the formation of hydrogels. This screening process resulted in the determination of design rules, for predicting self-assembling tripeptides.

Seven tripeptides were chosen of which five obeyed the design rules while the other two were control peptides. Extended coarse-grain molecular dynamics simulations indicated that the formation of nanofibrous was promoted where the N-terminal amino acid was cationic, in this case lysine, and the second and third amino acid were aromatic (KYF, KYW and KFF). Experimental methods such as FTIR, TEM and rheology indicated that there was a high degree of ordered upon the formation of these structures. It was evident that alteration of the aromatic residue alters the packing of the peptide molecules resulting in different hydrogel strengths. The control peptides, where the full reversal of the amino acid sequence and the substitution of aromatic residues with hydrophobic (FYK and KLL), has a

detrimental affect on the peptide assemblies. Alteration of the sequence indicated that the loss of the internal salt bridge between the lysine and C-terminus had an affect on the ability of the peptide to self-assemble. The change between leucine and aromatic amino acids indicated the importance of the additional π-interaction. This π-interaction is thought to increase the ordering of the tripeptide allowing for the formation of nanostructures. Atomistic molecular dynamics of a single molecule tripeptide molecule shows changes in conformation for a period of 50 ns. Measuring the dihedral angle between aromatic side chains indicated that preferred conformation of the self-assembly peptides was to adopt a *syn* conformation, where both aromatic residues as located on the same side with the lysine groups rotating and forming salt bridge with the C-terminus. This was not observed in the control peptides. In addition, anionic peptides, which followed the design rules, were also examined. In this case, DFF and FFD were used. Using similar techniques, these peptides indicated the formation of bilayers-like structures using CG MD, however experimental methods indicated the presence of no highly ordered structures. TEM analysis shows an amorphous aggregate for DFF whereas the formation of nanotubes was observed for FFD. However, these peptides did not form hydrogels and are thought to assemble in a more traditional 'surfactant' like mode- forming micelles and bilayers rather than fibers.

The application in cosmetics, biomedicine and food science has always been a goal for these self-assembling systems. To this extent, upon emulsifying peptides KYF, KYW, KFF, DFF and FFD in the presence of water and rapeseed oil, a variety of different types of emulsions could be formed. The observation that tripeptides such as KYF, KYW and KFF, which form nanofibers, were capable of assembling into interfacial nanofibrous networks at the water/oil interface. This phenomenon has been seen before with the use of N-protected peptide however, in the presence of unmodified tripeptides this was a new discovery. Through FTIR and TEM, it was observed that the peptide formed similar structures to that in the aqueous phase, however these fibers were localized at the interface. The amphiphilic nature of amino acids allow for the stabilization of the interfacial tension between the two phases. On the other hand, tripeptides DFF and FFD did not form nanofibers, however emulsions were created. This indicated that these emulsions were

stabilized *via* a different self-assembling mechanism. Thermal studies identified that emulsions formed *via* nanofibrous networks could withstand a greater temperature before de-emulsification. In contrast, DFF and FFD, which were predicted to form surfactant-like assemblies de-emulsified at a greater rate. The utilization of CG MD identified that, although no nanofibers formed, the nanofibrous peptides had a greater absorption to the interface than the surfactant-like peptides. Upon reaching longer timescales, oil droplet began to coalesce into a single droplet whereas oil droplets in the presence of fiber forming peptides remained dispersed.

After showing the formation of new nanomaterials can be achieved, methods for synthesizing peptides were explored to find new routes for making active tripeptides without the use of harsh chemicals. Enzymes, such as α-chymotrypsin, are widely available and are excellent for selectively making and breaking peptide bonds. Using the common and low cost peptide sweeter Aspartame (DF-OMe) and readily available amino acid amides as starting materials, reaction conditions such as temperature and pH were controlled to alter the equilibrium of the reaction mechanism. At higher temperature it was observed that the enzyme began to denature which prevents the hydrolysis of the peptide. This allows for the isolation of the selected tripeptide used for developing new materials. Changing pH of the solution resulted in slower kinetics of the hydrolysis. A lower pH changes to the ionization state of the enzyme meant that the hydrolysis process was retarded, preventing further hydrolysis. Subtle changes in the pH of the solutions controlled the rate of the hydrolysis meaning different peptides could be isolated at different times.

Finally, in the food, cosmetics and personal care industries, many different products are a combination of a series of additives. How these additives affect the self-assembling process was explored. In this case the non-hydrogelating peptide FFD, was used in the presence of different salts to examine how salts interact with the peptide. In the presence of sodium, the peptide did not form any order nanostructures capable of forming hydrogels, however, in the presence of calcium, the calcium ions crosslink between the FFD peptides allowing for the formation of

nanofibers resulting in hydrogelation. Furthermore, the anionic counter ion was identified to affect the packing of the peptide molecules and results obtained *via* rheology indicated that the anions that had greater salting out ability (kosmotropes) resulted in stronger hydrogels, whereas the salting in peptide (chaotropes) formed weaker hydrogels.

In summary, this thesis has shown the development, using combined experimental and computational methods, of new tripeptide nanostructures that are capable of self-assembling to form highly ordered materials that can be tuned for applications in the food, cosmetic and biomedical industries.

7. Future Work

During the course of this thesis, there have been many challenges and accomplishments for 4 years worth of research. However, as with the majority of science, the progression of research continually grows leading to a number of different exciting opportunities. Within each chapter, the research could be expanded. In this section, an overview of the future work will be discussed on what the next steps for the research can be.

Within Chapter 2, the premise of using both computational and experimental methods was discussed to try and predict self-assembling tripeptides for the purpose of hydrogel formation. In this section, there were only seven tripeptides investigated in detail out of a possible 8,000 in total and several hundred that have promising self-assembling behavior. The design rules can be used further to determine why amino acids such as lysine have a greater affinity to self-assemble over arginine and also likewise for aspartic acid and glutamic acid. One of the main studies that were not fully described was the determination of the packing of the peptide in order to form nanofibers. In order to explore this, X-ray and light scattering methods such as XRD and WAXS could be used to determine the distances between peptide molecules. This would give a deeper insight into how these peptides interact.

Chapter 3 discussed the potential applications for exploiting peptide self-assembly as tunable emulsifiers and surfactants. The formation of emulsions was a key step into understanding the materials that can be formed from these peptides. As only a selection of five different peptides were used to determine the emulsifying capability. Further analysis of other tripeptides could be of interest to determine the other potential emulsifiers. In this chapter, a single concentration and oil was used, however, being able to fine tune the concentration of the peptide used to give similar physical properties was never explored. This would allow industry to keep down the costs. In addition, as these emulsions were primarily examined for the food industry, methods to develop the application of these systems were never

explored. Identification of the peptides for cosmetics of biomedical applications would allow the peptides to be used for a more diverse range of applications.

Chapter 4 examined the enzymatic approaches for synthesizing self-assembling peptides. The key idea of this chapter was to examine green approaches for synthesizing peptides. However, in this chapter only a single dipeptide ester was used to measure examine the enzymatic synthesis. In order to fully understand and see the advantages of these methods a number of dipeptide methyl esters can be used, such as KY-OMe, KF-OMe, *etc*. In addition, an investigation into the gradual heating of the enzyme solutions can be beneficial to understand the enzyme kinetics.

Finally Chapter 5, explored how different salts affect the self-assembly of the tripeptide FFD. In this case, it was evident that there was a clear distinction between the nanostructures formed in the presence of calcium rather than sodium. To follow on from this work, changes in supramolecular structures for different tripeptides such as KYF could be explored, where preliminary data has been obtained. In the presence of all salts, KYF forms hydrogels, however there are differences in the mechanical properties of the hydrogels, which could be further examined. In addition, throughout the chapter it was briefly mentioned that the high salt concentrations affect the hydrogelation ability. An in depth characterization of these systems, would give a greater insight into how the salt interferes with the peptides. Finally, within the cosmetics, food and personal care industries there are many more additives that are used, for example sugars. Understanding how these additives affect the self-assembling ability of the peptides could be beneficial across a number of industries.

8. References

(1) Kushner, D. J., *Bac Rev*, **1969,** *33* (2), 302-345.
(2) Pauling, L.; Corey, R. B., *Proc. Nat. Acad. Sci. U.S.A*, **1951,** *37* (11), 729-740.
(3) Pauling, L.; Corey, R. B., *Nature*, **1953,** *171*, 59-61.
(4) Crick, F. H. C., *Acta Crystallogr*, **1953,** *6*, 689-697.
(5) Watson, J. D.; Crick, F. H. C., *Nature*, **1953,** *171*, 737-738.
(6) Hartgerink, J. D.; Beniash, E.; Stupp, S. I., *PNAS*, **2002,** *99* (8), 5133-5138.
(7) Reches, M.; Gazit, E., *Science*, **2003,** *300*, 625-627.
(8) Damodaran, S., *Amino acids, peptides, and proteins*. CRC Press: Boca Raton, L: 2008; Vol. 4.
(9) Jeffrey, G. A., *An Introduction to Hydrogen Bonding*. Oxford Univeristy Press: New York, 1997; Vol. 32.
(10) Emsley, J., *Chemical Society reviews*, **1980,** *9* (1), 91-124.
(11) Tuttle, T.; Kraka, E.; Wu, A.; Cremer, D., *J. Am. Chem. Soc.*, **2004,** *126*, 5093.
(12) Tuttle, T.; Grafenstein, J.; Wu, A.; Kraka, E.; Cremer, D., *J. Phys. Chem. B*, **2004,** *108* (1115).
(13) Jeffrey, G. A.; Saenger, W., *Hydrogen bonding in biological structures*. Springer Science & Business Media: 2012.
(14) Steed, J. W.; Atowood, J. L., *Supramolecular Chemistry*. John Wiley and Sons: 2009.
(15) Gao, J.; Kelly, J. W., *Protein Science*, **2008,** *17* (9), 1096-1101.
(16) Ghelis, C., Protein Folding. Academic Press: 1982.
(17) Birchall, L. S.; Roy, S.; Jayawarna, V.; Hughes, M.; irvine, E.; Okorogheye, G. T.; Saudi, N.; Santis, E. D.; Tuttle, T.; Edwards, A. A.; Ulijn, R. V., *Chem. Sci.*, **2011,** *2* (1349).
(18) Adler-Abramovich, L.; Vaks, L.; Carny, O.; Trudler, D.; Magno, A.; Caflisch, A.; Frenkel, D.; Gazit, E., *Nat. Chem. Biol.*, **2012,** *8*, 701.
(19) Martinez, C. R.; Iverson, B. L., *Chemical Science*, **2012,** *3* (7), 2191-2201.
(20) Nelson, D. L.; Cox, M. M., *Lehninger Principles of Biochmeistry*. 6th Ed. ed.; Macmillan Gordonsville: U.S.A, 2005.
(21) Moore, D. S., *Biochem. Edu.*, **1985,** *13* (1), 10-11.
(22) Kumar, S.; Nussinov, R., *Chem. Bio. Chem*, **2002,** *3* (7), 604-617.
(23) Tang, C.; Smith, A. M.; Collins, R. F.; Ulijn, R. V.; Saiani, A., *Langmuir*, **2009,** *25* (16), 9447-9453.
(24) Schulz, G. E.; Schirmer, R. H., Principles of Protein Strucutres. Springer-Verlag KG: 1979.
(25) Castillo, J.; Sasso, L.; Svendsen, W. E., *CRC Press*, **2012**.
(26) Ha, J.-H.; Spolar, R. S.; Record, M. T., *Journal of molecular biology*, **1989,** *209* (4), 801-816.

(27) Spolar, R. S.; Ha, J.-H.; Record, M. T., *Proceedings of the National Academy of Sciences*, **1989,** *86* (21), 8382-8385.
(28) Spolar, R. S.; Record Jr, M. T., *Science*, **1994,** *263*, 11.
(29) Vegners, R.; Shestakova, I.; Kalvinsh, I.; Ezzell, R. M.; Janmey, P. A., *Journal of Peptide Science*, **1995,** *1* (6), 371-378.
(30) Zhang, Y.; Gu, H.; Yang, Z.; Xu, B., *Journal of the American Chemical Society*, **2003,** *125* (45), 13680-13681.

(31) Yang, Z.; Gu, H.; Zhang, Y.; Wnag, L.; Xu, B., *Chem Commun*, **2004**, 208-209.
(32) Fleming, S.; Ulijn, R. V., *Chemical Society reviews*, **2014,** *43* (23), 8150-8177.
(33) Chen, L.; Morris, K.; Laybourn, A.; Elias, D.; Hicks, M. R.; Rodger, A.; Serpell, L.; Adams, D. J., *Langmuir*, **2009,** *26* (7), 5232-5242.
(34) Chen, L.; Revel, S.; Morris, K.; C. Serpell, L.; Adams, D. J., *Langmuir*, **2010,** *26* (16), 13466-13471.
(35) Adams, D. J.; Topham, P. D., *Soft Matter*, **2010,** *6* (16), 3707-3721.
(36) Webber, M. J.; Kessler, J. A.; Stupp, S. I., *Journal of internal medicine*, **2010,** *267* (1), 71-88.
(37) Altunbas, A.; Pochan, D. J., Peptide-based and polypeptide-based hydrogels for drug delivery and tissue engineering. In *Peptide-Based Materials*, Springer: 2011; pp 135-167.
(38) Fleming, S.; Debnath, S.; Frederix, P. W. J. M.; Hunt, N. T.; Ulijn, R. V., *Biomacromolecules*, **2014,** *15* (4), 1171-1184.
(39) Jayawarna, V.; Richardson, S. M.; Hirst, A. R.; Hodson, N. W.; Saiani, A.; Gough, J. E.; Ulijn, R. V., *Acta Biomaterialia*, **2009,** *5* (3), 934-943.
(40) Ulijn, R. V.; Smith, A. M., *Chemical Society reviews*, **2008,** *37* (4), 664-675.
(41) Dudukovic, N. A.; Zukoski, C. F., *Soft matter*, **2015,** *11* (38), 7663-7673.
(42) Lin, Y.; Qiao, Y.; Tang, P.; Li, Z.; Huang, J., *Soft Matter*, **2011,** *7* (6), 2762-2769.
(43) Behrendt, R.; Renner, C.; Schenk, M.; Wang, F.; Wachtveitl, J.; Oesterhelt, D.; Moroder, L., *Angewandte Chemie International Edition*, **1999,** *38* (18), 2771-2774.
(44) Guler, M. O.; Claussen, R. C.; Stupp, S. I., *Journal of Materials Chemistry*, **2005,** *15* (42), 4507-4512.
(45) Zhang, Y.; Yang, Z.; Yuan, F.; Gu, H.; Gao, P.; Xu, B., *Journal of the American Chemical Society*, **2004,** *126* (46), 15028-15029.
(46) Ma, M.; Kuang, Y.; Gao, Y.; Zhang, Y.; Gao, P.; Xu, B., *Journal of the American Chemical Society*, **2010,** *132* (8), 2719-2728.
(47) Adhikari, B.; Nanda, J.; Banerjee, A., *Chemistry–A European Journal*, **2011,** *17* (41), 11488-11496.
(48) Hamley, I. W., *Soft Matter*, **2011,** *7* (9), 4122-4138.
(49) Dastidar, P., *Chem. Soc. Rev*, **2008,** (37), 2699-2715.
(50) Yang, Z.; Liang, G.; Ma, M.; Gao, Y.; Xu, B., *J. Mater. Chem.*, **2007,** (17), 850-854.

(51) Fleming, S.; Debnath, S.; Frederix, P. W.; Tuttle, T.; Ulijn, R. V., *Chem Commun*, **2013,** (49), 10587-10589.
(52) Ishi-i, T.; Iguchi, R.; Snip, E.; Ikeda, M.; Shinkai, S., *Langmuir*, **2001,** (17), 5825-5833.
(53) Wolfe, A.; Shimer, G. H.; Meehan, T., *Biochemistry*, **1987,** *26* (20), 6392-6396.
(54) Long, E. C.; Barton, J. K., *Accounts of Chemical Research*, **1990,** *23* (9), 271-273.
(55) Sipe, J. D.; Cohen, A. S., *Journal of structural biology*, **2000,** *130* (2-3), 88-98.
(56) Westermark, P.; Engström, U.; Johnson, K. H.; Westermark, G. T.; Betsholtz, C., *Proceedings of the National Academy of Sciences*, **1990,** *87* (13), 5036-5040.
(57) Castaño, E. M.; Ghiso, J.; Prelli, F.; Gorevic, P. D.; Migheli, A.; Frangione, B., *Biochemical and biophysical research communications*, **1986,** *141* (2), 782-789.
(58) Glenner, G. G.; Wong, C. W., *Biochemical and biophysical research communications*, **1984,** *122* (3), 1131-1135.
(59) Lorenzo, A.; Yankner, B. A., *Annals of the New York Academy of Sciences*, **1996,** *777* (1), 89-95.
(60) Tjernberg, L. O.; Naslund, J.; Lindqvist, F.; Johansson, J.; Karlstrom, A. R.; Thyberg, J.; Terenius, L.; Nordstedt, C., *Journal of Biological Chemistry*, **1996,** *271* (15), 8545-8548.
(61) Tjernberg, L. O.; Hosia, W.; Bark, N.; Thyberg, J.; Johansson, J., *Journal of Biological Chemistry*, **2002,** *277* (45), 43243-43246.
(62) Gorbitz, C. H., *Chem. Eur. J*, **2001,** *7* (23).
(63) Gorbitz, C. H., *Chemical communications*, **2006,** (22), 2332-2334.
(64) Reches, M.; Gazit, E., *Nat Nano*, **2006,** *1* (3), 195-200.
(65) Reches, M.; Gazit, E., *Nano Lett*, **2004,** *4* (4).
(66) Scanlon, S.; Aggeli, A., *Nano Today*, **2008,** *3* (3-4), 22-30.
(67) Marchesan, S.; Vargiu, A. V.; Styan, K. E., *Molecules*, **2015,** *20* (11), 19775-19788.
(68) De Groot, N. S.; Parella, T.; Aviles, R. X.; Vendrell, J.; Ventura, S., *Biphysical Journal*, **2007,** *92*, 1732-1741.
(69) Whimley, W. C.; White, S. H.; Creamer, T. P., *Biochemistry*, **1996,** *35*, 5109-5124.
(70) White, S. H.; Whimley, W. C., *Biochim. Biophys. Acta BBA - Rev. Biomembr*, **1998,** *1376*, 339-352.
(71) Colombo, G.; Soto, P.; Gazit, E., *Trends in biotechnology*, **2007,** *25* (5), 211-218.
(72) Rymer, S.-J.; Tendler, A. T. B.; Bosquillon, C.; Washington, C.; Roberts, C. J., *Therapeutic Delivery*, **2011,** *2* (8), 1043-1056.
(73) Tamamis, P.; Adler-Abramovich, L.; Reches, M.; Marshall, K.; Sikorski, P.; Serpell, L.; Gazit, E.; Archontis, G., *Biophysical journal*, **2009,** *96* (12), 5020-5029.

(74) Arnon, Z.; Adler-Abramovich, L.; Levin, A.; Gazit, E., *Israel Journal of Chemistry*, **2015**, n/a-n/a.
(75) Pappas, C. G.; Shafi, R.; Sasselli, I. R.; Siccardi, H.; Wang, T.; Narang, V.; Abzalimov, R.; Wijerathne, N.; Ulijn, R. V., *Nat Nano*, **2016,** *11* (11), 960-967.
(76) Marchesan, S.; Easton, C. D.; Kushkaki, F.; Waddington, L.; Hartley, P. G., *Chemical communications*, **2012,** *48* (16), 2195-2197.
(77) Marchesan, S.; Easton, C. D.; Styan, K. E.; Waddington, L. J.; Kushkaki, F.; Goodall, L.; McLean, K. M.; Forsythe, J. S.; Hartley, P. G., *Nanoscale*, **2014,** *6* (10), 5172-5180.
(78) Marchesan, S.; Qu, Y.; Waddington, L. J.; Easton, C. D.; Glattauer, V.; Lithgow, T. J.; McLean, K. M.; Forsythe, J. S.; Hartley, P. G., *Biomaterials*, **2013,** *34* (14), 3678-3687.
(79) Marchesan, S.; Waddington, L.; Easton, C. D.; Kushkaki, F.; McLean, K. M.; Forsythe, J. S.; Hartley, P. G., *BioNanoScience*, **2013,** *3* (1), 21-29.
(80) Marchesan, S.; Waddington, L.; Easton, C. D.; Winkler, D. A.; Goodall, L.; Forsythe, J.; Hartley, P. G., *Nanoscale*, **2012,** *4* (21), 6752-6760.
(81) Merkler, D. J., *Enzyme and microbial technology*, **1994,** *16* (6), 450-456.
(82) Eipper, B. A.; Mains, R. E., *Annual review of physiology*, **1988,** *50* (1), 333-344.
(83) Cao, M.; Cao, C.; Zhang, L.; Xia, D.; Xu, H., *Journal of colloid and interface science*, **2013,** *407*, 287-295.
(84) Shlomo, Z.; Vinod, T. P.; Jelinek, R.; Rapaport, H., *Chem Commun*, **2015,** *51*, 3154-3157.
(85) Hauser, C. A.; Deng, R.; Mishra, A.; Loo, Y.; Khoe, U.; Zhuang, F.; Cheong, D. W.; Accardo, A.; Sullivan, M. B.; Riekel, C.; Ying, J. Y.; Hauser, U. A., *Proceedings of the National Academy of Sciences of the United States of America*, **2011,** *108* (4), 1361-1366.
(86) Lakshmanan, A.; Zhang, S.; Hauser, C. A., *Trends in biotechnology*, **2012,** *30* (3), 155-165.
(87) James, J.; Mandal, A. B., *Journal of colloid and interface science*, **2011,** *360* (2), 600-605.
(88) Wright, E. R.; Conticello, V. P., *Adv. Drug. Del. Rev*, **2002,** *54*, 17.
(89) Leach, A. R., *Molecular Modelling: Principles and Applications*. 2001.
(90) Kmiecik, S.; Gront, D.; Kolinski, M.; Wieteska, L.; Dawid, A. E.; Kolinski, A., *Chemical Reviews*, **2016,** *116* (14), 7898-7936.
(91) Goodman, J. M., *Chemical Applications of Molecular Modelling*. 1998.
(92) Debye, P., *Physikalische Zeitschrift*, **1920,** *21*, 178.
(93) Mackerell, A. D., Jr.; Banavali, N.; Foloppe, N., *Biopolymers*, **2001,** *56*, 257-265.
(94) Vanommeslaeghe, K.; Hatcher, E.; Acharya, C.; Kundu, S.; Zhong, S.; Shim, J.; Darian, E.; Guvench, O.; Lopes, P.; Vorobyov, I.; Mackerell, A. D., Jr., *Journal of computational chemistry*, **2010,** *31* (4), 671-690.

(95) Klauda, J. B.; Venable, R. M.; Freites, J. A.; O'Connor, J. W.; Tobias, D. J.; Mondragon-Ramirez, C.; Vorobyov, I.; Mackerell, A. D., Jr.; Pastor, R. W., *J Phys Chem B*, **2010,** *114*, 7830-7843.

(96) Soares, T. A.; Hunenberger, P. H.; Kastenholz, M. A.; Krautler, V.; Lenz, T.; Lins, R. D.; Oostenbrink, C.; van Gunsteren, W. F., *Journal of computational chemistry*, **2005,** *26* (7), 725-737.

(97) Lins, R. D.; Hunenberger, P. H., *Journal of computational chemistry*, **2005,** *26* (13), 1400-1412.

(98) Oostenbrink, C.; Soares, T. A.; van der Vegt, N. F.; van Gunsteren, W. F., *European biophysics journal : EBJ*, **2005,** *34* (4), 273-284.

(99) Meagher, K. L.; Redman, L. T.; Carlson, H. A., *Journal of computational chemistry*, **2002,** *24*, 10.

(100) Wang, J.; Wolf, R. M.; Caldwell, J. W.; Kollman, P. A.; Case, D. A., *Journal of computational chemistry*, **2004,** *25*, 8.

(101) Wu. C; Lei, H.; Duan, Y., *Journal of the American Chemical Society*, **2005,** *127*, 13530-13537.

(102) Wu, C.; Lei, H.; Duan, Y., *Journal of the American Chemical Society*, **2005,** *127* (39), 13530-13537.

(103) Noid, W. G.; Chu, J.-W.; Ayton, G. S.; Krishna, V.; Izvekov, S.; Voth, G. A.; Das, A.; Andersen, H. C., *The Journal of Chemical Physics*, **2008,** *128* (24), -.

(104) Bahar, I.; Rader, A. J., *Struc. Biol.*, **2005,** *15*, 586-592.

(105) Levitt, M., *J Mol Biol*, **1976,** *104*, 59-107.

(106) Marrink, S. J.; Risselada, H. J.; Yefimov, S.; Tieleman, D. P.; De Vries, A. H., *J Phys Chem B*, **2007,** *111*, 13.

(107) Zuckerman, D. M., *The Journal of Physical Chemistry B*, **2004,** *108* (16), 5127-5137.

(108) Tozzini, V.; Rocchia, W.; McCammon, J. A., *Journal of Chemical Theory and Computation*, **2006,** *2* (3), 667-673.

(109) Tozzini, V.; McCammon, J. A., *Chemical Physics Letters*, **2005,** *413* (1–3), 123-128.

(110) Pizzitutti, F.; Marchi, M.; Borgis, D., *Journal of Chemical Theory and Computation*, **2007,** *3* (5), 1867-1876.

(111) Basdevant, N.; Borgis, D.; a-Duong, T., *The Journal of Physical Chemistry B*, **2007,** *111* (31), 9390-9399.

(112) Tozzini, V., *Current opinion in structural biology*, **2005,** *15* (2), 144-150.

(113) Tirion, M. M., *Physical Review Letters*, **1996,** *77* (9), 1905-1908.

(114) Haliloglu, T.; Bahar, I.; Erman, B., *Phys. Rev. Lett.*, **1997,** *79*, 3090-3093.

(115) Bahar, I.; Atilgan, A. R.; Erman, B., *Folding and Design* **1997,** *2*, 173-181.

(116) Monticelli, L.; Kandasamy, S. K.; Periole, X.; Larson, R. G.; Tieleman, D. P.; Marrink, S. J., *J Chem Theory Comput*, **2008,** *4*, 7830-7843.

(117) de Jong, D. H.; Singh, G.; Bennett, W. F. D.; Arnarez, C.; Wassenaar, T. A.; Schäfer, L. V.; Periole, X.; Tieleman, D. P.; Marrink, S. J., *Journal of Chemical Theory and Computation*, **2013,** *9* (1), 687-697.

(118) Lopez, C. A.; Rzepiela, A. J.; De Vries, A. H.; Dijkhuizen, L.; Hunenberger, P. H.; Marrink, S. J., *J Chem Theory Comput*, **2009,** *5*.
(119) López, C. A.; Sovova, Z.; van Eerden, F. J.; de Vries, A. H.; Marrink, S. J., *Journal of Chemical Theory and Computation*, **2013,** *9* (3), 1694-1708.
(120) Marrink, S. J.; Tieleman, D. P., *Chemical Society reviews*, **2013,** *42* (16), 6801-6822.
(121) Frederix, P. W.; Ulijn, R. V.; Hunt, N. T.; Tuttle, T., *The journal of physical chemistry letters*, **2011,** *2* (19), 2380-2384.
(122) Guo, C.; Luo, Y.; Zhou, R.; Wei, G., *ACS Nano*, **2012,** *6* (5), 3907-3918.
(123) Azuri, I.; Adler-Abramovich, L.; Gazit, E.; Hod, O.; Kronik, L., *Journal of the American Chemical Society*, **2014,** *136* (3), 963-969.
(124) Frederix, P. W.; Scott, G. G.; Abul-Haija, Y. M.; Javid, N.; Kalafatovic, D.; Pappas, C. G.; Hunt, N. T.; Ulijn, R. V.; Tuttle, T., *Nat. Chem.*, **2014,** (7), 30.
(125) Xie, A.; Hoff, W. D.; Kroon, A. R.; Hellingwerf, K. J., *Biochemistry*, **1996,** *35* (47), 14671-14678.
(126) Jackson, M.; Mantsch, H. H., *Critical reviews in biochemistry and molecular biology*, **1995,** *30* (2), 95-120.
(127) Byler, D. M.; Susi, H., *Biopolymers*, **1986,** *25* (3), 469-487.
(128) Cosgrove, T., *Colloid science: principles, methods and applications*. John Wiley & Sons: 2010.
(129) Tadros, T. F., *Applied surfactants: principles and applications*. John Wiley & Sons: 2006.
(130) Tadros, T. F., *Emulsion formation and stability*. John Wiley & Sons: 2013.
(131) Cao, Z.; Sun, Y., *ACS applied materials & interfaces*, **2009,** *1* (2), 494-504.
(132) Iacoviello, J. G.; Daniels, W. E., Vinyl acetate copolymer emulsions for paint. Google Patents: 1980.
(133) Tadros, T. F., *Surfactants in agrochemicals*. CRC press: 1994; Vol. 54.
(134) Cyril, S. T., Emulsions and processes for their production. Google Patents: 1945.
(135) Bais, D.; Trevisan, A.; Lapasin, R.; Partal, P.; Gallegos, C., *Journal of colloid and interface science*, **2005,** *290* (2), 546-556.
(136) Bouchemal, K.; Briançon, S.; Perrier, E.; Fessi, H., *International Journal of Pharmaceutics*, **2004,** *280* (1–2), 241-251.
(137) Garti, N., *LWT - Food Science and Technology*, **1997,** *30* (3), 222-235.
(138) McClements, D. J.; Li, Y., *Advances in Colloid and Interface Science*, **2010,** *159* (2), 213-228.
(139) Miller, D. J.; Henning, T.; Grünbein, W., *Colloids and Surfaces A: Physicochemical and Engineering Aspects*, **2001,** *183–185* (0), 681-688.
(140) Sanguansri, P.; Augustin, M. A., *Trends in Food Science & Technology*, **2006,** *17* (10), 547-556.
(141) Weiss, J.; Takhistov, P.; McClements, D. J., *J. Food Sci.*, **2006,** *71*, R107.
(142) Lim, G. K.; Wang, J.; Ng, S. C.; Gan, L. M., *Langmuir*, **1999,** *15* (22), 7472-7477.

(143) Chu, Z.; Feng, Y., *Chemical communications*, **2011,** *47* (25), 7191-7193.
(144) Fowler, C. I.; Muchemu, C. M.; Miller, R. E.; Phan, L.; O'Neill, C.; Jessop, P. G.; Cunningham, M. F., *Macromolecules*, **2011,** *44* (8), 2501-2509.
(145) Liu, Y.; Jessop, P. G.; Cunningham, M.; Eckert, C. A.; Liotta, C. L., *Science*, **2006,** *313* (5789), 958-960.
(146) Minkenberg, C. B.; Florusse, L.; Eelkema, R.; Koper, G. J. M.; van Esch, J. H., *Journal of the American Chemical Society*, **2009,** *131* (32), 11274-11275.
(147) Ristenpart, W. D.; Bird, J. C.; Belmonte, A.; Dollar, F.; Stone, H. A., *Nature*, **2009,** *461* (7262), 377-380.
(148) Menger, F. M.; Littau, C. A., *J. Am. Chem. Soc.*, **1993,** (115), 10083-10090.
(149) Menger, F. M.; Yamasaki, Y., *J. Am. Chem. Soc.*, **1993,** (115), 3840-3841.
(150) Rosen, M. J.; Zhen Huo, Z.; Yuan Hua, X., *J. Am. Oil. Chem. Soc.*, **1992,** *69* (1), 30-33.
(151) Pickering, S. U., *J. Soc. Client Ind. London*, **1910,** *29*, 129.
(152) Ramsden, W., *Proceedings of the royal Society of London*, **1903,** *72*, 156-164.
(153) Zoppe, J. O.; Venditti, R. A.; Rojas, O. J., *Journal of colloid and interface science*, **2012,** *369* (1), 202-209.
(154) Rayner, M.; Marku, D.; Eriksson, M.; Sjöö, M.; Dejmek, P.; Wahlgren, M., *Colloids and Surfaces A: Physicochemical and Engineering Aspects*, **2014,** *458*, 48-62.
(155) Marku, D.; Wahlgren, M.; Rayner, M.; Sjöö, M.; Timgren, A., *International journal of pharmaceutics*, **2012,** *428* (1), 1-7.
(156) Rayner, M.; Timgren, A.; Sjöö, M.; Dejmek, P., *Journal of the Science of Food and Agriculture*, **2012,** *92* (9), 1841-1847.
(157) Lam, S.; Velikov, K. P.; Velev, O. D., *Current Opinion in Colloid & Interface Science*, **2014,** *19* (5), 490-500.
(158) Frelichowska, J.; Bolzinger, M.-A.; Pelletier, J.; Valour, J.-P.; Chevalier, Y., *International journal of pharmaceutics*, **2009,** *371* (1), 56-63.
(159) Destribats, M.; Rouvet, M.; Gehin-Delval, C.; Schmitt, C.; Binks, B. P., *Soft matter*, **2014,** *10* (36), 6941-6954.
(160) Berton-Carabin, C. C.; Schroën, K., *Annual review of food science and technology*, **2015,** *6*, 263-297.
(161) Besnard, L.; Marcheal, F.; Paredes, J. F.; Daillant, J.; Pantoustier, N.; Perrin, P.; Guenoun, P., *Adv Mater.*, **2013,** (25), 2844-2848.
(162) Garcia-Tunon, E.; Barg, S.; Bell, R.; Weaver, J.; Walter, C.; Goyos, L.; Saiz, E., *Angewandte Chemie (International ed. in English)*, **2013,** *52* (30), 7805-7808.
(163) Zhang, J.; Coulston, R. J.; Jones, S. T.; Geng, J.; Scherman, O. A.; Abell, C., *Science*, **2012,** *335* (6069), 690.
(164) Molau, G. E., Collodial and Morphoplogical Behaviour of Block and Graft Copolymers. In *Block Copolymers*, Plenum Press: 1970; p 79.
(165) Cölfen, H., *Macromol. Rapid Commun*, **2001,** *22*, 219.
(166) Bahdadur, P.; Reiss, G., *Tenside, Surfactants, Detergents*, **1991,** *28*, 173.

(167) Tan, B.; Lee, J.-Y.; Cooper, A. I., *Macromolecules*, **2007,** *40* (6), 1945-1954.
(168) Louie, J. S.; Pinnau, I.; Ciobanu, I.; Ishida, K. P.; Ng, A.; Reinhard, M., *Journal of Membrane Science*, **2006,** *280* (1), 762-770.
(169) Tadros, T. F.; Vandamme, A.; Levecke, B.; Booten, K.; Stevens, C. V., *Advances in colloid and interface science*, **2004,** *108*, 207-226
(170) Reiss, G.; Labbe, C., *Macromole. Rapid. Commun*, **2004,** *25*, 401-435.
(171) Zhang, S., *Nat Biotech*, **2003,** *21* (10), 1171-1178.
(172) Santoso, S. S.; Vauthey, S.; Zhang, S., *Current Opinion in Colloid & Interface Science*, **2002,** *7* (5–6), 262-266.
(173) Vauthey, S.; Santoso, S.; Gong, H.; Watson, N.; Zhang, S., *Proceedings of the National Academy of Sciences*, **2002,** *99* (8), 5355-5360.
(174) Bai, S.; Pappas, C.; Debnath, S.; Frederix, P. W. J. M.; Leckie, J.; Fleming, S.; Ulijn, R. V., *ACS Nano*, **2014,** *8* (7), 7005-7013.
(175) Mahler, A.; Reches, M.; Rechter, M.; Cohen, S.; Gazit, E., *Adv Mater.*, **2006,** *18*, 1365.
(176) Biancalana, M.; Koide, S., *Biochimica et biophysica acta*, **2010,** *1804* (7), 1405-1412
(177) Hudson, S. A.; Ecroyd, H.; Kee, T. W.; Carver, J. A., *FEBS Journal*, **2009,** *276* (20), 5960-5972.
(178) Hanselman, D.; Littlefield, B., *Mastering MATLAB 6: a comprehensive tutorial and reference*. Pearson: 2001.
(179) Koshland, D. E., *Proceedings of the National Academy of Sciences*, **1958,** *44* (2), 98-104.
(180) Whittaker, R. G.; Bryant, K. J.; Hamilton, E. A.; McVittie, L. T.; Schober, P. A., *Annals of the New York Academy of Sciences*, **1992,** *672* (1), 387-395.
(181) Bongers, J.; Heimer, E. P., *Peptides*, **1994,** *15* (1), 183-193.
(182) Wong, C. H., *Science*, **1989,** *244* (4909), 1145-1153.
(183) Scott, G. G.; McKnight, P. J.; Tuttle, T.; Ulijn, R. V., *Adv Mater.*, **2016,** *28* (7), 1381-1386.
(184) Fichman, G.; Gazit, E., *Acta Biomaterialia*, **2014,** *10* (4), 1671-1682.
(185) Zhao, X.; Pan, F.; Xu, H.; Yaseen, M.; Shan, H.; Hauser, C. A.; Zhang, S.; Lu, J. R., *Chemical Society reviews*, **2010,** *39* (9), 3480-3498.
(186) Rudra, J. S.; Tian, Y. F.; Jung, J. P.; Collier, J. H., *Proc. Nat. Acad Sci.*, **2010,** *107* (2), 622-627.
(187) Gao, X.; Matsui, H., *Adv. Mater.*, **2005,** *17* (17), 2037-2050.
(188) Gruchlik, A.; Jurzak, M.; Chodurek, E.; Dzierzewicz, Z., *Acta poloniae pharmaceutica*, **2012,** *69* (6), 1303-1306.
(189) Hern, D. L.; Hubbell, J. A., *J. Biomed. Mat. Res.*, **1998,** *39* (2), 266-276.
(190) Tchuenbou-Magaia, F. L.; Norton, I. T.; Cox, P. W., *Food Hydrocolloids*, **2009,** *23* (7), 1877-1885.
(191) Montalbetti, C. A. G. N.; Falque, V., *Tetrahedron*, **2005,** *61* (46), 10827-10852.
(192) Morihara, K., *Trends Biotechnol.*, **1987,** *5* (6), 164-170.

(193) Schellenberger, V.; Jakubke, H. D., *Angew. Chem. Int. Ed.*, **1991,** *30* (11), 1437-1449.
(194) Chaiken, I. M.; Komoriya, A.; Ohno, M.; Widmer, F., *App. Biochem. Biotechnol.*, **1982,** *7* (5), 385-399.
(195) Guzman, F.; Barberis, S.; Illanes, A., *J. Biotechnol*, **2007,** *10* (2), 279-314.
(196) Koeller, K. M.; Wong, C.-H., *Nature*, **2001,** *409* (6817), 232-240.
(197) Das, A. K.; Collins, R. F.; Ulijn, R. V., *Small*, **2008,** *4* (2), 279-287.
(198) Ulijn, R. V.; Bisek, N.; Halling, P. J.; Flitsch, S. L., *Org. Biomol. Chem.*, **2003,** *1* (8), 1277-1281
(199) Ulijn, R. V.; Baragana, B.; Halling, P. J.; Flitsch, S. L., *J. Am. Chem. Soc.*, **2002,** *124* (37), 10988-10989.
(200) Halling, P. J., *Current Opinion in Chemical Biology*, **2000,** *4* (1), 74-80.
(201) Carrea, G.; Riva, S., *Angew Chem Int Ed*, **2000,** *39* (13), 2226-2254.
(202) Klibanov, A. M., *Nature*, **2001,** *409* (6817), 241-246.
(203) Khmelnitsky, Y. L.; Rich, J. O., *Current Opinion in Chemical Biology*, **1999,** *3* (1), 47-53.
(204) Ulijn, R. V.; Janssen, A. E. M.; Moore, B. D.; Halling, P. J., *Chem. Eur. J*, **2001,** *7* (10), 2089-2099.
(205) Semenov, S. N.; Wong, A. S. Y.; van der Made, R. M.; Postma, S. G. J.; Groen, J.; van Roekel, H. W. H.; de Greef, T. F. A.; Huck, W. T. S., *Nature chemistry*, **2015,** *7* (2), 160-165.
(206) Meyer, A. S.; Isaksen, A., *Trends Food Sci. Technol.*, **1995,** *6* (9), 300-304.
(207) Sarney, D. B.; Vulfson, E. N., *Trends biotechnol.*, **1995,** *13* (5), 164-172.
(208) Godfrey, T.; Reichelt, J., **1982**.
(209) Vellard, M., *Curr. Opin. Biotechnol.*, **2003,** *14* (4), 444-450.
(210) James, J.; Simpson, B. K.; Marshall, M. R., *Crit. Rev. Food Sci. Nut.*, **1996,** *36* (5), 437-463.
(211) Asgeirsson, B.; Bjarnason, J. B., *Comp. Biochem. Physiol*, **1991,** *998* (2), 327-335.
(212) Frankenberger, W. T.; Johanson, J. B., *Soil Biol. Biochem.*, **1982,** *14* (5), 433-437.
(213) Pavasovic, M.; Richardson, N. A.; Anderson, A. J.; Mann, D.; Mather, P. B., *Aquaculture*, **2004,** *242* (1–4), 641-654.
(214) Stevens, E. D.; McLeese, J. M., *Am. J. Physiol.*, **1984,** *246* (4), R487-R494.
(215) Iyer, P. V.; Ananthanarayan, L., *Process Biochem.*, **2008,** *43* (10), 1019-1032.
(216) Eijsink, V. G. H.; Gåseidnes, S.; Borchert, T. V.; van den Burg, B., *Biomol. Eng.*, **2005,** *22* (1–3), 21-30.
(217) Lumry, R.; Biltonen, R., *J. Am. Chem. Soc.*, **1971,** *93* (1), 224-230.
(218) Carrasquillo, K. G.; Sanchez, C.; Griebenow, K., *Biotechnol. App. Biochem.*, **2000,** *31* (1), 41-53.
(219) Heremans, L.; Heremans, K., *Biochim. Biophys. Acta*, **1989,** *999* (2), 192-197.
(220) Pace, C. N.; Grimsley, G. R.; Scholtz, J. M., *J. Biol. Chem.*, **2009,** *284* (20), 13285-13289.

(221) Hedstrom, L., *Chem. Rev.*, **2002,** *102* (12), 4501-4524.
(222) Morihara, K.; Oka, T., *Biochem. J.*, **1976,** *163*, 531-542.
(223) Kumar, A.; Venkatesu, P., *Chem. Rev.*, **2012,** *112*, 4283-4307.
(224) Boekhoven, J.; Brizard, A. M.; Kowlgi, K. N. K.; Koper, G. J. M.; Eelkema, R.; van Esch, J. H., *Angewandte Chemie*, **2010,** *122* (28), 4935-4938.
(225) Boekhoven, J.; Poolman, J. M.; Maity, C.; Li, F.; van der Mee, L.; Minkenberg, C. B.; Mendes, E.; van EschJan, H.; Eelkema, R., *Nature chemistry*, **2013,** *5* (5), 433-437.
(226) Pappas, C. G.; Sasselli, I. R.; Ulijn, R. V., *Angew Chem Int Ed* **2015,** *54* (28), 8119-8123.
(227) Rezaei-Ghaleh, N.; Ramshini, H.; Ebrahim-Habibi, A.; Moosavi-Movahedi, A. A.; Nemat-Gorgani, M., *Biophys.Chem.*, **2008,** *132* (1), 23-32.
(228) Colowick, S. P.; Kaplan, N. O., *Methods in Enzymology - Proteolytic Enzymes*. 1970; Vol. 19.
(229) Hennessey Jr, J. P.; Johnson Jr, W. C., *Biochemistry*, **1981,** *20* (5), 1085-1094.
(230) You, C.-C.; De, M.; Han, G.; Rotello, V. M., *J. Am. Chem. Soc.*, **2005,** *127* (37), 12873-12881.
(231) Bizzozero, S. A.; Baumann, W. K.; Dutler, H., *Eur. J. Biochem.*, **1975,** *15*, 167-176.
(232) Parker, L.; Wang, J. H., *J. Biol. Chem.*, **1968,** *23* (13), 3729-3734.
(233) Jayawarna, V.; Ali, M.; Jowitt, T. A.; Miller, A. F.; Saiani, A.; Ulijn, R. V., *Adv Mater.*, **2006,** *18*, 611.
(234) Hofmeister, F., *Arch. Exp. Pathol. Pharmakol.*, **1888,** *24*, 247.
(235) Silva, G. A.; Czeisler, C.; Niece, K. L.; Beniash, E.; Harrington, D. A.; Kessler, J. A.; Stupp, S. I., *Science*, **2004,** *303* (5662), 1352-1355.
(236) Haine, L.; Butterick, S.; Rajagopal, K.; Branco, M.; Salick, D.; Rughani, R.; Oilarz, M.; Lamm, M. S.; Pochan, D. J.; Schneider, J. P., *Proceedings of the National Academy of Sciences of the United States of America*, **2007,** *104*, 7791-7796.
(237) Kunz, W.; Lo Nostro, P.; Ninham, B. W., *Curr Opin Colloid Interface Sci*, **2004,** *9*, 7.
(238) Lo Nostro, P.; Lo Nostro, A.; Ninham, B. W.; Pesavento, G.; Frantoni, L.; Baglioni, P., *Curr Opin Colloid Interface Sci*, **2004,** *9*, 97-101.
(239) Lo Nostro, P.; Ninham, B. W., *Chem. Rev.*, **2012,** *112*, 2286-2322.
(240) Segarra-Maset, M. D.; Nebot, N. J.; Miravet, J. F.; Escuder, B., *Chem. Soc. Rev*, **2013,** *42*, 7086-7098.
(241) Yang, X. Y.; Zhang, G. X.; Zhang, D. Q., *J. Mater. Chem.*, **2012,** *22 38-50*.
(242) Foster, J. A.; Piepenbrock, M. O. M.; Lloyd, G. O.; Clarke, N.; Howard, J. A. K.; Steed, J. W., *Nat. Chem.*, **2010,** *2*, 1037-1043.
(243) Lloyd, G. O.; Steed, J. W., *Nat. Chem.*, **2009,** *1*, 437-442.
(244) Maeda, H., *Chem. Eur. J*, **2008,** *14*, 11274-11282.
(245) Piepenbrock, M. O. M.; Lloyd, G. O.; Clarke, N.; Steed, J. W., *Chem. Rev.*, **2010,** *110*, 1960-2004.

(246) Steed, J. W., *Chem. Soc. Rev*, **2010,** *39*, 3686-3699.
(247) Roberts, D.; Rochas, C.; Saiani, A.; Miller, A. F., *Langmuir*, **2012,** *28*, 16196-16206.
(248) Aggeli, A.; Bell, M.; Carrick, L. M.; Fishwick, C. W. G.; Harding, R.; Mawer, P. J.; Radford, S. E.; Strong, A. E.; Boden, N., *Journal of the American Chemical Society*, **2003,** *125* (32), 9619-9628.
(249) Hartgerink, J. D.; Beniash, E.; Stupp, S. I., *Science*, **2001,** *294* (5547), 1684.
(250) Cohn, E. J.; Edsall, J. T., *Proteins, amino acids and peptides as ions and dipolar ions*. Reinhold Publishing Corporation; New York: 1943.
(251) Zhang, Y.; Cremer, P. S., *Curr Opin Chem Biol*, **2006,** *10*, 658-663.
(252) Stryer, L., *Biochemistry*. 4th Edition ed.; New York, 1995.
(253) Urry, D. W.; Peng, S. Q.; Parker, T. M.; Gowda, D.; Harris, R. D., *Angewandte Chemie International Edition in English*, **1993,** *32* (10), 1440-1442.
(254) Kanicky, J. R.; Poniatowski, A. F.; Mehta, N. R.; Shah, D. O., *Langmuir*, **2000,** *16* (1), 172-177.
(255) Ulijn, R. V.; Moore, B. D.; Janssen, A. E. M.; Halling, P. J., *Journal of the Chemical Society, Perkin Transactions 2*, **2002,** (5), 1024-1028.
(256) Tang, C.; Ulijn, R. V.; Saiani, A., *Langmuir*, **2011,** *27* (23), 14438-14449.
(257) Roy, S.; Javid, N.; Frederix, P. W.; Lamprou, D. A.; Urquhart, A. J.; Hunt, N. T.; Halling, P. J.; Ulijn, R. V., *Chem. Eur. J*, **2012,** *18* 11723-11731.
(258) Nebot, N. J.; Ojeda-Flores, J. J.; Smets, J.; Fernábdez-Prieto, S.; Escuder, B.; Miravet, J. F., *Chem. Eur. J*, **2014,** *20*, 14465-14472.
(259) Chen, L.; Pont, G.; Morris, K.; Lotze, G.; Squires, A.; Serpell, L. C.; Adams, D. J., *Chemical communications*, **2011,** *47* (44), 12071-12073.
(260) Chen, L.; McDonald, T. O.; Adams, D. J., *RSC Advances*, **2013,** *3* (23), 8714-8720.
(261) Mart, R. J.; Osbourne, R. D.; Stevens, M., M.; Ulijn, R. V., *Soft Matter*, **2006,** *2*, 822-835.
(262) Xie, Y.; Zhao, J.; Huang, R.; Wei, Q.; Wang, Y.; Su, R.; He, Z., *Nanoscale Res. Lett.*, **2016,** *11* (184).
(263) Ozbas, B.; Kretsinger, J.; Rajagopal, K.; Schneider, J. P.; Pochan, D. J., *Macromolecules*, **2004,** *37* (19), 7331-7337.